A REAL TIME FLUORESCENT PARTICLE COUNTER

FOR

ATMOSPHERIC DISPERSION STUDIES

BY

WILLIAM LEWIS ERROL DAVEY, B. Sc. Eng., M. Sc. Eng.

Submitted in partial fulfilment of the requirements for the degree of Doctor of Philosophy in the Department of Chemical Engineering University of Natal, Durban.

1985

SUMMARY

A new instrument which can automatically measure the concentration of fluorescent pigment (FP2267) in the atmosphere and record the readings continuously on magnetic tape has been developed. In principle air is sampled through a small bore pipe, and at a discrete break in the pipe the sampled air is irradiated with ultra-violet light and simultaneously the fluorescence from any particles of pigment present in the air is detected by a photomultiplier. The fluorescent particle counter was rigorously tested in the laboratory yielding the following characteristics:

aerosol transmission efficiency	:	better than 90%
highest detectable concentration	:	4×10^5 particles/m^3
lowest detectable concentration	:	600 particles/m^3
response to step changes	:	less than 2s
minimum time resolution	:	2s
calibration equation	:	$A = 4{,}21\ B^{1{,}45}$

(where A is the actual concentration in particles/m^3 and B is the electronic count in counts/minute)

As a means of determining the ability of the new instrument to measure atmospheric dispersion a field trial was conducted from which some 37 hours of useful data was accumulated out of a total of 41 hours operation.

Eddy diffusivities, of between 1 and 11 m^2/s, were estimated from the data collected at 20 m from the source by fitting a K-theory model modified to allow for a fluctuating wind direction. These estimates of the eddy diffusivities are shown to be within an order of magnitude of data extrapolated from the published results of other workers.

ACKNOWLEDGEMENTS

The work described herein was supervised first by Dr. M.T. Scholtz, then by Professor E.T. Woodburn, and finally by Professor D. Raal. Both the research and the author were supported by a grant from the Atomic Energy Board who also undertook the design and construction of the Fluorescent Particle Analyser. Most of the regressions reported in this work were carried out on a computer belcnging to AECI Limited.

I wish to record my sincere appreciation to the following people :

To Professor D. Raal for his helpful and constructive criticism of my work ;

To Dr. R. Fogel for never failing to believe that I would eventually finish the work ;

To my father who has waited patiently for ten years to see this work completed and who has kindly paid for the typing and binding of this work ;

To Dr. E.A. Zaloumis who was responsible for stimulating my interest in environmental problems ;

To my wife who threatened on several occasions to burn the growing volume of paper ;

And finally to Mrs. Vera Swart for giving up time which should have been devoted to her faimily to type this thesis.

CHRONOLOGICAL NOTE

The work reported in this thesis was initiated in 1973. Development of the fluorescent particle counter, calibration and field test were carried out on a full-time basis until the end of 1976 at the University of Natal, Durban. Thereafter the modelling work and preparation of this thesis was carried out on a part-time basis until it was first submitted to the University of Natal for adjudication in June 1983. The extended period of time over which this work was carried out therefore raises the question as to how it relates to other work in the field of fluctuating concentrations in the atmosphere. A recent review by Hanna (85) in 1984 gives some perspective to this problem. Following the publication of Gifford's (22) and Csanady's (10) work in 1959 and in 1969 respectively, apparently the next and subsequent reports on the modelling of concentration fluctuations appeared in the literature from 1979 onwards. With regard to experimental measurements following the work at Hanford (43,44,45,54) over the period 1967 to 1971 apparently reports of two field experiments and three laboratory experiments have appeared in the literature since 1981. The dearth of experimental data has led Hanna to remark "There are not many observations of concentration fluctuations available due to the difficulties involved in obtaining and interpreting the data. In addition there are far fewer field data than laboratory data."

DECLARATION

I hereby certify that this research, unless where specifically acknowledged, is the result of my own investigation which has not already been accepted in substance for any degree and is not being concurrently submitted in candidature for any other degree.

W.L.E. DAVEY

VITA

Name :	William Lewis Errol Davey
Place and year of birth :	Scottburgh, Natal, 1946
Education :	Primary education at Sezela Government School followed by Treverton Primary School. Secondary education at St Charles College ; matriculated 1963 University of Natal 1965 - 1969 ; awarded B.Sc. Chem. Eng. 1969 University of Natal 1970 - 1973 ; awarded M. Sc. Chem. Eng. 1973 University of Natal 1974 - 1976 ; present project
Experience :	Engineer's assistant. SAICCOR Ltd., Umkomaas, Summers of 1965, 1966, 1967. Engineer's assistant, Hulett's Refinery, Durban, Summer 1968. Chief Technical Officer, AECI Ltd, Modderfontein, Transvaal 1977 onwards.
Awards :	National Institute of Metallurgy, Bursary
Publications :	'The Conditioning of an Apatite Ore for Flotation'. M.Sc. Thesis, Department of Chemical Engineering, University of Natal, Durban, 1973

Publications (cont.)

Davey W.L.E., 'Recovery of Useful Products from Koppers-Totzek Gasifier Flyash ; The Manufacture of a Reductant'. Proceedings of a Conference on the Utilisation of Pulverised Fuel Ash, Council for Scientific and Industrial Research, Pretoria, South Africa (1979)

Davey W.L.E. and Engelbrecht A.D., 'Recovery of Useful Products from Koppers-Totzek Gasifier Flyash ; Combustion to Raise Steam'. Proceedings of the Third National Meeting of S.A.I. Chem. E., Johannesburg, South Africa (1980) and subsequently published in CHEMSA (April 1982)

Couch A.T. and Davey W.L.E., 'The Use of Fluidised Combustion to Burn the Flyash from Koppers-Totzek Gasifiers'. Proceedings of the International Conference on Coal Conversion, Council for Scientific and Industrial Research, Pretoria, South Africa (August 1982).

Davey W.L.E., Turner M.J. and Marshall A.R., 'A Fluidised Bed Boiler to Burn Waste Flyash from Koppers-Totzek Gasifiers'. Proceedings of an International Conference on Fluidised Combustion, The Institute of Energy, London (October 1984).

Couch A.T. and Davey W.L.E., 'Fluidised Bed Boiler will Burn Ammonia Plant Flyash Waste'. Modern Power Systems, 3, 56 (October 1983).

Couch A.T., Cruickshank T.D., Marshall A.R., Wakeford D.R., Tydd C.B. and Davey W.L.E., 'Fluidised Bed Combustion Apparatus'. Patent applied for in Great Britain, E.E.C., U.S.A., Canada, R.S.A. and Australia (1983).

CONTENTS

TABLES

FIGURES

NOTATION

A	Actual concentration derived from the filter located in the housing below the sample chamber in figure 3.8 (particles/m^3)
B	Electronic counting rate derived from the photomultiplier in the detection system (counts /minute)
C_y, C_z	Constants in the expression for the spreading coefficients for the horizontal and vertical planes respectively
K_y, K_z	Eddy diffusivities in the horizontal and vertical planes respectively (m^2/s)
n	Exponent in the expression for the spreading coefficients
$P(\chi > \chi')$	Cumulative probability that χ will exceed χ'
$p(\theta)d\theta$	Probability density or probability that θ will be between θ and $\theta + d\theta$
Q	Tracer release rate (particles/s)
S	Horizontal distance between the tracer source and the sampler (m)
T	Temperature (^oC)
u	Wind velocity m/s
x	Horizontal co-ordinate of the sampling nozzle in relation to the tracer source along the mean wind direction (m)
y	Horizontal co-ordinate of the sampling nozzle in relation to the tracer source at right angles to the mean wind direction (m)
z	Vertical co-ordinate of the sampling nozzle in relation to the tracer source at right angles to the mean wind direction (m)

α	Angle between the azimuths of the sampler and the instantaneous wind in relation to the tracer source
ψ_s	Elevation of the sampler in relation to the source
θ	Instantaneous azimuth of wind direction in relation to the tracer source
$\bar{\theta}$	Mean azimuth of wind direction in relation to the tracer source
θ_s	Azimuth of the sampler in relation to the tracer source
σ_c	Coefficient, or standard deviation, of plume meander in the horizontal plane (m)
σ_y, σ_z	Spreading coefficients, or standard deviations of the plume cross-section in the horizontal and vertical planes respectively (m)
σ_θ	Standard deviation of fluctuations in the azimuth of wind direction
x	Instantaneous concentration of a tracer measured by a sampler (particles/m^3)
$\bar{x}$	Mean concentration of a tracer measured by a sampler (particles/m^3)

GLOSSARY

Fluorescent Particle Counter	:	That part of the instrument embodying the illumination and detection sections and through which a sample of the air is continuously drawn.
Fluorescent Particle Analyser	:	That part of the supporting equipment which processes the signal from the Fluorescent Particle Counter.

CHAPTER ONE : INTRODUCTION

It is necessary to measure atmospheric dispersion for two main reasons, and these are:

a) to verify mathematical models of dispersion, and

b) to estimate the parameters by which atmospheric dispersion is characterised.

Atmospheric dispersion parameters, commonly reported either as eddy diffusivities in the K-theory model, or as spreading coefficients in the gaussian plume formulae, have been found to be a complex function of distance downwind, topography and surface roughness and consequently it has proved necessary to measure these parameters for each location under consideration in order to obtain a more exact understanding of the dispersion process.

The classical method by which dispersion has been measured is to release a tracer from one point and measure its concentration in the atmosphere at a number of points downwind of the source. These sampling points are usually located in the horizontal plane at about ground level but

on occasions have also been located in the vertical. The atmosphere is usually sampled by drawing a stream of air through some form of capture apparatus such as an absorber for gaseous tracers, or a filter paper for solid tracers. Samples are collected for periods of time ranging from three minutes to sixty minutes and then analysed and such samples have been termed "time mean samples".

This method of measuring atmospheric dispersion, by time mean samples, has in the past been used very successfully in a large number of field programs but has its limitations, in that :

a) the spatial variation in concentration is well described but temporal variations are poorly described

b) although the method has been successfully applied in unstable atmospheric conditions its application to neutral and stable atmospheres has been much less successful.

The aim of the work reported in this thesis has therefore been to overcome these limitations by the development of a

new instrument which measures the concentration of a tracer continuously and records this information in real time. In this way information about the temporal variation of concentration may be obtained and this is significant in circumstances where the concentration of a pollutant is more important than the dose.

Under stable atmospheric conditions the dispersion of a plume is very gradual making it necessary to know the path of the plume before samples can be taken. Invariably the plume does not follow a fixed path for any length of time but meanders very slowly. Sampling such a plume from fixed samplers therefore becomes a rather "hit and miss" affair which results in a rather poor rate of success. With a real time sampler however the air can be sampled continuously for long periods of time, making it feasible to monitor the passage of a plume as and when it meanders past the sampler.

The tracer chosen for the purpose of this thesis was the solid tracer zinc cadmium sulphide which has been used in a large number of studies reported in the literature. The conventional method of detection for this tracer is to collect it on a filter paper , irradiate it with ultraviolet light and then count the number of fluorescing particles

using a microscope. In order to detect this tracer continuously, however, air being sampled was drawn in a collimated stream through a zone which was irradiated with an intense beam of ultra-violet light. The zone of irradiation was simultaneously monitored by a photo-multiplier designed to record the passage of any particles fluorescing with a yellow colour. In this way the number of particles in the sampled stream of air could be counted and recorded continuously.

The new instrument was calibrated in two ways :- firstly an aerosol containing known concentrations of the tracer were created in the laboratory and sampled. The nature of the aerosol generation rig also made it possible to generate step changes in concentration with which to demonstrate the dynamic behaviour of the instrument.

For the second method of calibration the Fluorescent Particle Counter was placed in the field downwind from a tracer source and real atmospheric dispersion data was collected. This data was then used in conjunction with a modified version of the K-theory solution for a continuous source to estimate the eddy diffusivities. The resulting diffusivities were then compared with data

published by a number of authors and found to compare favourably considering the restricted conditions of the test.

The overall purpose, then, of the work reported in this thesis was to devise a continuous analyser for an atmospheric tracer which would enable the dispersion process to be better understood by resolving the temporal variations in concentration.

CHAPTER TWO: LITERATURE SURVEY

2.1 Introduction

For the purpose of this work the literature is surveyed and analysed with four main objectives :

1) review previous attempts to measure the temporal variations in concentration in the atmosphere

2) review the various tracers which have in the past been used to characterise atmospheric dispersion

3) review the various methods by which the tracer fluorescent pigment, have been detected

4) review the design of previous continuous analysers designed to detect fluorescent pigment.

2.2 Review of Field Programs Designed to Measure Real-Time Concentration Histories.

Atmospheric dispersion is normally investigated by releasing a tracer continuously into the atmosphere over a period of time and by measuring the concentration of that tracer at a number of locations downwind of the source. Because of the very powerful mixing action of the atmosphere the concentration of the tracer becomes very low at distances of more than a few hundred metres from the source. In addition eddies in the atmosphere are subject to random movements leading to random fluctuations in the instantaneous concentration at any downwind location. Thus in order to collect sufficient sample for subsequent assessment and also to smooth out the fluctuations samples are traditionally collected for a sampling period of not less than 3 minutes and usually not longer than 30 minutes. This method of sampling is known as "time-mean" sampling and as its name implies it yields a measure of the average concentration for the period over which the sample was taken.

Field studies of atmospheric dispersion have been reported from a fairly considerable number of locations throughout the developed world and most are based on data derived from time-mean sampling techniques. By contrast there are very few reported studies based on continuous on-line techniques of measurement and in fact for the purpose of this review it was possible to acquire only three such studies.

It is important at this point to distinguish between semi-continuous sampling and continuous sampling. It is apparent from the literature that some attempts have been made to study the time variation in concentration by taking a large number of sequential samples each of fairly short duration. Such methods suffer first from the problem that the volume of assessment becomes very large, and second from the problem that many of the samples contain insufficient tracer to be detected. The three papers to be reviewed therefore are based on detectors which operated continuously.

One of the earliest investigations of the instantaneous dosage field reported was by Gosline (26) who measured real-time concentration histories of NO_2 released from a 24 m high stack at distances of up to 488 m downwind of the stack. Gosline used a direct reading photoelectric gas analyser from which he took readings every ten seconds. He mounted the gas analyser in a jeep and this enabled him to visit in succession each of a series of preselected sampling sites. From this data Gosline was able to construct cumulative frequency curves for different distances and meteorological conditions.

Gosline's work was followed by an investigation, reported in 1958 by Davidson and Halitsky (11a), in which a smoke plume was photographed at 10 second intervals from a point at ground level and normal to the mean wind direction. The measurement technique in this study is clearly not a continuous one but the interval between photographs is sufficiently small for it to be nearly continuous.

Although Davidson and Halitsky were interested only in the vertical motions of the plume their work enabled them to postulate that segments of the plume appear to travel in straight lines from the source even though the paths followed by successive segments were unrelated to each other.

More recently Nickola (43,44) and his co-workers described a comprehensive and well instrumented investigation using 85 Kr as tracer and geiger counters as detectors. 64 Geiger counters were distributed on two sampling arcs at distances of 200m and 800m from the release point. The data from each counter was routed to a central point where it was collected in a hard wired memory system which in turn periodically read out to a tape recorder. In this way Nickola was able to obtain real-time histories arising from continuous and puff releases with a resolution of as little as 4,8 seconds.

In considering these three methods of measuring

real-time variations the following conclusions can be drawn :

1) Although nitrogen peroxide can be detected at relatively low concentrations using a fairly simple method of measurement it is today regarded as highly toxic and its release into the atmosphere is strictly controlled by legislation.

2) Photographic techniques have in the past been very useful in studying "gross" atmospheric movements but yield information which is qualitative rather than quantitative.

3) In using a radioactive tracer Nickola and his co-workers found that to achieve concentration levels downwind of the source which would exceed the background noise level large quantities of tracer had to be released, making the use of

this tracer a health hazard to both the workers and the public

2.3 Review of Atmospheric Tracers

Dumbauld (15) summarized the properties, methods of release and detection, and limitations of the many tracers reported to have been used at one time or another. His data, modified and updated for the purpose of this study, are presented in table 2.1.

The most frequently used tracer is seen to be zinc-cadmium sulphide, also known as Fluorescent Pigment or "FP", the usual source for this tracer being the U.S. Radium Corp. FP2210 was the tracer used in earlier work but this has been succeeded by FP2267 which fluoresces with a spectral peak of 577 nm when irradiated with the 365 nm line of the mercury spectrum. FP2267 has a particle size range of 1-5 microns and single particles are easily distinguised by eye using a magnification of about 100X. Each gram of the tracer is reported to contain about 1×10^{10} particles.

Table 2.1: Summary of the properties and methods of release and detection for various tracers which have been used to study atmospheric dispersion

Tracer	Smoke	Pollen	Natural aerosols	Sulphur dioxide	Glass microspheres	Sulphur hexafluoride	Uranine dye	Flourescent pigment(ZnCdS and ZnS)	Radioactive gases (^{41}Ar and ^{85}Kr)
		Particulate tracer. Size: 20-30 μm. Setting rate 15,6 mm St.	Particulate tracer. Size: 0,13 - 1,5 μm	Gaseous tracer.	Particulate tracer Size: 50 - 200 μm	Non-toxic gaseous tracer.	Particulate tracer Soluble in H O. Fluorescent peak at 518 nm. Size: adjustable.	Particulate tracer. Soluble in H20. ZnCd toxic. Size: 0,5 - 5 μm. S.G. : 4 Fluorescent peak at 597 nm	Gaseous tracer.
Method or release	Smoke generator	Occurs naturally from trees and ragweed	Occurs naturally from industrial and city sources	Direct from gas bottle	Hopper feed to moving belt or high velocity air stream	Direct from gas bottle	Water solution sprayed with pneumatic nozzle. Particle size adjustable with nozzle design	Dry powder dispenser or by acetone slurry in pneumatic nozzle	Continuous release from cylinder, or instantaneous release from glass bomb
Method of detection	Densitometer or plume photography	Collected on filter papers, stained and determined microscopically	Aerosol particle counter or densitometer. Real-time history possible.	Absorbed in H_2O_2 and measure conductivity. Detection limit: 0,01 ppm	Capture on sticky paper, assessment with stereo microscope. Also treated with FP, assessed visually with UV light.	Gas chromatograph with electron capture detector. Detection limit: 10^{-6} ppm. Can be improved to 10^{-8} ppm.	Collection on filter paper. Assessment with microscope or in aqueous solution with fluorometer. Detection limit: 1×10^{-11} gm ml^{-1}	Collection on filter paper. Assessment by microscope with U.V. light. Various automatic methods not very sensitive	By β -particle geiger counter tubes
General comments	Limited downwind travel	Has been used to study mesoscale transport of airborne biogenic particles to distances of 100 km	Used to study long range transport to 120 km	Has been studied over distances up to 1 000 km from industrial sources. Artificial sources limited by background from industry	Used to study dust fallout	Useful over long distance. Most promising tracer yet	A somewhat neglected tracer. Has been used over distances to 20 km. Possible problems with nozzle settings	Most popular tracer, well described. Used to distances of 100 km. Awkward to handle, assessment tedious	Quantity of gas required is large-health hazard. Useful to distances of 1 000 m
References	14	52, 53	5, 63	14, 16, 36 54, 58	66, 73	6, 8, 11, 12, 56	14, 32, 55, 57	2, 3, 4, 13, 14, 18, 19, 29, 39, 46, 71, 72	40, 41, 65

The properties and techniques for the use of FP were well described by Leighton and his co-workers (32,49). Probably as a result of Leighton's work FP has been used in a number of important investigations in atmospheric dispersion. These include the New Mexico Study (5) where plume cross-sections were measured to a distance of 235km from the source. The Lake Erie study (3,4) where the effect of a lake shore was investigated, the Green Glow Program and Hanford 30 series (19,20) where diffusion patterns were studied to a distance of 25,6km from the source, the St. Louis Study (40,51) where dispersion over an urban area was compared to that over a rural area and the Pretoria Study (79,80) where the Sutton diffusion parameters were measured for the Transvaal Highveld.

Until fairly recently zinc-cadmium-sulphide was generally regarded as non-toxic, however a recent paper by Spomer (69) has thrown some doubt on this assumption. Spomer reports the Threshold Limit Values for Cd metal and CdO as 0,2 mg/m^3 per 8 hour day and 0,05 mg/m^3 per 8 hour day respectively

and makes the point that zinc cadmium sulphide is readily dissolved by dilute acids. Whilst he does not exclude its use as an atmospheric tracer Spomer at least draws attention to the health hazard to which research workers using this tracer may expose themselves. From Spomer's figures it may be concluded that the threshold limit values would be exceeded by a concentration of more than 1×10^7 particles/m^3 and the greatest danger posed to research workers is likely to occur within the immediate vicinity of the source.

Other tracers which have received far less attention include oilfog, sulphur dioxide, uranine dye and lycopodium spores. These are reported in table 2.1 together with their appropriate references.

Of more recent origin is the finding that sulphur hexafluoride may be determined chromatographically using an electron capture detector at concentrations as low as 10pl/l (7,9,61). Furthermore, it appears that samples may be concentrated and hence the detection limit improved by as much as 1000

times. With the improvement of gas chromotography as an analytical tool the use of SF_6 is likely to succeed the use of ZnCdS as an atmospheric tracer.

For the purpose of this study however, ZnCdS was chosen as tracer for the following reasons :

1) Its use as a tracer to study atmospheric dispersion has been widely reported and its properties, advantages and disadvantages were therefore well known.

2) Some expertise in its use as a tracer existed in South Africa as a consequence of atmospheric dispersion studies carried out by the Council for Scientific and Industrial Research.

3) It was conceivable that FP could be counted in real-time in a manner analogous to the counting of radioactivity. As the ability to be assessed in real time was of fundamental importance in this study SF_6, which may have had advantages over FP, was excluded. At the

with an aspiration rate of 10 to 12 litres per minute concentrations of as low as 10 particles per m^3 can be reliably determined. The aspirated filter yields a time-mean concentration and in this way it has been used in almost every study of atmospheric dispersion in which FP has been used as a tracer.

The rotary drum impactor comprises a drum around the periphery of which is mounted a strip of sticky tape. Air is sampled continuously and is directed at high velocity at the sticky tape. Sufficient momentum is imparted to the particles of FP carried in the air stream to enable them to cross the streamlines and impact on the sticky tape. By rotating the drum very slowly or incrementally a real time history of concentration can be obtained. Assessment is carried out by microscopic examination under ultra-violet illumination. Clearly this method of analysis is more complex than the aspirated filter and its use has consequently not been widely reported. Conceptually the method appears to have merit,

however, it may suffer from a number of disadvantages namely :

1) There may be a cut off in the smallest size of particle which can successfully be impacted.

2) Determination of the tapes by microscope appears to be a very tedious task.

3) For sampling times of one minute or less each tape would last for only about two hours before a tape change became necessary. The instrument would, therefore, demand a high degree of attention if an experiment were to last for a substantial period of time.

The tedious task of assessing membrane filters was quite successfully solved by Rankin (55) who described a method whereby the filters were first

exposed to an alpha-emitting isotope. The filters were then placed under a photomultiplier which measured the level of fluorescence, and by means of suitable calibrations the concentrations could be estimated. Whilst substantially increasing the rate at which filters could be determined this method still does not lend itself to the measurement of real-time concentration histories.

Another automatic method for the assessment of fluorescent particles was described by van Buijtenen and Clarenburg (78). In this method filter papers are viewed through a microscope with a photomultiplier. Rotating chopper discs in the illumination and fluorescence beams are synchronised in such a way as to ensure that the photomultiplier only sees the FP when the illumination is cut off. In this way any interference in the determination by reflected ultra-violet light is completely eliminated. Whilst this idea appears to have merit and could conceivably be

adapted for the rapid assessment of drum impactor tapes, its use in atmospheric dispersion work has apparently not been further developed or reported.

2.5 Continuous Real-Time Methods for the Instantaneous Assessment of Fluorescent Pigment

Two instruments designed to measure real-time concentration histories have been described in the literature. The first instrument is described by Nickola and his co-workers (45), and in this instrument a continuous stream of air is drawn through an excitation chamber where the FP is irradiated with ultra-violet light. The FP is then drawn through a detection chamber in which the average level of fluorescence is determined using a photomultiplier and by measuring the photomultiplier current. The two chambers are separated by a labyrinth to prevent any interference in the detection chamber by ultra-violet light. Figure 2.1 is a sketch of the apparatus which shows clearly the parts described.

Nickola et al speculate on their instrument's ability to detect concentrations as low as 300 particles/m^3 but give what they consider to be a realistic lower detection limit of 2500 particles/m^3. The maximum concentration measured appears to have been about 6×10^6 particles/m^3.

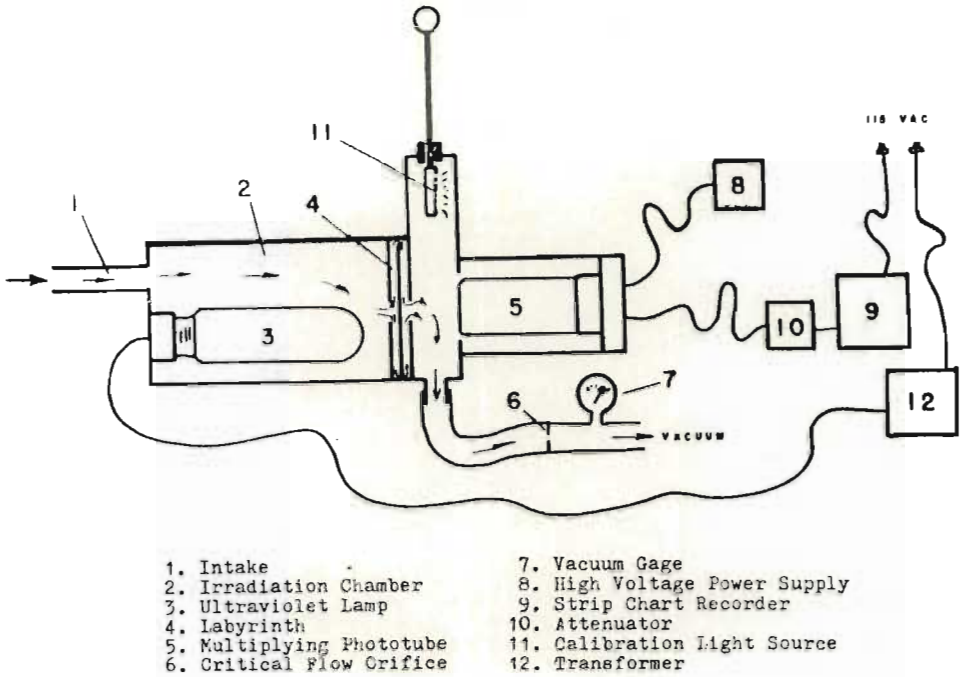

Figure 2.1: Schematic drawing of the real-time sampler reported by Nickola (45)

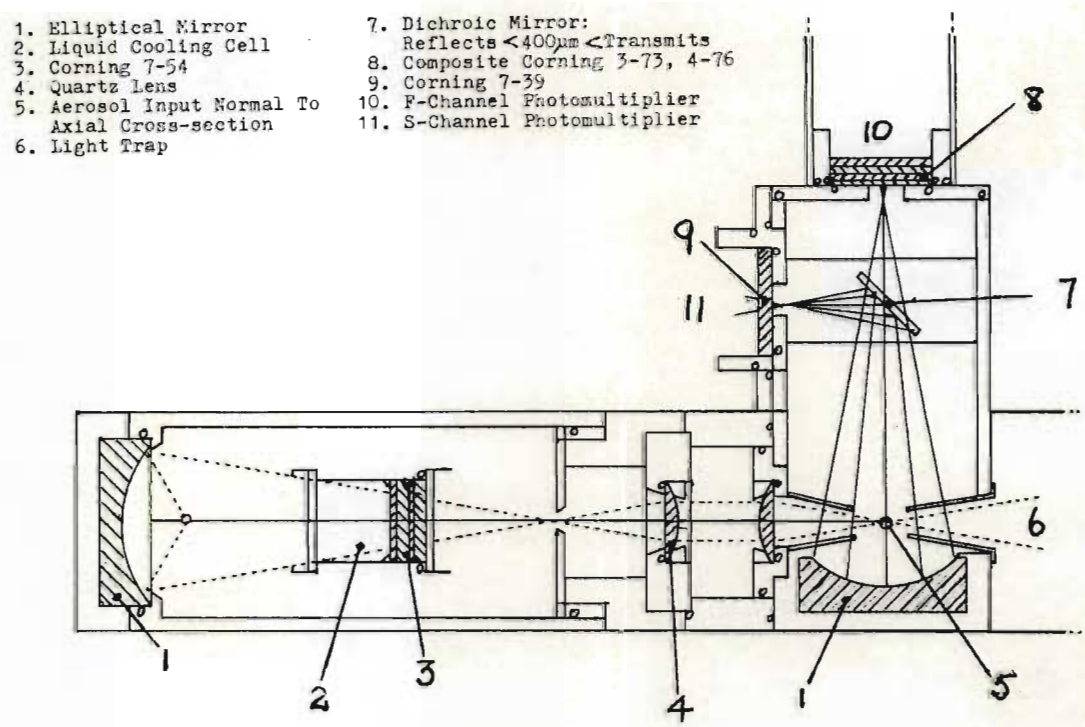

Figure 2.2: Schematic drawing of the real time counter reported by Goldberg (25)

Nickola calibrated this instrument by placing it in the field alongside a filter collector during atmospheric dispersion trials. By accumulating data over a number of trials effective calibration was achieved by comparing the concentration measured by the filter collector with a trace of the photo-multiplier current. Nickola reports a calibration equation of the form:

$$C = 2{,}90 \times 10^{-8} \; R^{0{,}965}$$

where C is the concentration in grams/m^3 and R is a measure of the photomultiplier current (one unit equals $0{,}04 \times 10^{-9}$ amps).

The second instrument designed to measure very low concentrations of FP was described by Goldberg (25) in 1968, and which he called a Microaerofluorometer (MAFIA). Figure 2.2 is a schematic diagram of Goldberg's instrument and demonstrates its greater sophistication over that reported by Nickola. In principle the operation of Goldberg's instrument is somewhat different from Nickola's in that the irradiation and detection zones are not separated. By carefully focussing a beam of UV light from a mercury lamp along an imaginary x-axis Goldberg has created a small zone of intense illumination. Through this zone but at right angles to the UV beam or along the z-axis, a stream of sampled air

is drawn. Any fluorescent particles present in the sampled air will fluoresce when irradiated with UV light and this fluorescence is focussed along the y-axis on to the photo-cathode of a photomultiplier. Because of the momentary nature of the fluorescence the presence of a particle of FP is seen as a pulse of light and results in a voltage pulse on the anode of the photomultiplier. In this way it should be possible to detect single particles of FP.

In order to overcome the problem of detecting reflected UV light, which could occur when dust particles pass through the "detection zone", Goldberg filtered the excitation beam to pass only UV light and filtered the detection beam to pass only the yellow fluorescence. He further improved the instrument's ability to discriminate between dust and FP by reflecting that portion of the detection beam with a wavelength less than 400 nm, to a second photomultiplier and subtracting its output from that of the first photomultiplier, in this way reducing to zero any signal arising from reflected UV light.

Whilst Goldberg describes the operation of his instrument and its possible uses he gives very little information on any calibration nor on any

experiments for which the instrument was used. Although Goldberg claims a lower detection limit of 100 particles/m^3 this would appear from his paper to be equal to the background noise level. Thus if three times the background counting rate is taken as a reasonable criterion 300 particles/m^3 is probably a more realistic lower detection limit. The residence time of particles in the view volume is given as 100μs and, if this is true, Goldberg's instrument should be capable of measuring concentrations as high as $1x10^7$ particles/m^3. No calibration equation is given but from three simple tests conducted in the concentration range $2,43x10^5$ to $7,04x10^5$ particles/m^3 it would appear that the actual concentration is roughly 72% of that inferred directly from the instrument counting rate.

2.6 Discussion

For the purpose of this work it was important to choose an established tracer with a unique property by which it could be distinguished from naturally occurring contaminants in the atmosphere, and which would also enable it to be detected continuously and automatically. Sulphur hexafluoride has the advantage that it is a gas, is not normally present in the atmosphere, and can be detected at extremely

low concentrations. However, sulphur hexafluoride must be detected and analysed by gas chromatography, a technique which is normally a batch operation and which is not readily adapted for continuous monitoring.

On the other hand, although the particulate nature of fluorescent pigment might be regarded as a disadvantage, its use in atmospheric dispersion has been widely reported, and it can be automatically detected. Furthermore some experience in its use already existed in South Africa.

Whilst the real-time instrument described by Nickola has the advantage of simplicity in its design insufficient attention appears to have been paid to the problem of particles impacting on the labyrinth and other parts which could later come loose giving rise to misleading results. In fact Nickola himself reports that knocking the instrument gave rise to spurious results. On the other hand, whilst the instrument developed by Goldberg does not apparently suffer from any of these problems it is not clear from his paper whether the complexity of his instrument is justified. Furthermore, Goldberg did not report a rigorous calibration of his instrument, nor did he demonstrate its effectiveness

in a field test of any kind.

The most important difference between these two instruments is that whereas Nickola's instrument determines concentration by measuring an average light level Goldberg's instrument is designed to detect individual particles. For atmospheric dispersion work where the dilution of a tracer can be several orders of magnitude over relatively short distances the ability to detect very low concentrations is of paramount importance. Thus in principle the ability to count single particles, as in Goldberg's instrument, should place no limitation on the lowest detectable concentration. By contrast the lowest light level which can be detected, as in Nickola's instrument, is limited by the photomultiplier dark current.

The subject of this thesis is therefore the development of a new instrument incorporating some of the principles described by Goldberg but without the complexity of his optical system. Briefly, in the new instrument irradiation and detection are accomplished simultaneously by arranging the irradiation, detection and sampling axes orthogonal to one another. In this way the distance through which the sample of air is drawn is kept as short as possible thus

minimising losses due to impaction. Furthermore, by focussing the irradiation and detection beams to predetermined shapes the time duration of fluorescence can be controlled thereby defining the pulse shape from the photomultiplier.

In addition to a description of the development of the new instrument, the present work also covers an extensive calibration and characterisation in the laboratory, a field test, and the estimation of dispersion parameters from the field test data.

CHAPTER THREE: DESIGN FOR A FLUORESCENT PARTICLE COUNTER

3.1 Introduction

Assuming a single particle of fluorescent pigment is irradiated with ultra-violet light the amount of energy it will absorb will be a function of the projected area of the particle and therefore to the square of its equivalent diameter. The particle then fluoresces, reradiating a portion of the absorbed energy uniformly into the space surrounding the particle. If a light sensitive device such as a photomultiplier is then focussed on the fluorescing particle a portion of the fluorescence can be collected and converted to an electrical signal. In principle then, the presence or absence of particles of fluorescent pigment may in this way be detected.

In practise particles of dust are also present in the atmosphere and these could reflect some of the irradiating ultra-violet light into the light sensor thus yielding a spurious result. Fortunately

particles of fluorescent pigment fluoresce at a wavelength which is considerably longer than the irradiating ultra-violet light and so spurious results may be minimised by interposing a filter which passes only the ultra-violet light between the light source and particle, and by interposing a filter which passes only the fluorescence, but not the U V light, between the particle and light sensor.

Using information obtained from vendors the fluorescent flux reaching the light sensor can be estimated. These calculations are shown in appendix E. Assuming that the light sensor is a photomultiplier it was found that a signal level of between 0,1 and 10 volts could be expected for particles varying in size between 0,5 and 5 µm. By comparison the signal level in the absence of a fluorescent particle may be deduced from the manufacturers figures for the photomultiplier and was expected to be about 0,001 volts, some two to four orders of magnitude less than that in the presence of a particle. The expected

strength of this signal therefore provided the justification for the design of the instrument to be described.

In this chapter the design of the fluorescent particle counter will be discussed in detail. Following a description of the overall concept the instrument is broken down into its three main parts :

1) the excitation system, where the fluorescent particles are irradiated with ultra-violet light

2) the detection system, where the fluorescence from each particle is detected

and

3) the data processing system, where the signals generated by the detection of fluorescent particles are recorded in a retrievable form.

Calibration of the fluorescent particle counter is dealt with in chapter four.

3.2 Principle of Operation

In section 2.4 two instruments were discussed with which it was possible to count fluorescent particles on a real-time basis. Whereas the instrument described by Nickola would, it seems, have been better suited to the detection of fairly large concentrations of FP the instrument developed by Goldberg would have been very sensitive to extremely low concentrations of FP. However Goldberg did not report a rigorous calibration of his counter and there has been no further mention of its use in the literature.

As has already been discussed, Leighton et al attempted to count particles on a filter paper using simultaneous illumination with ultra-violet light and detection with a photomultiplier through a microscope. Although he found the filter paper reflected too much ultra-violet light to enable satisfactory determinations to be made in this way, he was able

to measure a luminous flux at the photo-cathode from single particles of FP of between 10^2 and 10^5 pico-lumens. In the absence of any other interference this is sufficient to yield a detectable current from the anode of a photo-multiplier.

Inspired by the various designs for light scattering aerosol photometers (8,30,38,56,84) a design similar to Goldberg's was developed and is shown in isometric view in figure 3.1 Essentially a stream of the gas to be sampled is drawn down the sample tube at right angles to both an excitation axis and a detection axis which are themselves at right angles to each other. The intersection of these three axes is termed the "view volume". The sampled gas is directed in a very narrow stream through the view volume which in turn is irradiated with ultra-violet light from a compact source mercury lamp. Lenses in the excitation beam serve to focus the light from the light source onto the view volume.

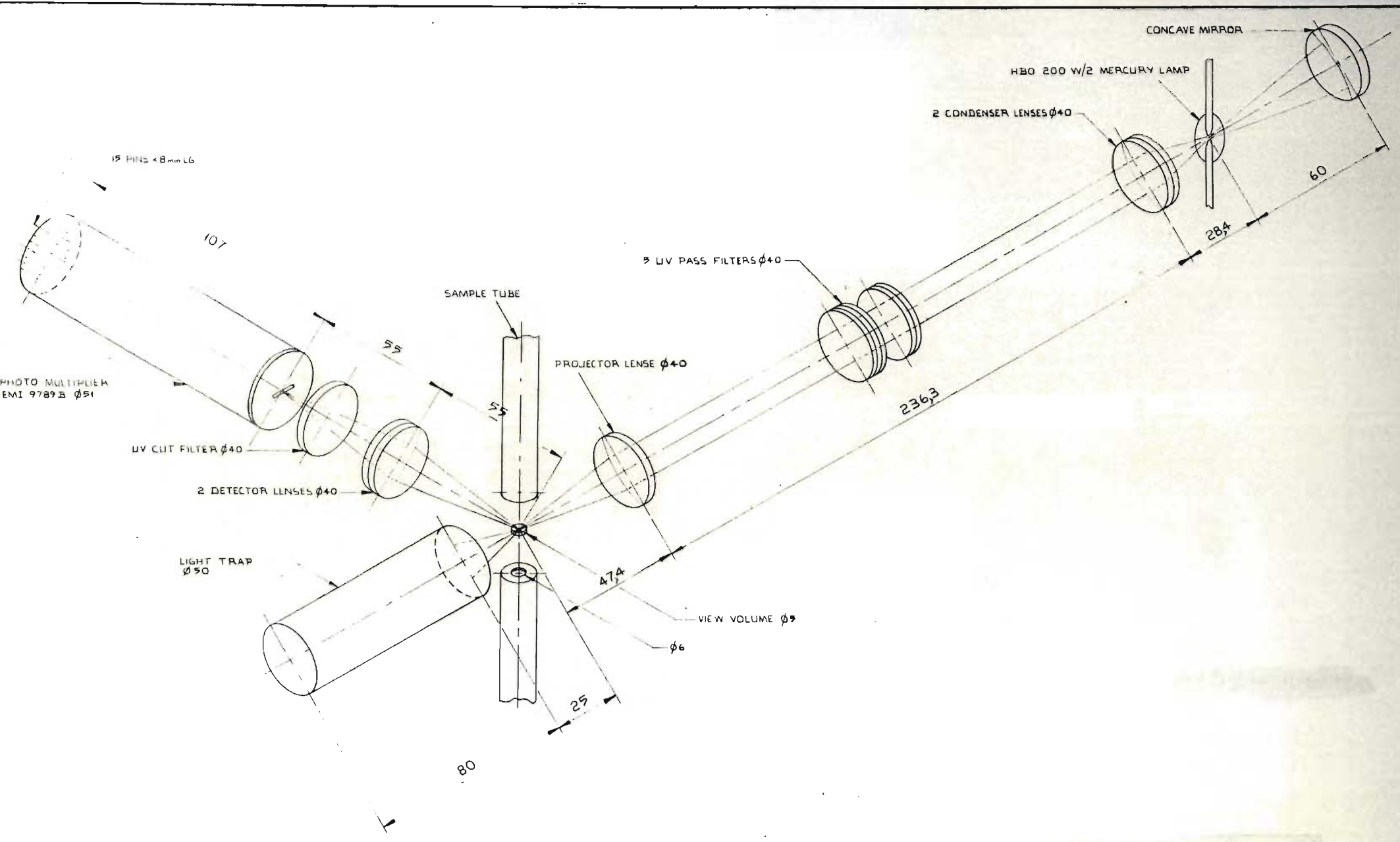

Figure 3.1: Isometric view of the optical layout of the fluorescent particle counter

At right angles to the excitation beam lenses focus the fluorescence which occurs when fluorescent particles pass through the view volume onto the photo-cathode of a photomultiplier. A slit in the detection system ensures that the photomultiplier sees only a thin slice of the view volume. As the particles are carried smoothly through the view volume with the sampled stream of air their passage gives rise to a pulse of light at the photo-cathode which is converted to a pulse of electricity, and which in turn is amplified, counted and recorded electronically. Clean pulses of light only occur provided particles do not stick to any object within the view volume and in order to ensure that this is the case the tube through which the sample is drawn is broken into two parts as shown in figure 3.1. Thus when passing through the view volume the sampled stream of air must cross a discrete gap making it impossible for any particles to remain in the view volume giving rise to a high background signal level.

The fluorescent particle counter was designed to sample air at the rate of 12 l / min. With a diameter of the stream of sampled air of about 5 mm the residence time of a particle in the excitation zone is about 1 ms which is well in excess of the response time of solid phosphors reported to be in the region of 10^{-8} to 10^{-5} seconds (36). Typical pulses from the photomultiplier had a period of about 1 ms for which electronic processing was a fairly straightforward matter.

3.3 The Optical Systems

3.3.1 The Excitation System

Figure 3.1, an isometric view of the fluorescent particle counter, shows the excitation system comprising a compact source mercury arc lamp, condenser, filters to isolate the 365 nm line of the mercury spectrum and a projector lens. The mercury lamp was the HBO 200 W/2 super pressure mercury lamp from Osram chosen for this

application chiefly for its very intense radiation at 365 nm, as shown by the typical spectrum for this lamp figure 3.2. The mercury arc in this lamp is very compact measuring typically 2,2 x 1,2mm. and may therefore be regarded as approximating a point source. With this approximation it becomes permissable to use simple optics design formulae and also simple convex lenses in the lens train.

Although a smaller lamp having a more powerful arc was available from the same Supplier the HBO 200W/2 was chosen for this application for its greater power. It is possible that an improved optical design may have permitted the use of the smaller lamp leading consequently to a lower heat dissipation, smaller lamp housing and smaller power supply, however such a detailed investigation was considered beyond the scope of the present study.

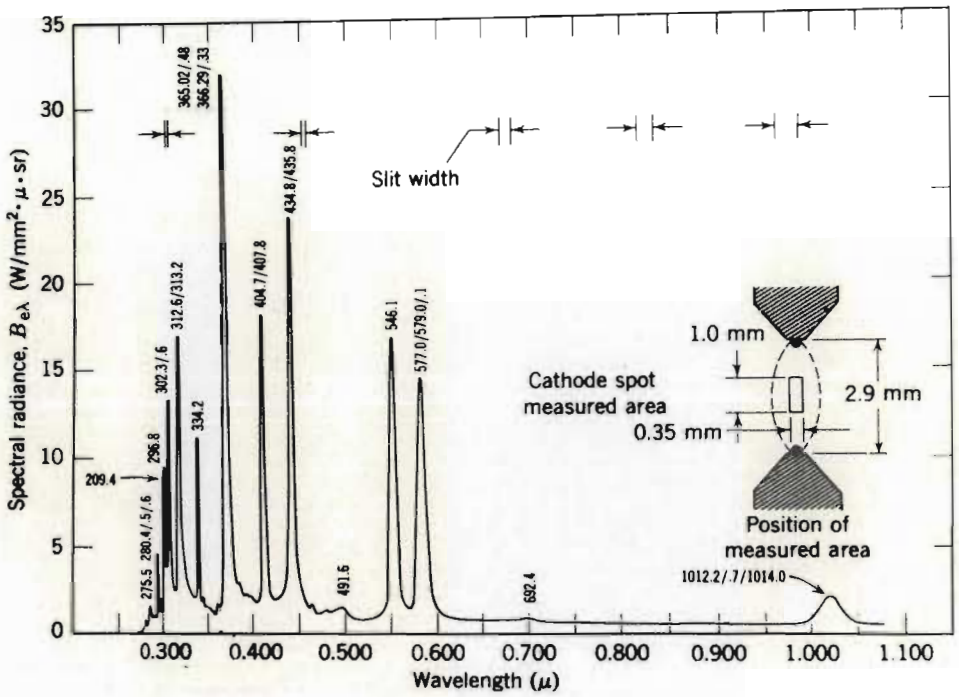

Figure 3.2: Spectral radiance of a 200W high-pressure mercury arc lamp. From Levi (33)

The convex lenses used in the excitation train were all stock lenses made of quartz, for improved transmission of ultra-violet light, with dimensions of 40mm diameter and 50 mm focal length. With these lenses there are three different arrangements which can be used to obtain a uniformly illuminated field, or view volume, and these are illustrated in figure 3.3.

If light rays are traced from the light source when placed at the focal point of a condenser it becomes apparent that at the opposite focal plane there is a zone of uniform illumination. In figure 3.3 (b) an aperture stop is located at this focal plane and an image of this aperture is focussed by the projector lens onto the view volume. Theoretically the illumination at the view volume should be completely uniform however in practise it proved impossible to count more than about 10% of the particles passing through the view volume with this arrangement.

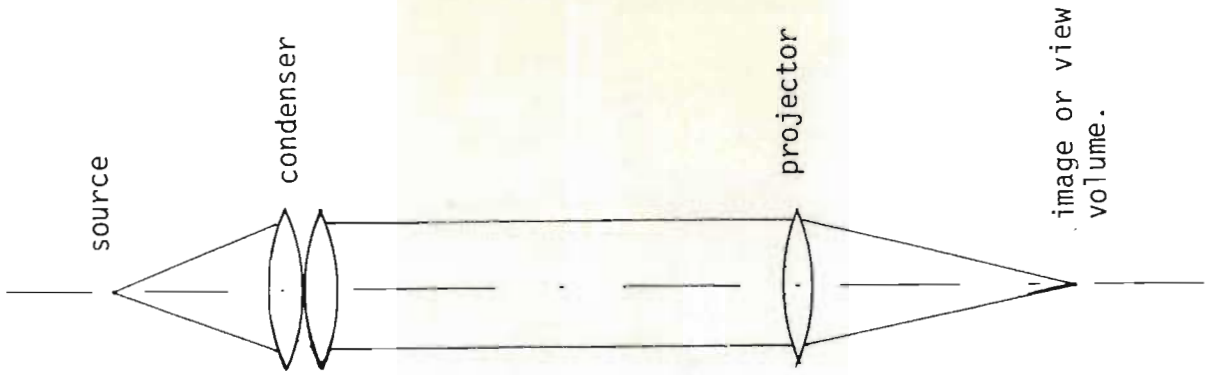

a) Arc image used to illuminate the view volume.

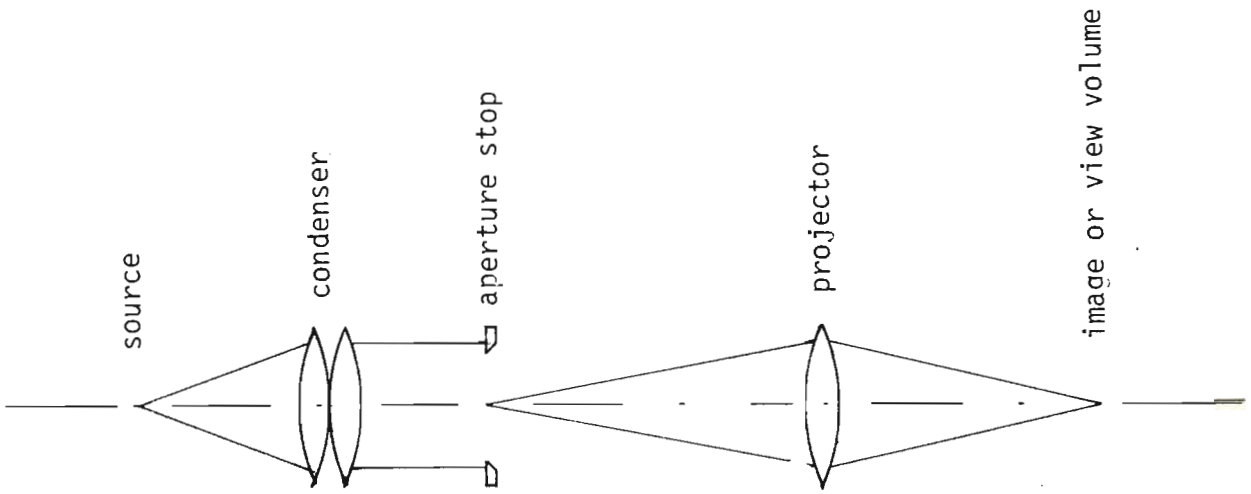

b) Uniformly illuminated view volume.

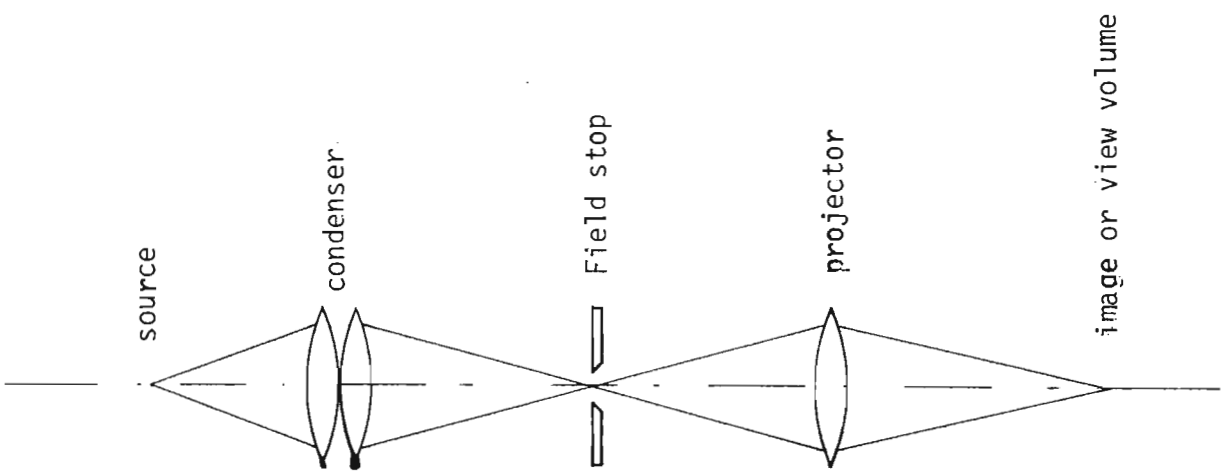

c) Shaped arc image used to illuminate the view volume.

Figure 3.3: Various optical arrangements which were investigated for the excitation system

To provide better shaping of the light beam and to eliminate scattered light it is possible to focus a real image of the light source at some finite point not far from the condenser and to surround this image with a field stop as shown in figure 3.3 (c). A real image of the field stop is then focussed at the view volume. Whilst this configuration was an improvement on figure 3.3 (b) it did not enable the detector to "see" more than about 30% of the particles passing through the view volume.

In figure 3.3 (a) the condenser is used to focus an image of the light-source at infinity and the projector lens is used to focus a real image of the light source at the view volume. A problem with this arrangement is the intensity of the light source which is not uniform over the cross-section as shown in figure 3.4 and this non-uniform distribution is projected on the view volume. However this problem was partially overcome by making the image of the light source slightly out of focus at the view volume. Although somewhat less

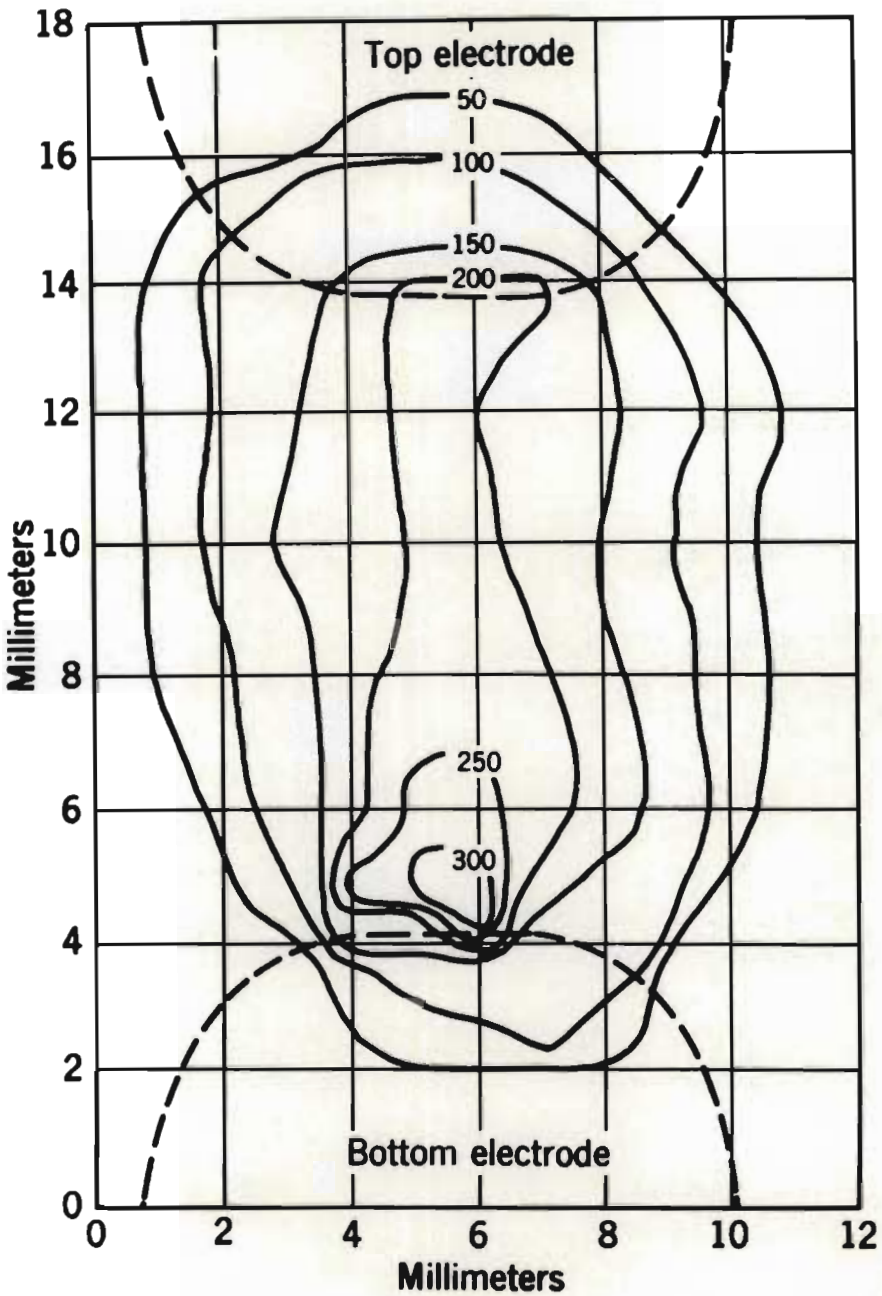

Figure 3.4: Luminance distribution of a 2500W short arc mercury lamp. Contours are in candles/mm^2. From Levi (33)

sophisticated than the other configurations this configuration proved in practise to give the best results, enabling the detector to "see" in excess of 60% of the particles passing through the view volume.

A measure of how much better the lens configuration in figure 3.3 (a) proved in practise over that in figure 3.3 (c) can be obtained by plotting the back-ground count rate as a function of the counting efficiency for each configuration and for various levels of gain in the detection system. Increasing the gain in the detector enables more particles to be "seen" but at the cost of a greater background counting rate. Although the actual values of gain for each point have been omitted from figure 3.5 the general trend can be clearly seen. The horizontal spread in the band of points representing the lens configuration 3.3 (a) can be ascribed to

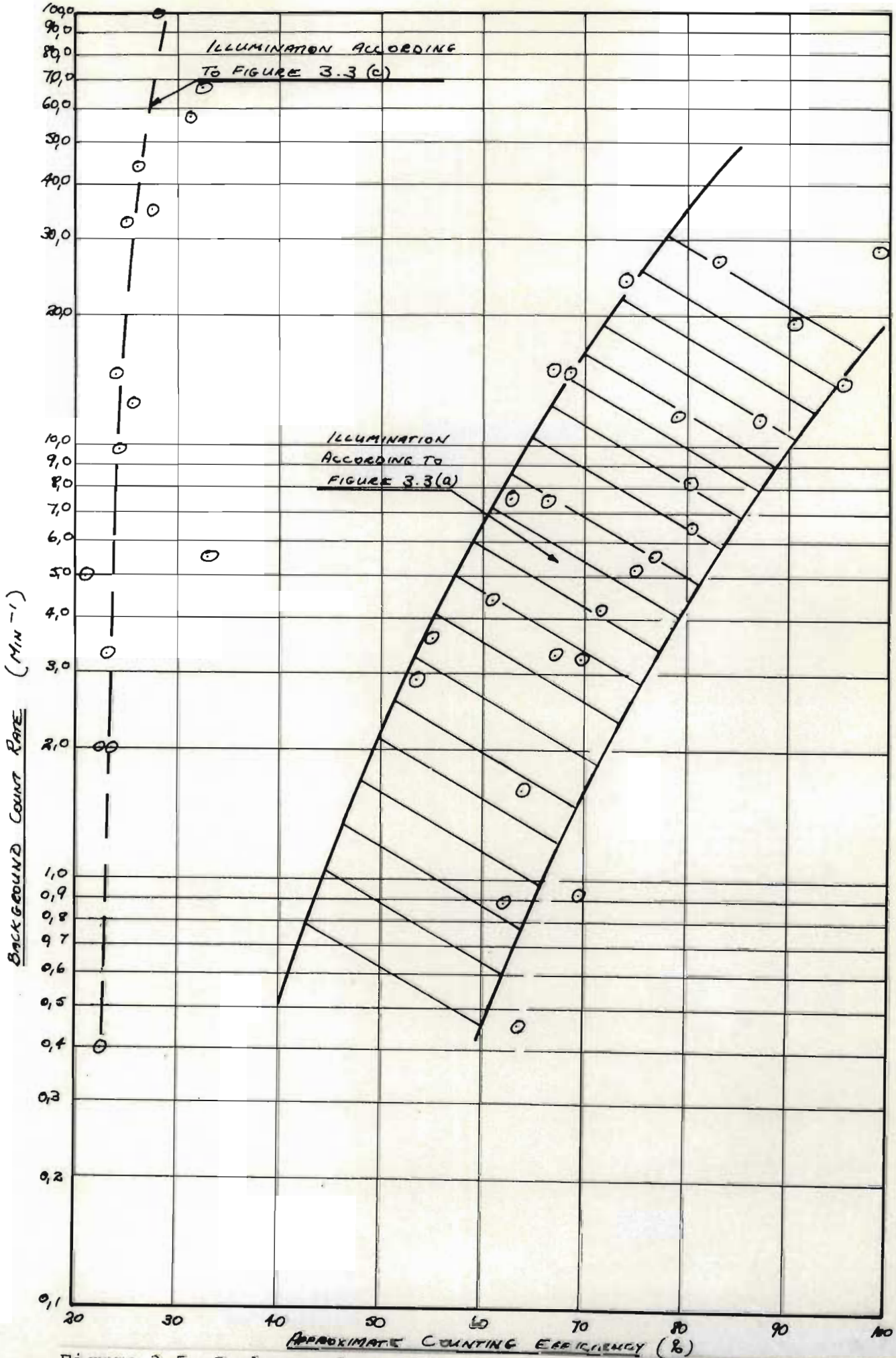

Figure 3.5: Background counting rate [illegible]

minor improvements which were made to the system in order to reduce the background counting rate.

The filter set used in the excitation train was one recommended for use in UV fluorescence microscopy by the vendor, Wild, and comprised the following filters in order from nearest the light source :

2 off KG1 heat absorbing filters
2 off UG5 U V pass filters
1 off BG38 red absorbing filter

The transmittance curves for each of these filters is plotted on common axes in figure 3.6 from which the narrow pass band for the combination around 365 nm can be clearly seen. Although the excitation system as described is unsophisticated it performed well and further development in this area was not pursued.

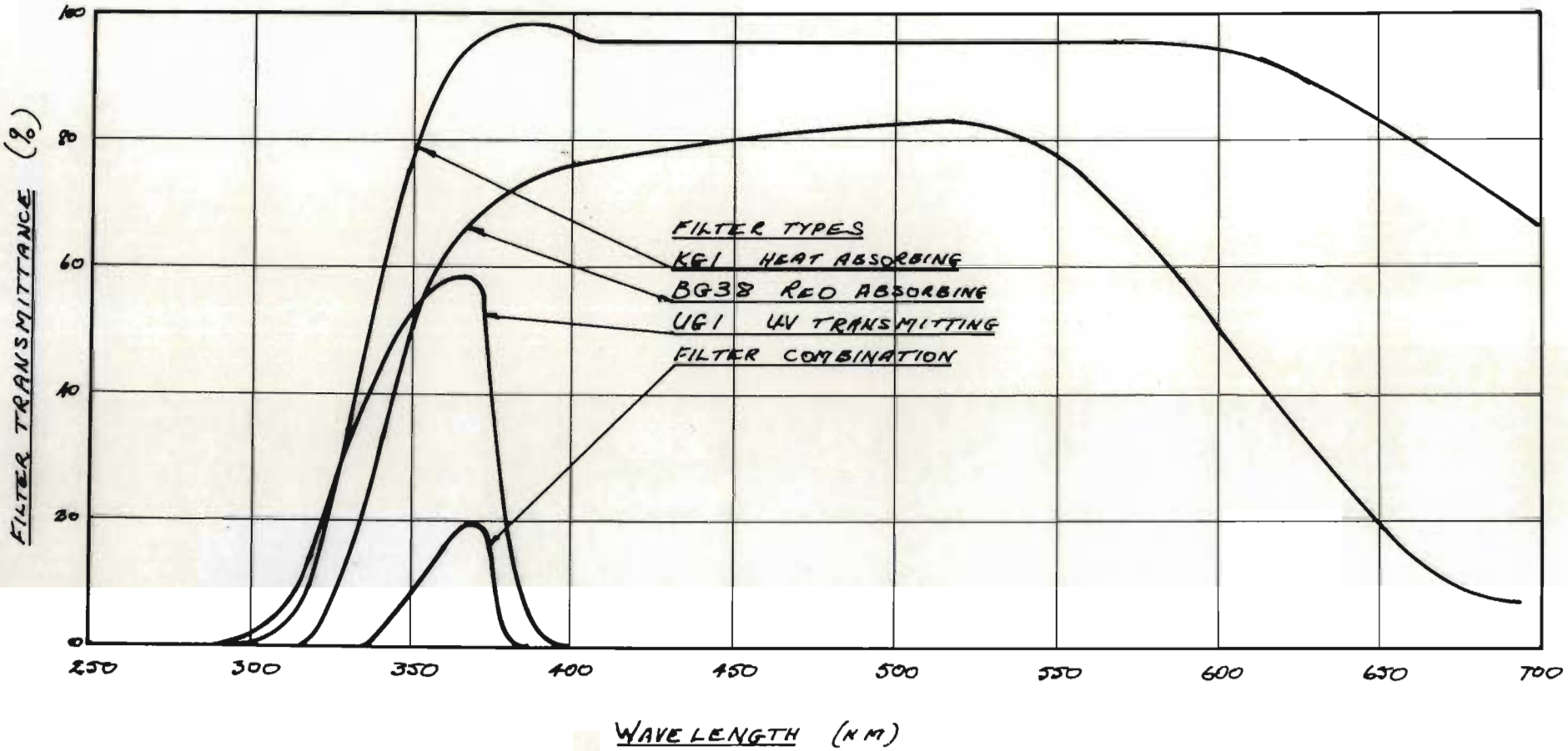

Figure 3.6: Transmittance of the filters used in the excitation system

3.3.2 The Detection System

In figure 3.1 the detection system is shown to comprise a collector lens, a U.V. cut filter, a slit and a photo-multiplier. The photomultiplier, an EMI 9789 B with bialkali photocathode, was chosen in this application for its high gain and low dark current (16). A problem with photomultipliers is their rather higher sensitivity to the blue end rather than to the red end of the spectrum and this is clearly shown by the photo-cathode response curve shown in figure 3.7. In this application where the light to be detected was yellow a photo-cathode with an extended red response might have been the better choice but these tubes are usually characterised by a higher dark current.

In an effort to limit the amount of reflected or stray U V light reaching the photo-multiplier, a U V filter the GG 13c was

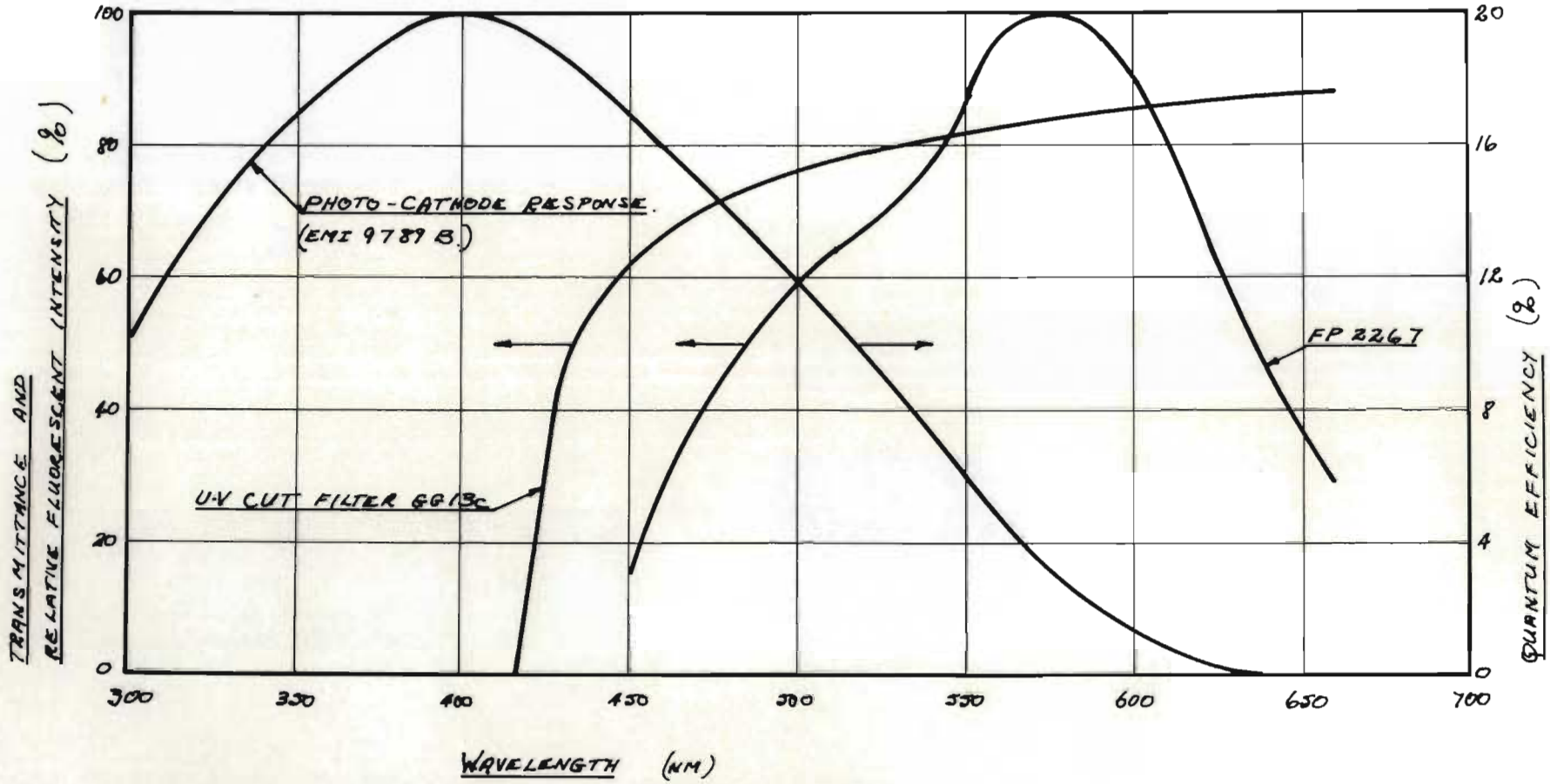

Figure 3.7: Spectrum of fluorescence for FP2267, transmittance of the filter and response of the photocathode used in the detection system

included in the detection system. This completed the set of filters recommended by the vendor, Wild, for U V fluorescence microscopy. The transmittance curve for this filter is also shown in figure 3.7 along with the fluorescent spectrum of FP 2267.

The sensitivity of the system to stray U V light is very evident from figure 3.7. Only a small part of the photomultiplier response curve is used and because of the greater response to U V light even very low levels of U V may give rise to signals of sufficient magnitude to interfere with the detection of yellow fluorescent particles.

A slit, of 1 mm width,was placed in front of the photocathode,as shown in figure 3.1, in order to limit its field of view and hence to limit the amount of background light reaching the photo-cathode. This slit was located in such a way that its

image in object space intersected the excitation beam and sample stream axes, in this way defining a small exclusive rectangular "view volume" in which fluorescing particles are "seen" by the photomultiplier. The detector lenses were stock convex lenses with diameter of 40 mm and focal length of 5o mm, made of glass, there being no need to ensure the maximum transmittance of U V light.

The voltage applied to the anode of the photomultiplier was fixed throughout the work at 1000 volts, giving the tube an overall sensitivity of 328 amps/lumen. Taking into account the design of the detector head as described in this chapter the detectable luminous flux at the photocathode from single fluorescent particles ranged from 300 to 17,000 picolumens giving rise to signal levels of between 0,1 and 6 volts.

3.4 The Construction of the Fluorescent Particle Counter (FPC)

In practise the view volume was enclosed in a light-tight box known as the sample chamber as shown in the assembly drawing figure 3.8. In view of the need to locate the intersection of three mutually perpendicular axes at some pre-assigned location within the sample chamber it was found necessary to machine and bore the box to a fairly high degree of precision. The completed instrument is shown in the two views figure 3.9 (a) and (b). A number of practical problems were encountered during the commissioning of the FPC and these and their solutions will be discussed in turn.

3.4.1 Air Circulation

If a stream of air leaves the end of a tube, as it does when crossing the discrete gap in the sample tube arrangement shown in figure 3.8, the air behaves as a free jet

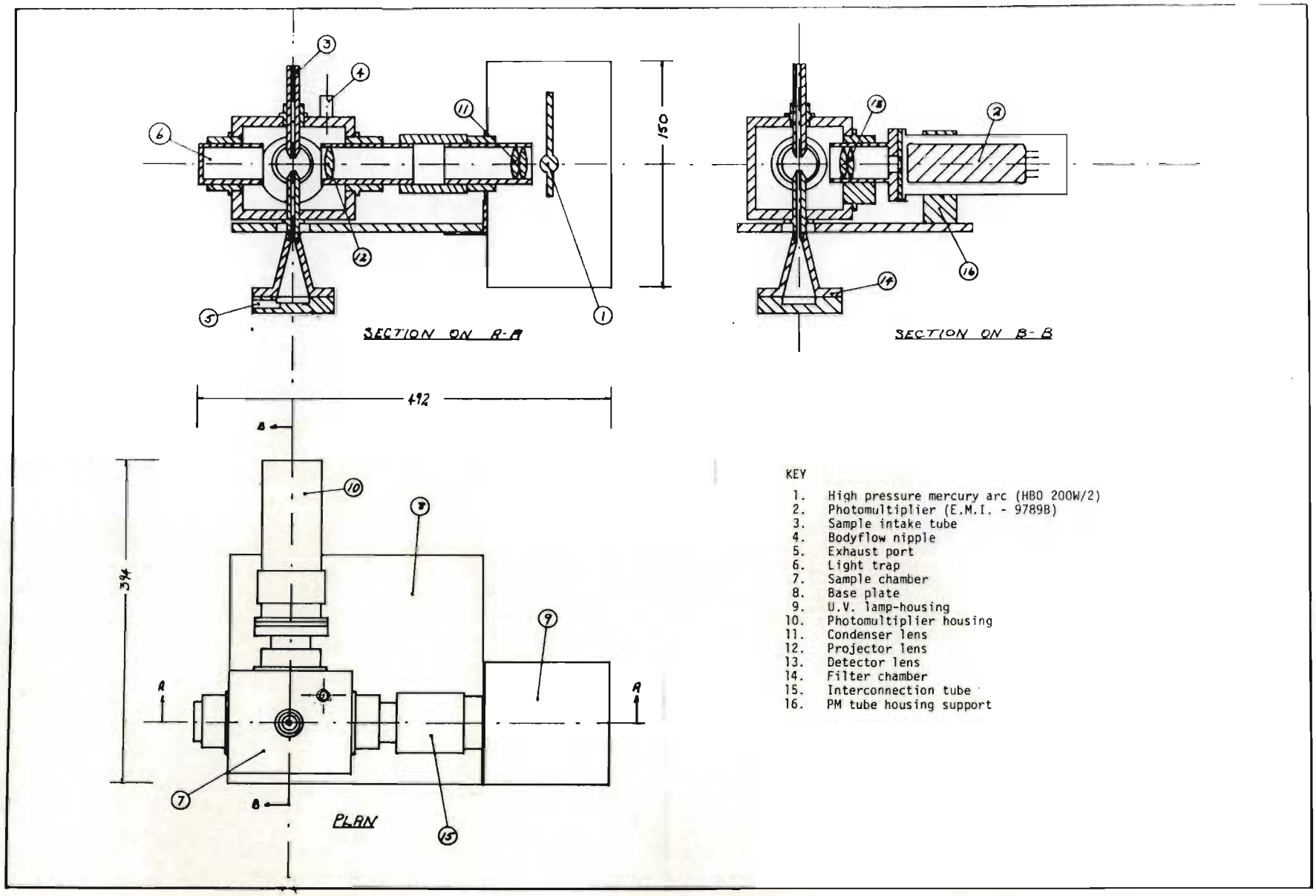

Figure 3.8: General arrangement drawing of the fluorescent particle counter

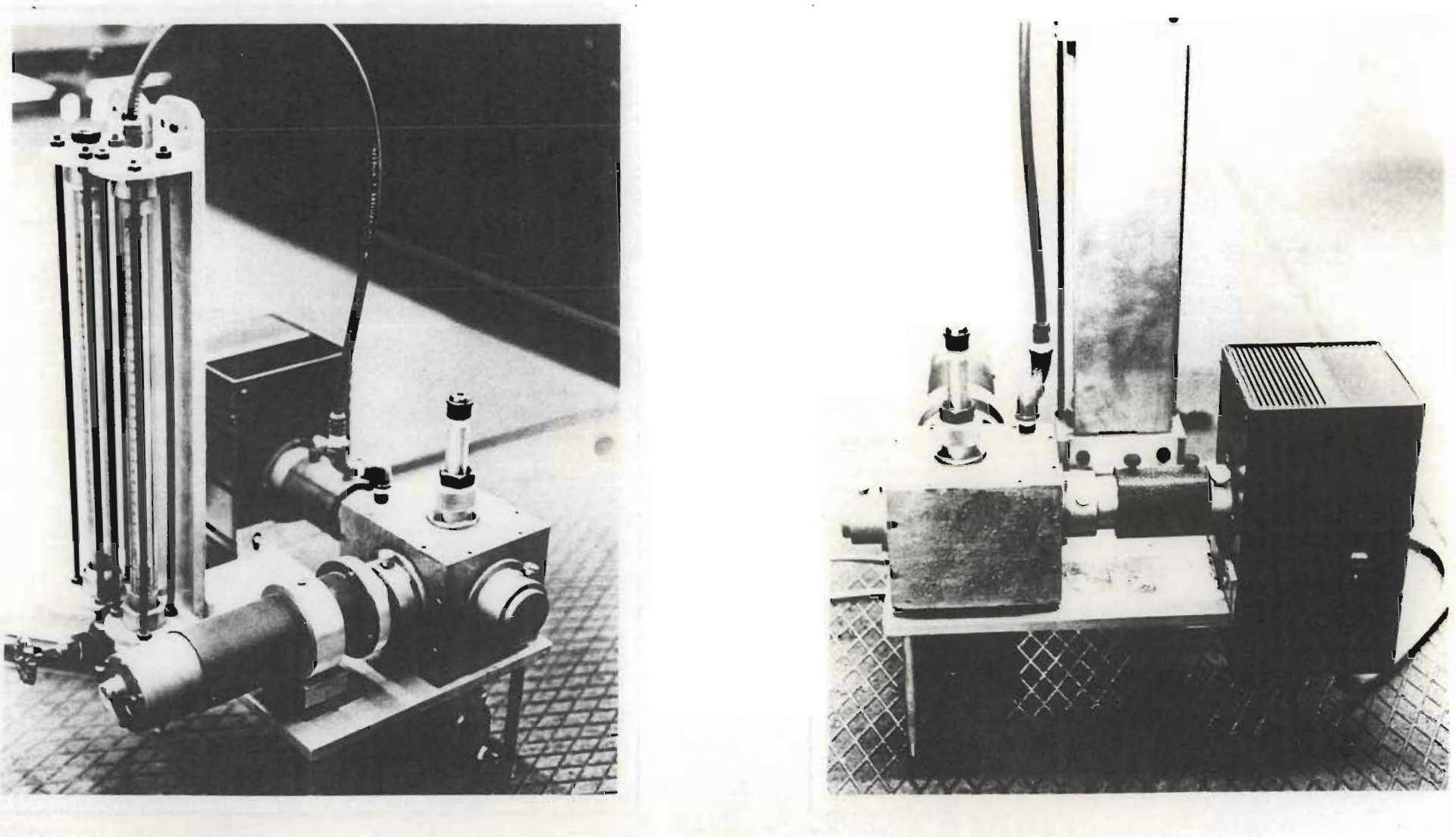

Figure 3.9: Two views of the fluorescent particle counter assembled

and expands with a core angle of about 20^{o}. To circumvent this problem Forestall and Shapiro (18) show that the sample stream or primary jet can be sheathed in a coaxial secondary jet of air. Provided that the velocity of primary and secondary jets is equal the primary jet should not expand at all. This was the approach used by Martens and Keller (38) in their Bosch and Lomb dust counter. However a concentric tube arrangement was found to be difficult to fabricate and so was discarded in favour of the simpler arrangement shown in figure 3.8. In this arrangement the sampled stream of air leaves a small bore sample pipe, passes the discrete gap and enters the lower pipe which has a larger bore. The sample stream is prevented from diverging by drawing additional air into the lower pipe. The additional air was supplied to the sample chamber via a separate nozzle. The bore of the lower tube was specified in such a way as to make the velocity

approximately equal to that in the sample intake tube.

With the need not only to draw a sample of air but also to supply additional or secondary clean air to the sample chamber the air circuit designed is shown in figure 3.10. The sampled air is drawn by means of a vacuum pump through the view volume and then through a millipore filter to collect the fluorescent pigment. The vacuum pump discharges through a second filter, to remove the fine oil spray generated by the pump, and a portion of the discharged air is recycled to the sample chamber. Rotameters were installed on the discharge and recycle lines to make it possible to adjust the primary to secondary air flow ratio. Primary and secondary air flow rates of 12 and 20 litres per minute respectively were found to be adequate in this work.

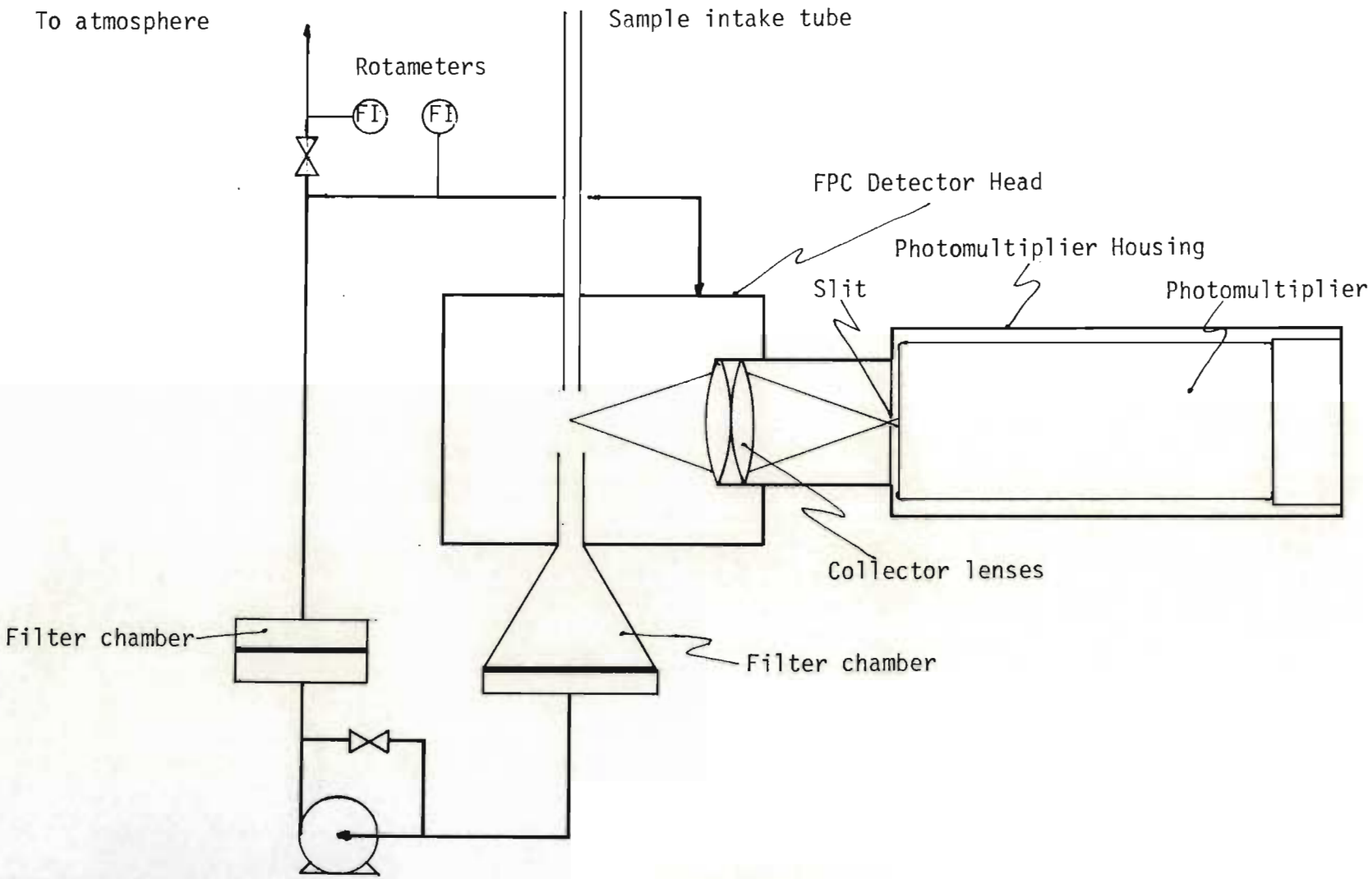

Figure 3.10: Flowsheet of the air circulation system for the fluorescent particle counter

The filter holder mounted directly beneath the sample chamber was designed for use with 47mm millipore filters. By examining these filters microscopically under U V irradiation it was possible to count the fluorescent particles which had passed through the view volume and thus calibrate and check on the performance of the counter.

3.4.2. Reduction of Stray Light

In an instrument as sensitive as the FPC it was of paramount importance to reduce as far as possible the incidence of stray light within the sample chamber. The greatest reduction in stray light was obtained by coating all the internal parts of the sample chamber with soot from burning cotton waste soaked with benzene. In addition reflection of light from the sample tube itself was reduced by cutting a bevel onto the

inlet and outlet tubes on either side of the view volume as shown on figure 3.8. By incorporating a filter in the air line following the vacuum pump the fine oil spray generated by the pump was removed from the air being recycled to the sample chamber. Although the entrance to the sample tube is shown as squared off, in practice this was found to be unsatisfactory particularly at mid-day with the sun virtually overhead. For the field trials a sampling tube resembling a pitot tube (with a right angle bend) was therefore used. Loss of material by deposition within this sample tube was calculated (75) to be less than 5% for particles of 3mm diameter and this was not regarded as significant.

3.4.3 Dissipation of Heat

A considerable amount of heat is generated by the U V lamp and it is therefore important to ensure that the temperature of the photomultiplier housing does not exceed 60^{o}C in order to avoid irreversibly damaging the photocathode. To protect the photomultiplier therefore the sleeve connecting the U V lamp with the sample chamber was machined from an insulating material and the photomultiplier housing itself was separated from the base plate by means of a wooden block.

3.5 Automatic Processing of Data

Clearly the fluorescent particle counter counts events i.e. the passage of one or more fluorescent particles, and from this information the concentration can be calculated. In the first instance, though, the data processing equipment

must be capable of distinguishing and counting the signals associated with the desired events and of storing this information in a retrievable form. The data storage requirements are also fairly difficult in that the instrument was designed to operate for long periods of time (in excess of eight hours) unattended.

The data processing requirements of the FPC parallel in some measure the measurement of radioactivity, which is also an event counting operation. It seemed attractive therefore to try to use the same type of equipment for the FPC as it is cheap and readily available. However radioactive events are characterised by pulses with a very steep leading edge (rise times of less than 1 μs) followed by an exponential decay, and the associated counting equipment is designed to count only pulses of this shape. The FPC, on the other hand, produced pulses roughly sinusoidal in shape with a pulse width of about 1ms, with the result that it became necessary to develop a new

data processing system.

The equipment required to support the FPC is shown in figure 3.11 and comprises the vacuum pump, a high voltage power supply to the photomultiplier and a direct current power supply to the mercury lamp. The signal from the photomultiplier, essentially a current signal, is converted to a voltage signal in a buffer amplifier before being recorded and stored by the Fluorescent Particle Analyser and tape recorder respectively. Decoding the data involved replaying the tape and feeding the signal via a decoder to the event counter terminals of a CDC 1700 computer as shown in figure 3.12. In the field all the electrical and electronic equipment, and vacuum pump was housed in a wooden box shown in figure 3.13 which afforded some protection against the weather. The FPC was mounted on top of the same box in order to keep the supply leads and piping as short as possible.

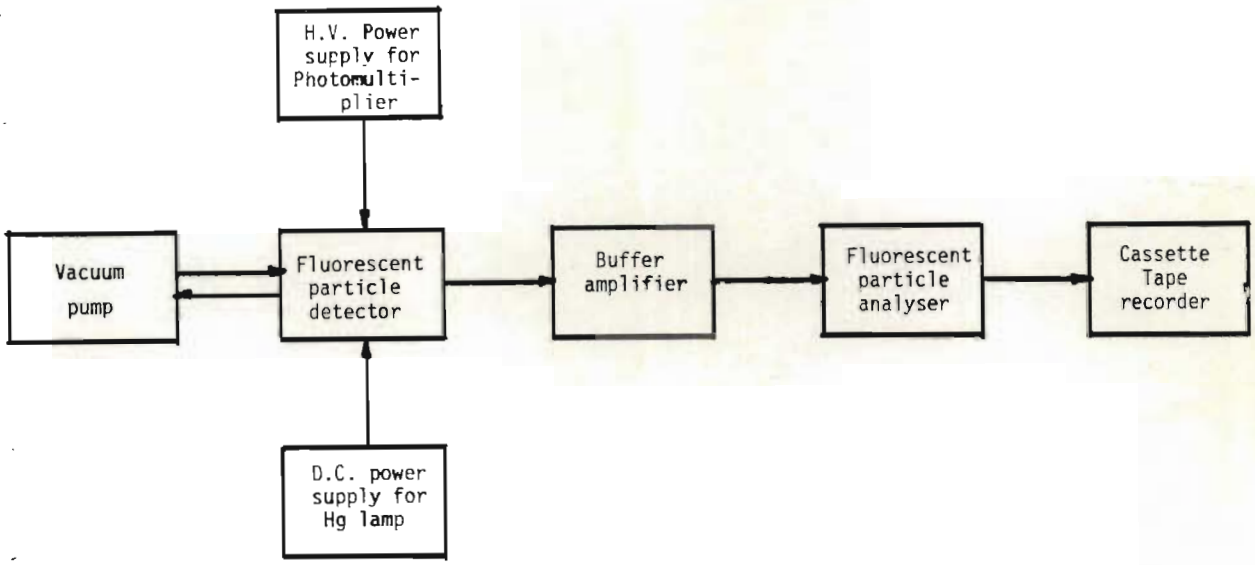

Figure 3.11: Block diagram of the fluorescent particle counter and supporting equipment

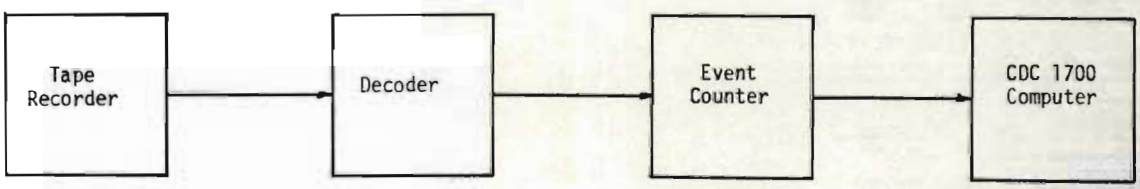

Figure 3.12: Block diagram of the equipment required to recover the data recorded by the fluorescent particle counter

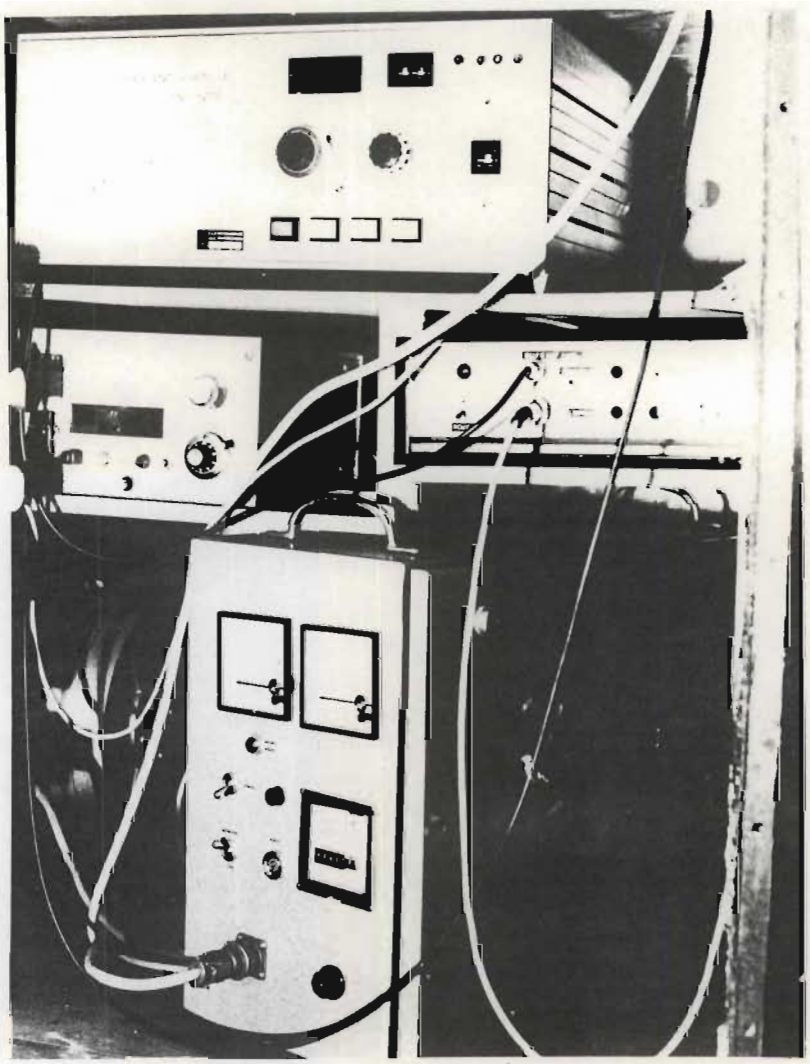

Figure 3.13: View of the supporting equipment for the fluorescent particle counter assembled in the instrument shelter

In the next three sections the method of processing the signal from the photomultiplier and the method of storing and retrieving the data are discussed in more detail.

3.5.1 The Photomultiplier

A photomultiplier is an extremely sensitive photon counting device and incorporates a photocathode and a very high gain amplifier. The photocathode on receiving photons of light emits electrons, in the ratio of about one electron per ten photons of light received. The electrons emitted from the photocathode are directed to the first dynode which is an amplifying device and emits a number of electrons for each electron it receives. The electrons emitted by the first dynode are directed to the second dynode which amplifies the signal still further. This amplification process is continued down a string of dynodes which for the photomultiplier used in this work

numbered nine. The electrons emitted by the last dynode are directed to the anode where the signal can then be measured as a current, or converted to a voltage signal by passing the current through a resistor. In this way gains in excess of 1000 can be achieved and single photons of light can be converted to measurable signal levels.

In order to function correctly adjacent dynodes must differ in electrical potential. To achieve this the dynodes are fitted with a string of resistors in the form of a potential divider and these are located external to the photomultiplier.

In this way adjacent dynodes are operated at a fixed potential difference which for a linear string is the same for all pairs of dynodes throughout the string, and in addition the potential increases progressively down the string from the photocathode to the anode.

The amplification of the photomultiplier is a direct function of the potential difference between adjacent dynodes and therefore of the overall potential difference between the photocathode and the anode. For the photomultiplier used in this work a potential difference of 1000 volts was applied between anode and photocathode giving an overall gain of about 500.

The circuit used to operate the photomultiplier is included in appendix A.3.

3.5.2 The Buffer Amplifier

Photomultipliers are inherently noisy devices owing to the discrete nature of the photon counting process and so a buffer amplifier incorporating some signal smoothing, was found necessary to prevent the larger of the spurious noise pulses from being mistaken for the passage of a fluorescent particle. A number of

different smoothing circuits were tried including second and fourth order filters of various designs (76) without much success. The circuit finally adopted comprised a simple integrator of the form:

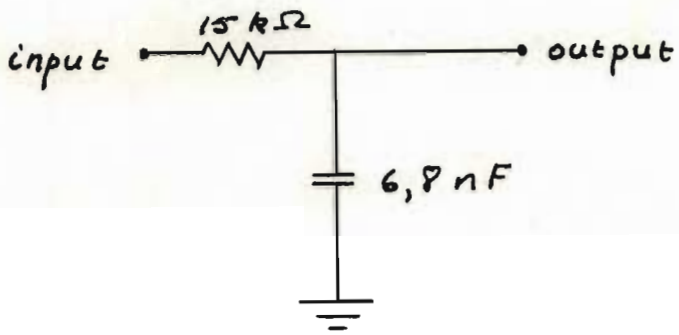

and having a time constant of about 100μs. This circuit effectively smoothed out all the 2 μs noise pulses whilst preserving the 1ms pulses arising from the passage of fluorescent particles. The noisy nature of the signal is clearly shown in figures 3.14 (a) (b) and (c) and the effect of the filter in figure 3.14 (d).

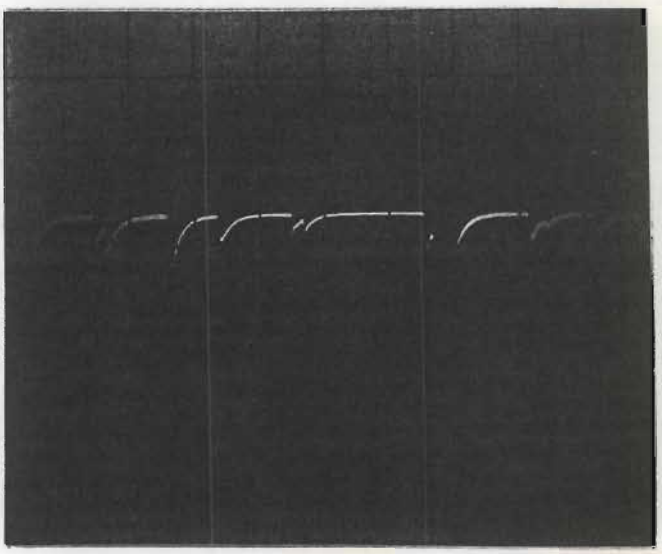

(a): Background noise.
x= 10μs/div; y = 0,2V/div.

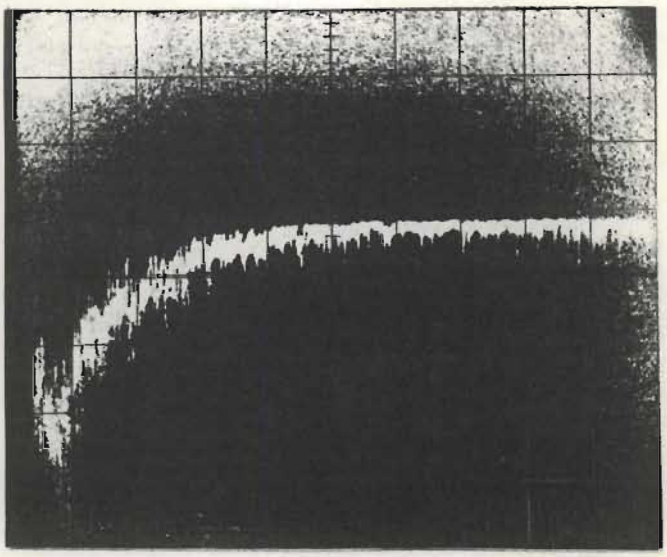

(b): Signal resulting from the passage of a large particle.
x=0,2ms/div; y= 0,5V/div.

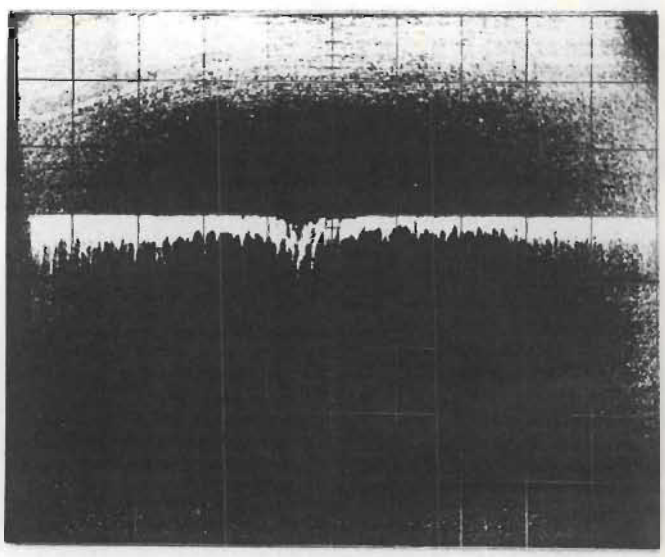

(c): Signal resulting from the passage of a small particle.
x= 0,5ms/div; y= 0,2V/div.

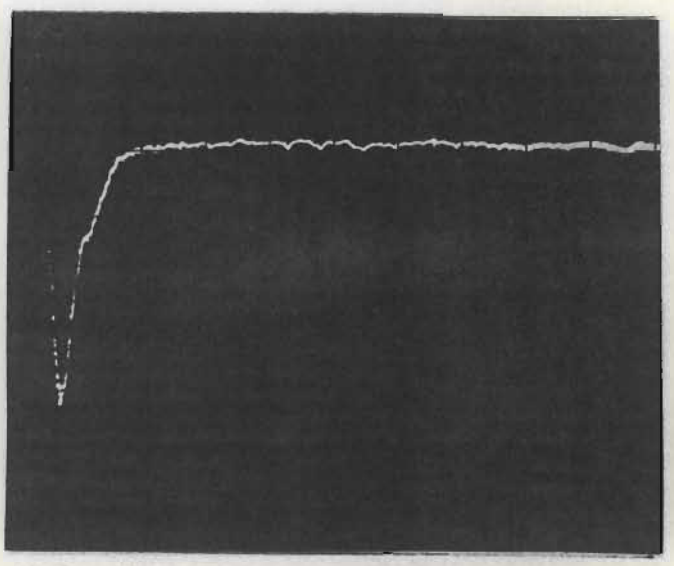

(d): Smoothed signal resulting from the passage of a particle.
x= 1,0ms/div; y= 0,1V/div.

Figure 3.14: Oscillographs of the signal arising from the photomultiplier.

Apart from smoothing the signal the buffer amplifier was also used to invert and amplify the signal and to eliminate the offset introduced by the preceding circuits.

3.5.3 Analysing and Storing the Signal

To analyse and store the signal a Fluorescent Particle Analyser (FPA) was designed and built by the Atomic Energy Board (71) to the author's specifications. Essentially this device counted and measured the height of each pulse in real time and then produced a record suitable for recording on a conventional cassette recorder. In view of the very long periods over which the instrument was expected to operate the FPA also controlled the tape recorder turning it on only when there was information to be recorded.

In concept the FPA comprised two memories each with 41 locations as shown in figure 3.15. The functions of the locations were designated as follows:

- record counter	1 location
- pulse height analyser (PHA)	10 locations
- time discrimination analyser (TDA)	30 locations

Each memory was filled in turn with data for a period of one minute. During each one minute period the alternate memory was read out to the tape recorder and then reset. During each period of one minute the following functions were performed.

a) the record counter was incremented by one.

b) the pulse height analyser comprising ten "windows", separated linearly, measured the height of each incoming pulse and incremented the value

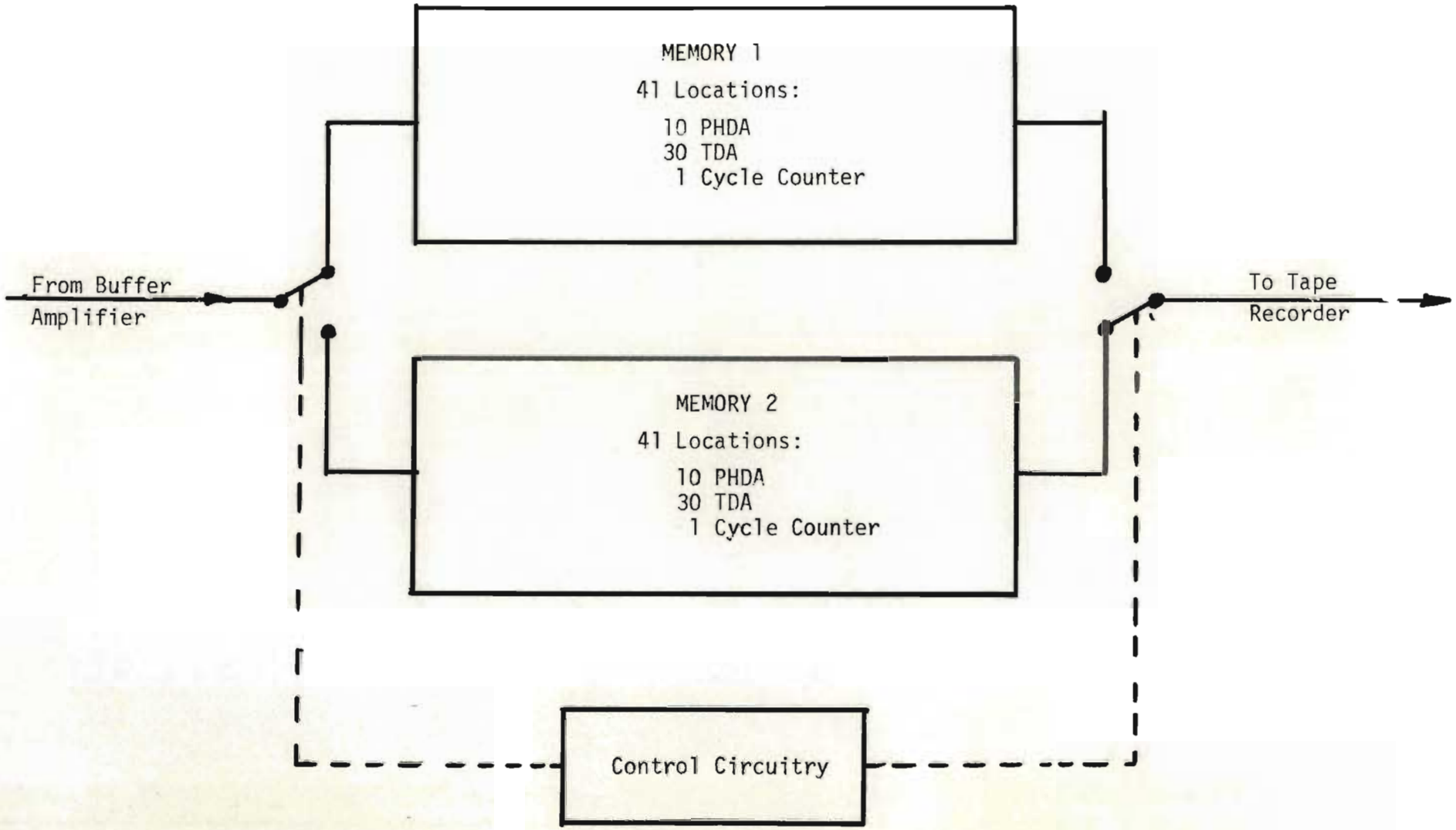

Figure 3.15: Block diagram showing the principle of operation of the fluorescent particle analyser

held in the corresponding location.

c) the time discrimination analyser counted the number of pulses occurring in each succeeding two second interval and stored the totals in successive locations.

To read this information to a conventional tape recorder the contents of each location, termed a "word", was transferred as a rapid sequence of identical pulses, the number of pulses being equal to the value of the word. The layout of the information in each record on tape is shown in figure 3.16 which also shows the difference in spacing between records and between words within a record which made it possible to decode the information. To further assist in decoding the information every location in memory, except for the record counter, was reset to 1 rather than 0 at the end of every cycle. Consequently every word on tape contained at least one pulse resulting in every

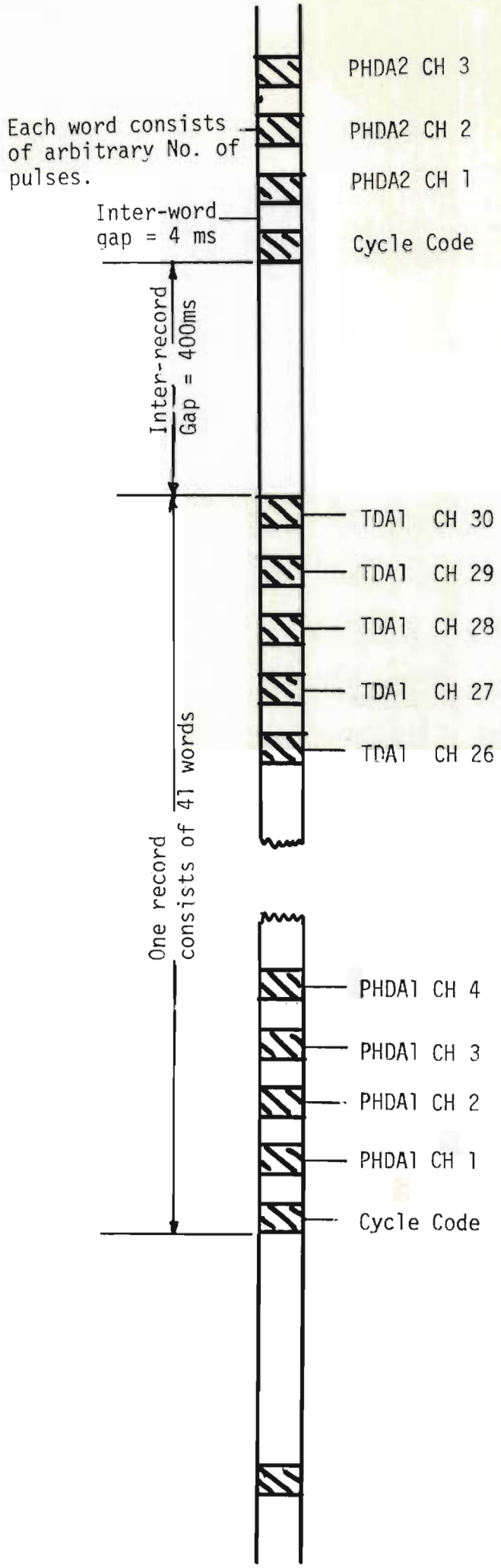

Figure 3.16: Typical section of recorded tape

record containing exactly 41 words.

The most important point about the Fluorescent Particle Analyser was that it effectively compressed real time information by a factor in excess of 10 times. In other words a full memory comprising one minute's information was despatched to tape in less than six seconds. Furthermore the tape recorder was turned on for only as long as there was information to transfer, consequently a blank memory was transferred in probably less than one second. As a result it was possible to use an ordinary 30 minute cassette tape for periods in excess of twelve hours.

3.5.4 Information Retrieval

The CDC 1700 computer housed in the Department of Chemical Engineering at the University of Natal is fitted with

four 8 bit event counters (a device which automatically counts incoming pulses of specified shape). By means of software the counters may be read, reset or pre-loaded at any point in time by the computer. If the counter overflows an interrupt signal is generated to the computer which, if recognised by the software, may be used to initiate a desired sequence of actions.

These event counters therefore presented themselves as an ideal way to decode the information on tape. As mentioned in section 3.5.3 different time delays were incorporated between words and between records when recording on tape. Decoding this information amounted therefore to setting up simple end of word and end of record detectors as shown in figure 3.17 each designed to drive an event counter arranged as an interrupt device. The interrupt signal thus generated enabled the computer to decide on the next course

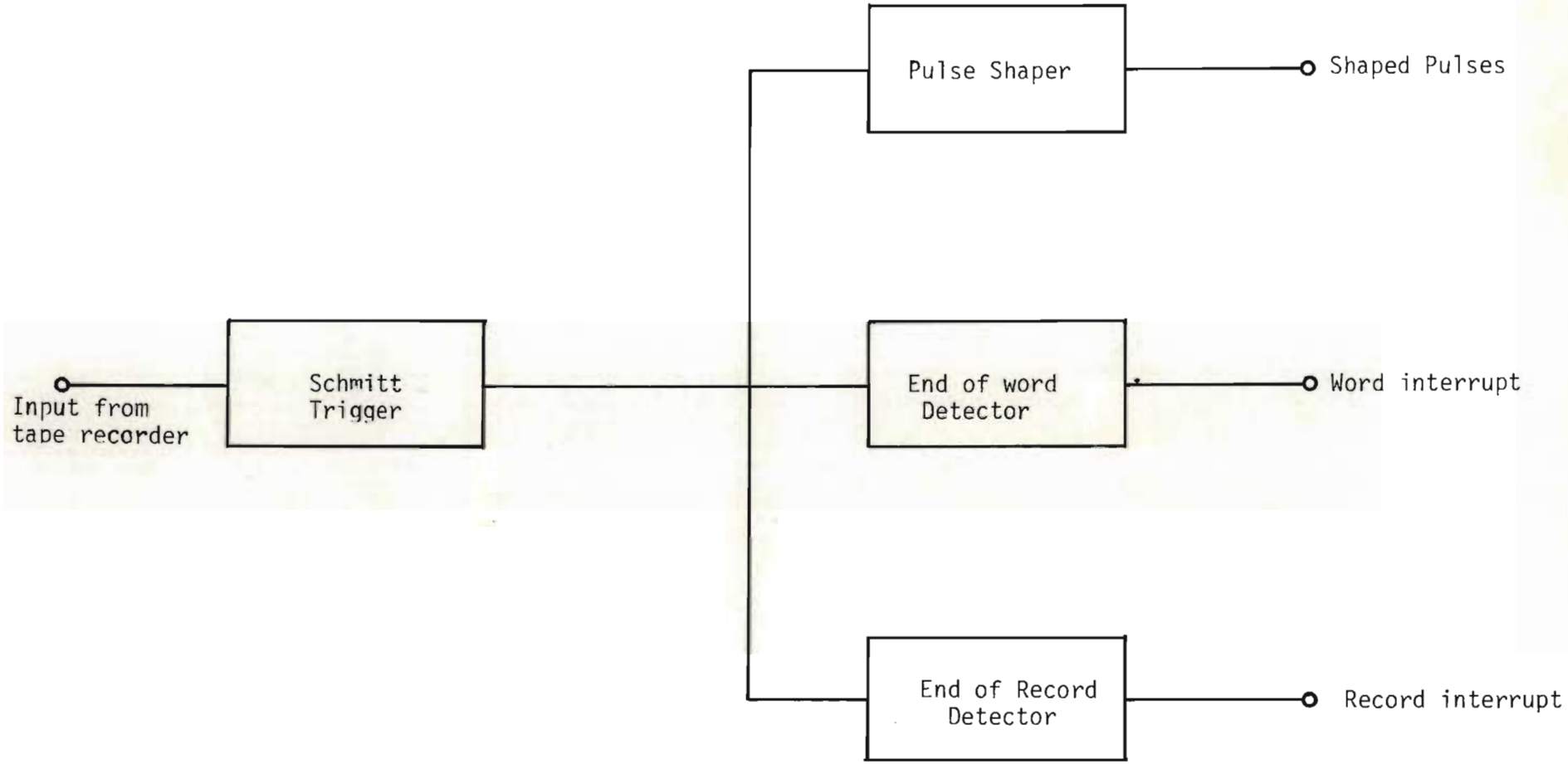

Figure 3.17: Block diagram of the decoder

of action. The value of each word was obtained by feeding its pulses into a third event counter.

Figure 3.18 shows the flow diagram of the software written to handle these signals. Essentially between interrupts pulses are counted by the event counter. On word interrupts the current value held by the event counter is read and the counter is reset to zero. On record interrupts the complete record now held in memory is transferred to a disc file thus completing the retrieval of information.

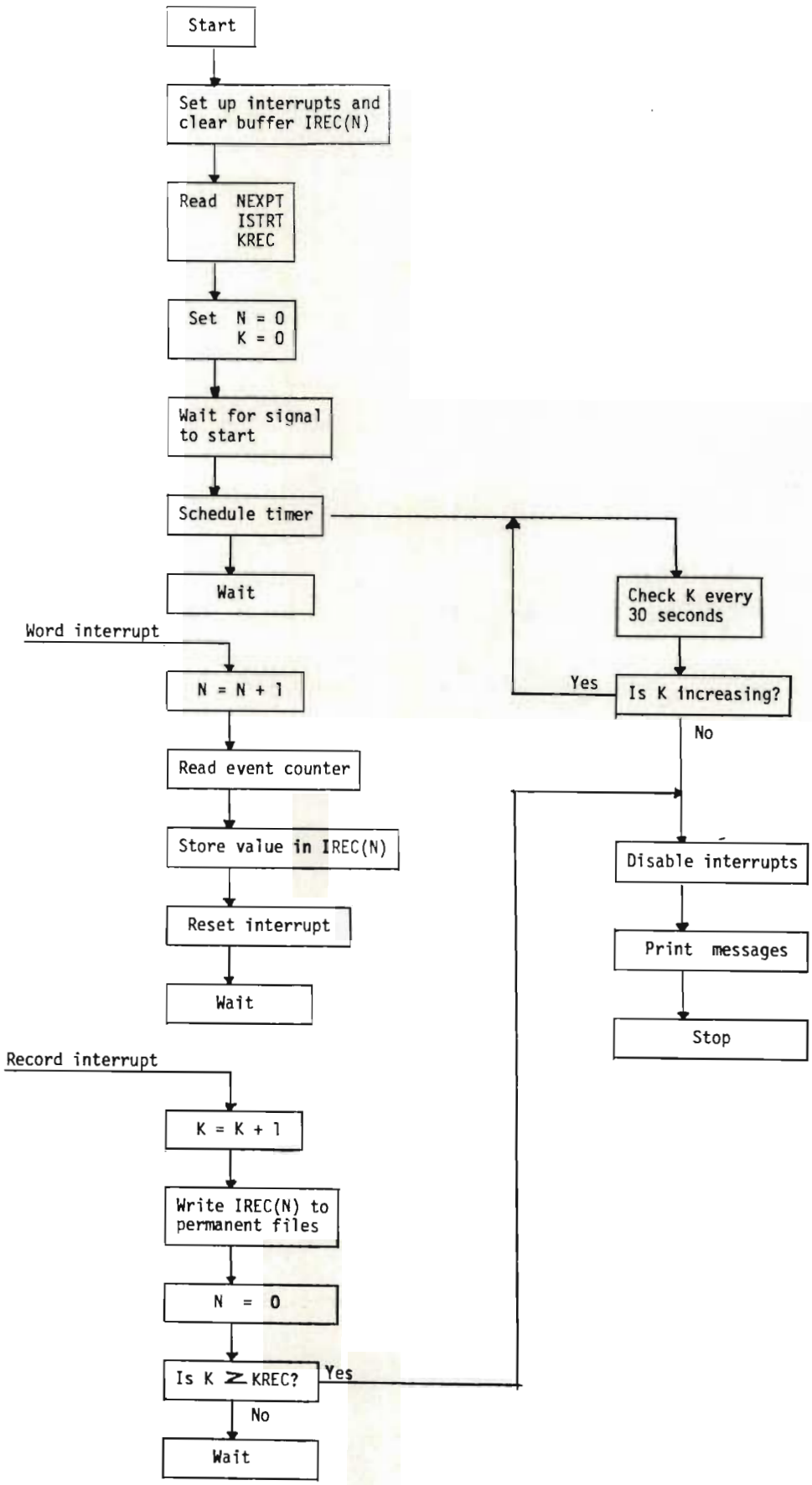

Figure 3.18: Flow diagram for the program DTAPE which was designed to enterpret the signals from the decoder and store the data in a disc file

CHAPTER FOUR: LABORATORY AND FIELD CHARACTERISATION OF THE FLUORESCENT PARTICLE COUNTER

4.1 Introduction

In order to investigate the performance of the fluorescent particle counter and to obtain quantitative data about its efficiency of counting it was necessary to sample the air from a controlled enviroment containing a known concentration of fluorescent pigment. Initially the method chosen for establishing such a controlled enviroment was to enclose and isolate a large volume of air either in a room or in a prefabricated structure and then inject into it a known mass of fluorescent pigment. In practise however this scheme did not prove to be effective for two main reasons :

1) For an enclosed volume of $2m^3$ the quantity of pigment required to generate a suitable aerosol was minute.

2) The aerosol thus generated persisted for a period very much shorter than expected, probably due to electostatic precipitation of the particles onto the walls of the enclosure.

A different scheme for the generation of an aerosol was therefore devised and this consisted of spraying a slurry of the pigment into the entrance of a long pipe through which a large volume of air was continuously drawn. The air was then sampled from the pipe at a point sufficiently far from the entrance for the slurry to have completely evaporated. The second scheme turned out to have a number of advantages over the former scheme and made it possible to :

1) Generate a reliable and reproducible aerosol for as long as it was required.

2) Estimate accurately the number concentration of particles per unit weight of pigment.

3) Calibrate the fluorescent particle counter and test its dynamic response.

4) Test the performance of the aerosol generation equipment which would be used in field trials.

After calibrating the fluorescent particle counter in the laboratory it was then tested in a field trial under the conditions for which it was designed. Although the instrument was originally intended for use over distances in excess of 10km the logistics and organisation required for atmospheric dispersion experiments of this magnitude are formidable. A field test on a very much reduced scale was therefore carried out and is reported. The data obtained from the test was used to estimate the atmospheric dispersion parameters which were then compared with data published by other workers. The field

test has served to :

a) Highlight the usefulness of real-time measurements of atmospheric dispersion.

b) Provide useful experience in the set-up and operation of the equipment.

c) Provide experience in the analysis of the data accumulated.

The site chosen for the field test was the top of a large submerged reservoir near the Dept. of Chemical Engineering building. Although this could not be regarded as the ideal site, located as it was on the crest of a hill, it had the advantage of being near to the laboratory and workshop from where the site could be reached, it had a lockable shelter in which to store the equipment when not in use, and power and

compressed air could be laid on from nearby buildings.

In this chapter then the laboratory and field characterisation tests are described. The data derived from the field tests is treated in detail in chapters 5 and 6.

4.2 Laboratory Characterisation

4.2.1 The Calibration Rig

As mentioned in section 4.1 the aerosol was generated by spraying a slurry of the pigment into the entrance of a long pipe. Figure 4.1 gives a flow sheet of this scheme and the dimensions and specifications of the main items of equipment. The pipe and fan were existing items of equipment in the laboratory and originally formed part of a flash drier.

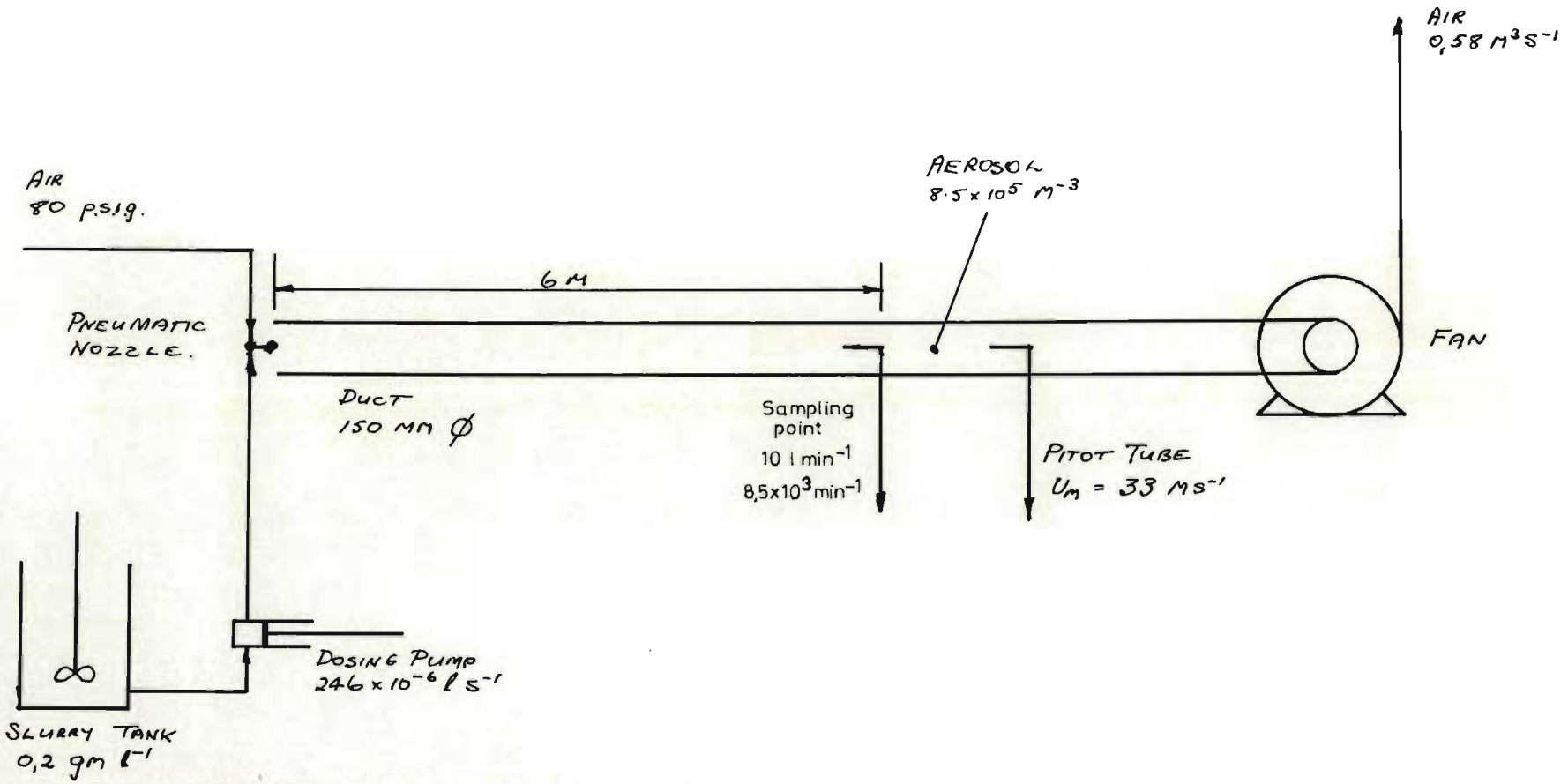

Figure 4.1: Schematic diagram of the laboratory calibration rig

It is important in an experiment of this nature to ensure that the flow at the sampling point is fully developed, that the velocity profile is symmetrical about the axis of the pipe and that the particles forming the aerosol are uniformly distributed over the cross-section of the pipe. The air velocity within the pipe was about 33 m/s giving a Reynolds no. of about $3,6 \times 10^5$ which suggests fully turbulent flow. The section of pipe between the entrance and the sampling point was absolutely straight, horizontal and about 6m in length, or about 40 pipe diameters, which is,within practical limitations,near enough to the 50 pipe diameters normally required to produce uniform flow.

A concentration traverse was also performed over the pipe cross-section and is shown in figure 4.2. Although there appears to be a higher concentration of particles in the lower half of the pipe the variation

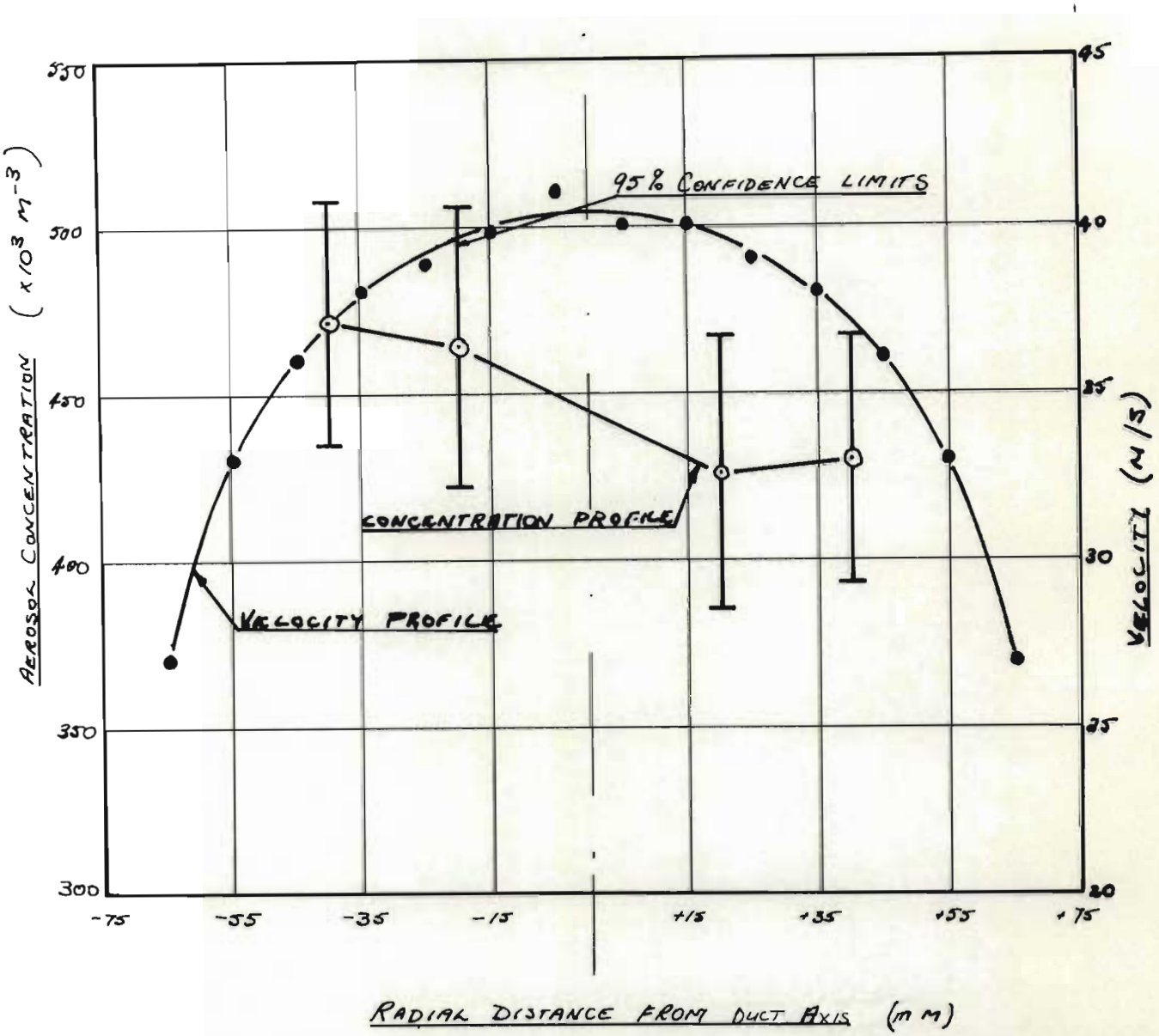

Figure 4.2: Concentration and velocity profiles across the calibration duct at the sampling point. The duct was horizontal and the measurements were taken over a vertical section, measurements above the duct axis are indicated by a positive value of radius and vice versa

between the four measurements is within the statistical error of measurement and it is therefore doubtful whether this variation is significant. In any event the difference between the highest and the lowest measurement represents a variation of about 11% which was not considered significant within the context of the experiment.

Figure 4.3 shows the fluorescent particle counter positioned beneath the calibration pipe with its sampling probe, a tube with bore of 4mm and bent in the shape of a pitot tube, protruding into the pipe. The pitot tube used for the measurement of velocity within the pipe is mounted on the pipe to the right of the counter and can be identified by its two tubes leading to the manometer whichis out of the picture.

4.2.2 The Aerosol Generation Equipment

A problem with generating an aerosol is

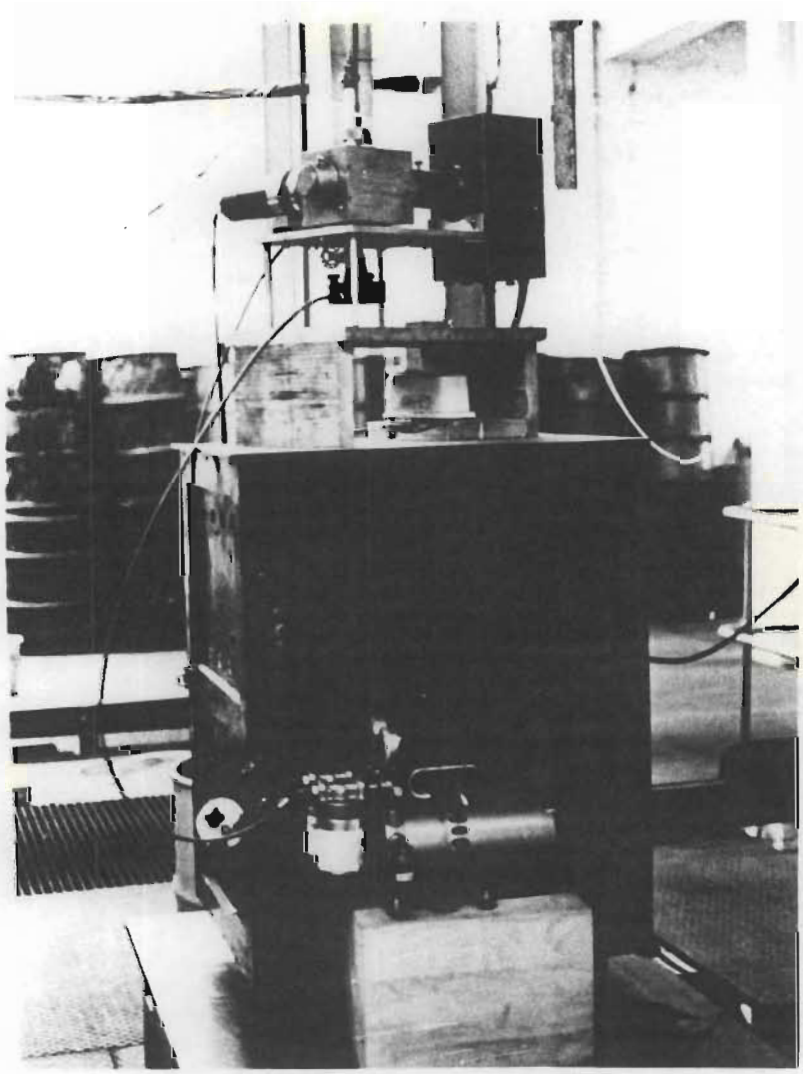

Figure 4.3: General view of the fluorescent particle counter in position to sample air from the calibration duct

that surface charges on individual particles cause the particles to agglomerate and a very high field of shear is required to break up these agglomerates. Leighton et at (32) described the use of a high speed fan to provide this shear field when dispersing the pigment as a dry powder. However in this experiment the use of a fan was considered inappropriate because of the large quantities of pigment normally fed to the fan. An alternative scheme was therefore considered whereby the pigment was slurried with acetone and the slurry pumped through a pneumatic spray nozzle. Pneumatic spray nozzles by nature have a very high shear field in order to atomise the liquid being sprayed, and the shear force can be increased and the droplet size decreased by simply increasing the air pressure. For the purpose of these experiments the maximum available air pressure of 544 kPa(g) was used. No attempt was made to measure the droplet size distribution or to check for

the presence of agglomerates as the results obtained from the calibrations did not seem to warrant such an investigation.

The pigment slurried in acetone, was stored in a glass vessel and was kept in suspension by a stirrer. The slurry was pumped to the nozzle with a reciprocating metering pump. As the pigment has a specific gravity of 4 it was found to be very prone to settling out in the pipes and in the valves of the pump. To overcome this problem a delivery tube with a bore of about 2mm was used with a fixed pumping rate of about $8,86 \times 10^{-4}$ m^3/h giving a velocity in the line of about 0,078m/s. The concentration of the aerosol was then varied by changing the concentration of pigment in the slurry.

As acetone is a solvent for plastics and rubber compounds and is also highly volatile and inflammable neoprene gaskets were required in the metering pump gland and flame

proof motors were required for the pump and stirrer. Although water would have been preferable in every respect to acetone the fluorescent pigment appeared to be hydrophobic and would not wet readily making it necessary to slurry with a non-polar liquid.

Figure 4.4 shows the slurry reservoir and metering pump assembled on a frame to make the apparatus portable, and figure 4.5 shows the pneumatic nozzle mounted at the entrance to the calibration pipe.

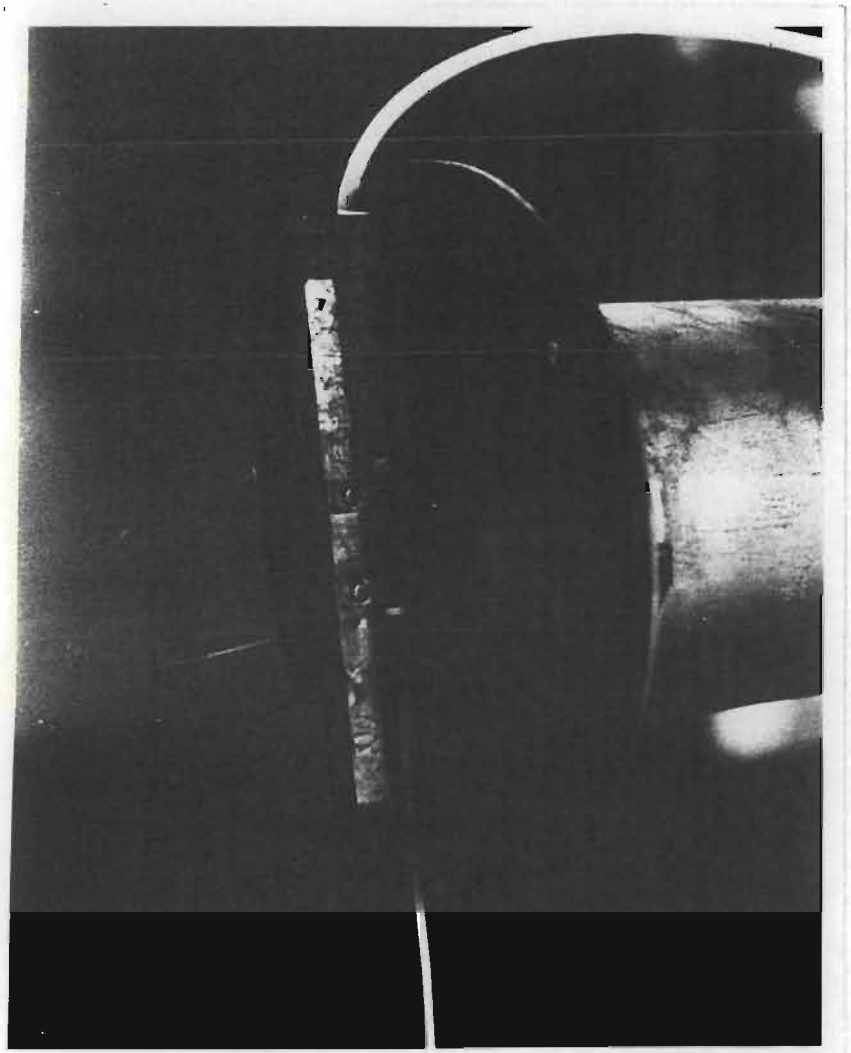

Figure 4.4: View of the pneumatic spray nozzle mounted on the intake of the calibration duct

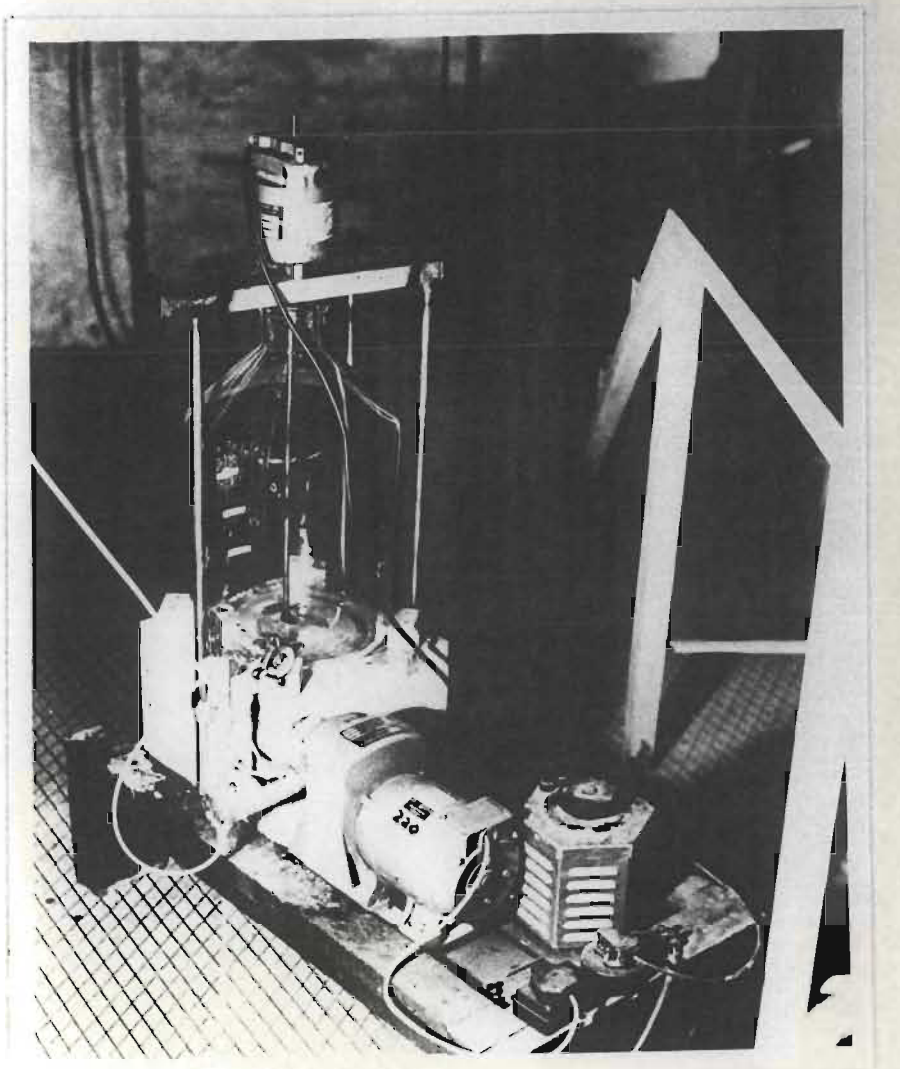

Figure 4.5: General view of the slurry reservoir and metering pump

4.2.3 Aerosol Sampling and Estimation

To characterise the calibration rig the aerosol was sampled through the same probe used for the fluorescent particle counter but the sampled air was drawn directly through a millipore filter and not through the fluorescent particle counter. Measurements of this kind were also used to estimate the transmission efficiency of the counter. The millipore filters used had a mean pore diameter of 0,8µm and were characterised by a very narrow pore size distribution and retained the aerosol particles on their surface, thus making subsequent determinations very much easier. When sampling with the fluorescent particle counter the millipore filter was then mounted in the filter holder following the sample chamber, as shown in figure 3.8 and was

used to calibrate the instrument.

In all sampling tests with or without the fluorescent particle counter the sampling probe was aligned with the axis of the calibration pipe with the entrance to the probe facing upstream. The sampling velocity was in every case adjusted to 16 m/s which is roughly half the velocity measured in the pipe. These velocities were to a large extent dictated by the equipment used for the tests. To have attempted to sample isokinetically would have meant fairly substantial alterations to the equipment. In any event Badzioch (2) showed in a paper on sampling of gas borne dust particles that under these conditions the aerosol concentration is likely to be overestimated by 7% for particles of 3μm in diameter and by 0,8% for particle of 1μm in diameter. Considering that about 80% of the particles are less than 3μm in size the error incurred by not sampling isokinetically

would probably be in the region of 5%. In the context of the experiment this error would only have affected the estimate of the number density of the fluorescent pigment and not the calibration of the fluorescent particle counter.

Estimation of the number of fluorescent particles on a filter paper was accomplished in much the same way as described by Leighton (32) and by Venter (80). Each filter paper was illuminated with the 365nm line from a 200W super pressure mercury lamp in a free-standing housing, and was visually observed using a microscope with a magnification of 100 X. The microscope was fitted with a UV cut filter to protect the eyes of the observer. On filter papers coloured black the fluorescent particles showed up very clearly as small bright yellow specks of light.

When estimating the number of particles on filter paper 49mm in diameter it is impractical to try and count every particle when there is a large number of particles. A counting graticule was therefore normally used in the eyepeice and in order to make it visible it was found necessary to supplement the illumination with a small amount of light from the standard microscope illuminator.

To estimate the number of particles on the filter paper ten fields were observed on every filter. Eight fields were selected to coincide very roughly with the intersections between two perpendicular diameters and two concentric circles of approximately 14 and 28mm in diameter. The remaining two fields were selected at random at the centre of the filter. If particles are assumed to be distributed across the filter paper with a Poisson distribution the precision

(or 95% confidence limits) with which the mean can be estimated varies from about ± 10% to about ± 16% for fields containing an average of 50 and 20 particles respectively. If the average number of particles falls to 10 the precision deteriorates quite sharply to about ± 23%. On the other hand with more than 50 particles per field counting becomes rather tedious. For these reasons the field was varied in size to always contain between 20 and 50 particles or more. This was achieved:

a) by changing the magnification from 100X to 60X and thus changing the projected area of the graticule from 0,49mm^2 to 1,33mm^2, or

b) by using the grid squares marked on the filter paper each of which covered an area of 9,61mm^2. For comparison the total useful area of the filter was 1354mm^2.

With this technique the number of particles

on a filter was estimated with a precision, on average, of about ± 12%.

By means of the techniques described in this section it was possible to estimate the number density of fluorescent pigment and this turned out to be about $1,09 \times 10^{10}$ particles/g. This number is overestimated by about 5% as a result of anisokinetic sampling discussed earlier in this section. However it is underestimated by the loss of particles arising from deposition onto the walls of the duct, and onto the walls and in the bend of the sampling probe. From Strom's work (75) it appears that loss due to deposition on horizontal parts of the duct and sampling probe may be less than 0,2%. However losses in the bend of the sampling probe may be very much higher but are difficult to calculate. Strom also points out that losses can be much higher if the particles carry a surface charge and earlier work discussed in section 4.1 suggests this might be the case. If then

the number density is regarded as being underestimated by about 5% owing to aerosol transmission losses this error is probably just compensated for by the error due to anisokinetic sampling, and the result of $1,09 \times 10^{10}$ particles per gram may be regarded as a fair estimate. Within 95% confidence limits of $\pm$ 12% this number compares quite favourably with that reported by Leighton (32) of $1,39 \times 10^{10}$ particles per gram.

4.2.4 Calibration of the Fluorescent Particle Counter

The fluorescent particle counter was characterised by three different measurements namely: the aerosol transmission efficiency, the calibration, and the dynamic response. Each is described in turn in this section.

When sampling aerosols through tubes of small bore there is always the risk that an

aerosol particle will collide with the tube wall and stick there leading to a loss in particles. The loss could be greater if the particles carried a surface charge and were attracted to the wall. This loss results in underestimation of the true concentration of the aerosol.

The losses likely to occur in the sampling probe have already been discussed in section 4.2.3 and will not be discussed any further. What is of concern here is the transmission of the fluorescent particle counter itself i.e. the transmission of the aerosol through the inlet pipe and view volume. This was measured by counting particles on filter papers with and without the counter coupled to the sampling probe. The measurement was made for three different ratios of secondary to primary air flow rate and is reported in figure 4.6. This graph shows that for a ratio between secondary and primary air of 1,67 the tansmission of the instrument was in the region of 90%.

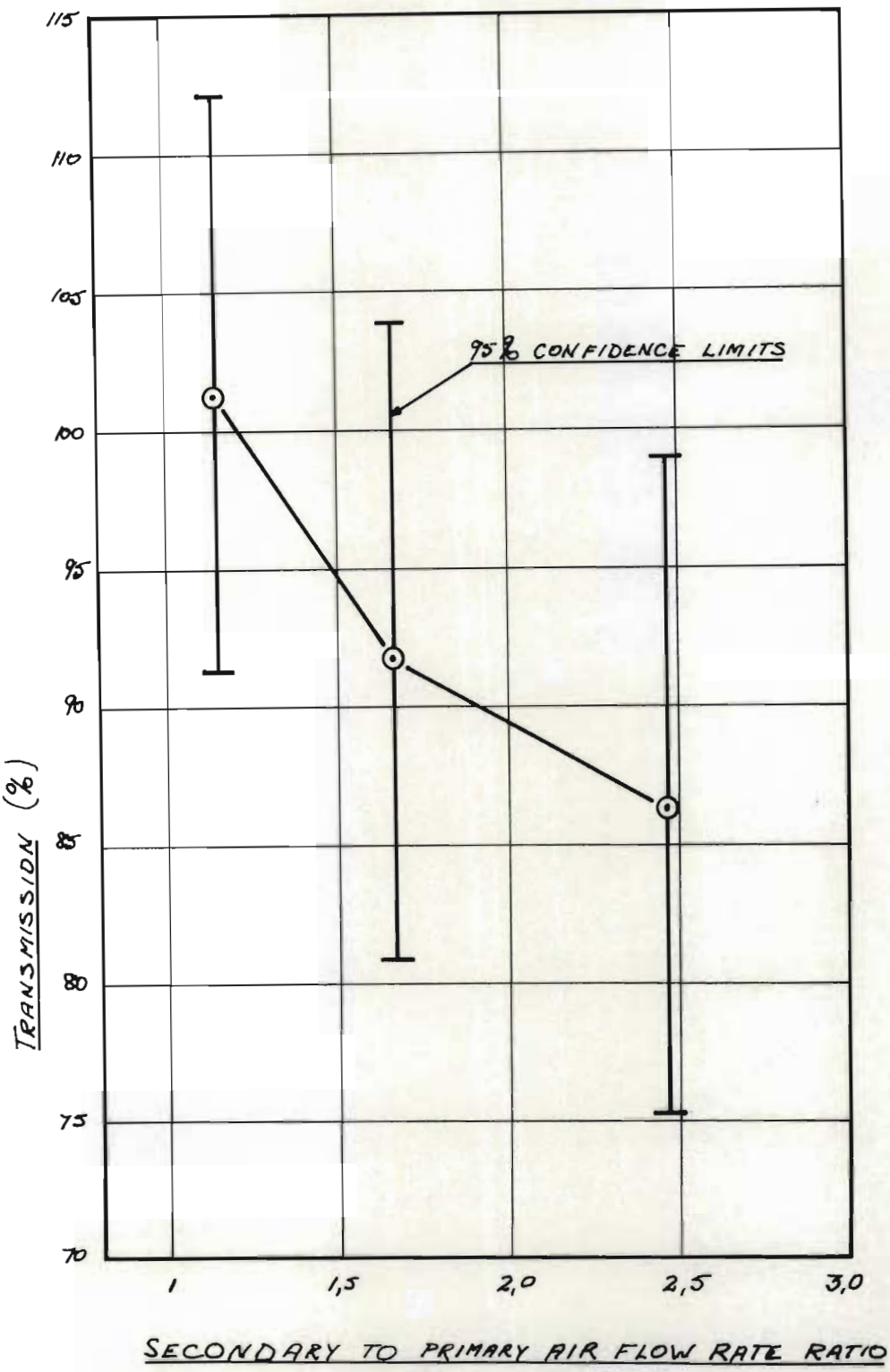

Figure 4.6: Aerosol transmission of the fluorescent particle counter as a function of the secondary to primary air flow ratio

Figure 4.6 also shows a trend which suggests that as the ratio increases the transmission decreases. The reason for this is not clear however the trend is rather heavily clouded by errors of estimation and so it is really of questionable significance.

To calibrate the fluorescent particle counter aerosols of different concentrations were sampled for different lengths of time and the number of particles counted electronically was compared with the number of particles on the filter. The period for which the aerosol was sampled was varied in order to get enough particles on the filter paper to fulfill the criteria discussed in section 4.2.3, consequently dilute aerosols were sampled for periods of up to 12 hours whereas concentrated aerosols were sampled for periods of as little as 20 minutes.

The accumulated results of some 68 sampling

trials are presented in figure 4.7 where the electronic count rate in counts per minute is plotted against the tracer concentration in particles/m^3 as estimated from the filter paper mounted directly beneath the sampling chamber (shown in figure 3.8). Also shown in figure 4.7 is the best regression line through the data together with its 95% confidence limits. These limits define the region within which the mean of several determinations of concentration for a single counting rate is most likely to fall. The determination of a single concentration from a single counting rate is however subject to additional variation about these limits and the corresponding 95% confidence limits are shown in figure 4.7 at the centre point and at each end of the regression. The equation giving the least squares fit to this data is:

$$B = 0,37\ A^{0,692} \qquad (4.1)$$

Where B is the electronic counting rate per minute and A is the actual concentration in particles/m^3. When measuring the concentration of tracer as opposed to calibrating the counter the inverse of equation (4.1) is useful:

$$A = 4,21\ B^{1,45} \qquad (4.2)$$

If the fluorescent particle counter had produced a pulse for every particle as it

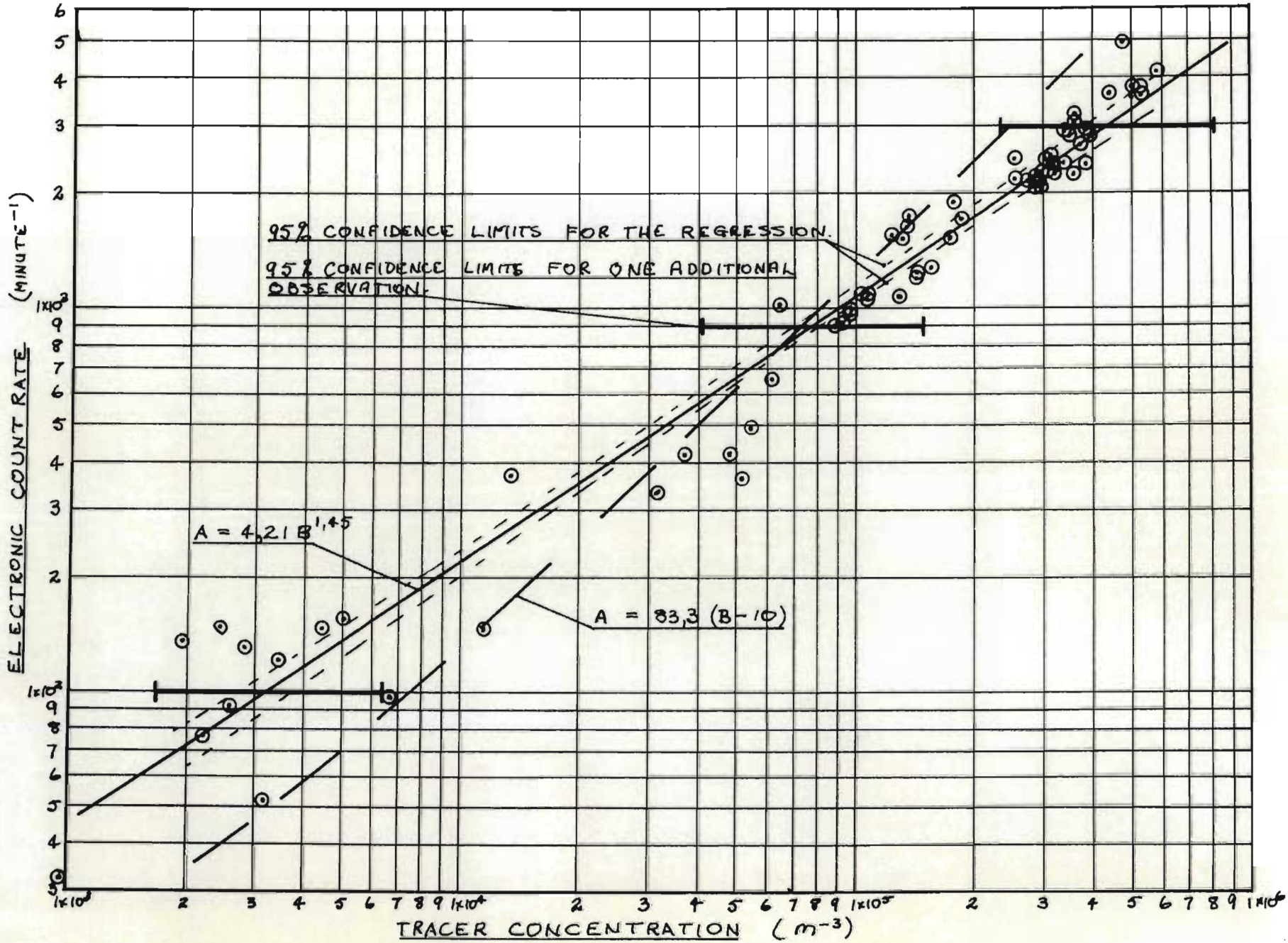

Figure 4.7: Calibration curve for the fluorescent particle counter.

might have been expected to do the calibration might have been expected to follow the equation

$$A = 83,33\ (B-10) \qquad (4.3)$$

where the background count rate of 10/minute has been subtracted from the observed counting rate. Ratios between concentrations given by equations (4.3) and (4.2) are given in the following table:

B	A from eqn (4.2)	A from eqn (4.3)	$\frac{A(4.3)}{A(4.2)}$
50	$1,2 \times 10^3$	$3,3 \times 10^3$	2,75
100	$3,3 \times 10^3$	$7,5 \times 10^3$	2,27
500	$3,5 \times 10^4$	$4,1 \times 10^4$	1,17
700	$5,6 \times 10^4$	$5,8 \times 10^4$	1,04
1000	$9,4 \times 10^4$	$8,3 \times 10^4$	0,88
3000	$4,6 \times 10^5$	$2,5 \times 10^5$	0,54

From these ratios it is clear that the linear calibration, equation (4.3), follows the actual calibration, equation (4.2), reasonably closely for counting rates in the range 500 to 1000 / minute. Outside of this range the correspondence between these equations diminishes, low concentrations being overestimated and high concentrations being underestimated by equation (4.3). Overestimation

at low concentrations can most probably be explained by the background noise from the photomultiplier which is significant in comparison with the observed counting rates. At high concentrations however it is to be expected that equation (4.3) will underestimate actual concentrations in view of the increased likelihood of more than one particle occurring in the view volume simultaneously, and for which only one count is recorded. Assuming a viewing window of 2ms and a Poisson distribution for particles in a gas, Davies and Goldsmith (11), the observed counting rate might be expected to fall to 98% and 92% respectively for concentrations of $1x10^5$ and $4x10^5$ particles/m^3. In practice the observed counting rate was only 56% of the linear counting rate for a concentration of $4x10^5$ particles/m^3. This fact cannot readily be explained and would be an area which would have to be addressed if the development of this prototype instrument was taken any further.

The apparent underestimation of the actual concentration when assuming a linear form for the calibration equation is clearly related in some way to the viewing window which from the oscillograph, figure 3.14(d), may be taken as 2ms.

Shortening this viewing window should diminish the chance of more than one particle occurring simultaneously in the view volume thereby raising the highest concentration which the counter can determine. A shorter viewing window could have been achieved by either shortening the gap in the sampling tube (difficult to accomplish without an improvement in the definition of the irradiation beam at the view volume) or by increasing the sampling flow rate (limited by the choice of vacuum pump). These effects were not investigated in any detail as the concentration range of the instrument was considered adequate, furthermore in the atmosphere where the dilution of a tracer is so great, the ability to measure very low concentrations accurately and reliably is of paramount importance.

Although Goldberg (25) did not apparently calibrate his instrument the data he does report suggests that a linear interpretation of its counting rate overestimates the actual concentration by about 42% at an actual mean of about $3{,}4 \times 10^5$ particles/m^3. The only valid comparison with the present instrument which can be drawn from this data is that the same ratio between linearly interpreted and actual concentrations

occurs at roughly $1,8x10^3$ particles/m^3, or about 1/20th of the above concentration, and this is perhaps consistent with the fact that Goldberg's instrument had a viewing window 1/20th that of the present instrument.

The third test was the dynamic response and this was accomplished by switching the metering pump on the aerosol generator off and then on again at roughly 20 second intervals. As the pneumatic nozzle created a back pressure in the liquid line, switching off the metering pump was expected to create a well defined cut off in aerosol concentration. This is quite accurately reflected in figure 4.8 where the counting rate of the fluorescent particle counter is plotted as a function of time.

Switching the pump on again was not as clean an operation as the liquid level in the pipe to the nozzle had usually dropped as a result of valves not sealing properly. The pump had therefore to recover the level and re-establish the liquid flow in the nozzle. Again this effect can be clearly seen in figure 4.8 . The momentary concentrations recorded at about 600 seconds are probably due to stray drops of slurry being emitted by the pneumatic

nozzle.

Clearly figure 4.8 suggests that the fluorescent particle counter responds quickly to changes in aerosol concentration.

4.2.5 Summary of Operating Characteristics

Outstanding features of the fluorescent particle counter which have still to be discussed include the highest and lowest concentrations which can be reliably determined for the instrument. The highest concentration is determined by the likelihood of more than one particle occurring in the view volume. Particles distribute themselves in a large volume of air according to a Poisson distribution, Davies and Goldsmith (11). Thus for a counting window of approximately 2 ms the maximum concentration which may be determined with a less than 1% chance of more than one particle occurring in the view volume simultaneously is approximately 4×10^5 particles/m^3. The figure of 1% was chosen arbitrarily and is not a physical limitation, however at concentrations greater than 4×10^5 particles/m^3 the instrument's ability to distinguish single particles will deteriorate.

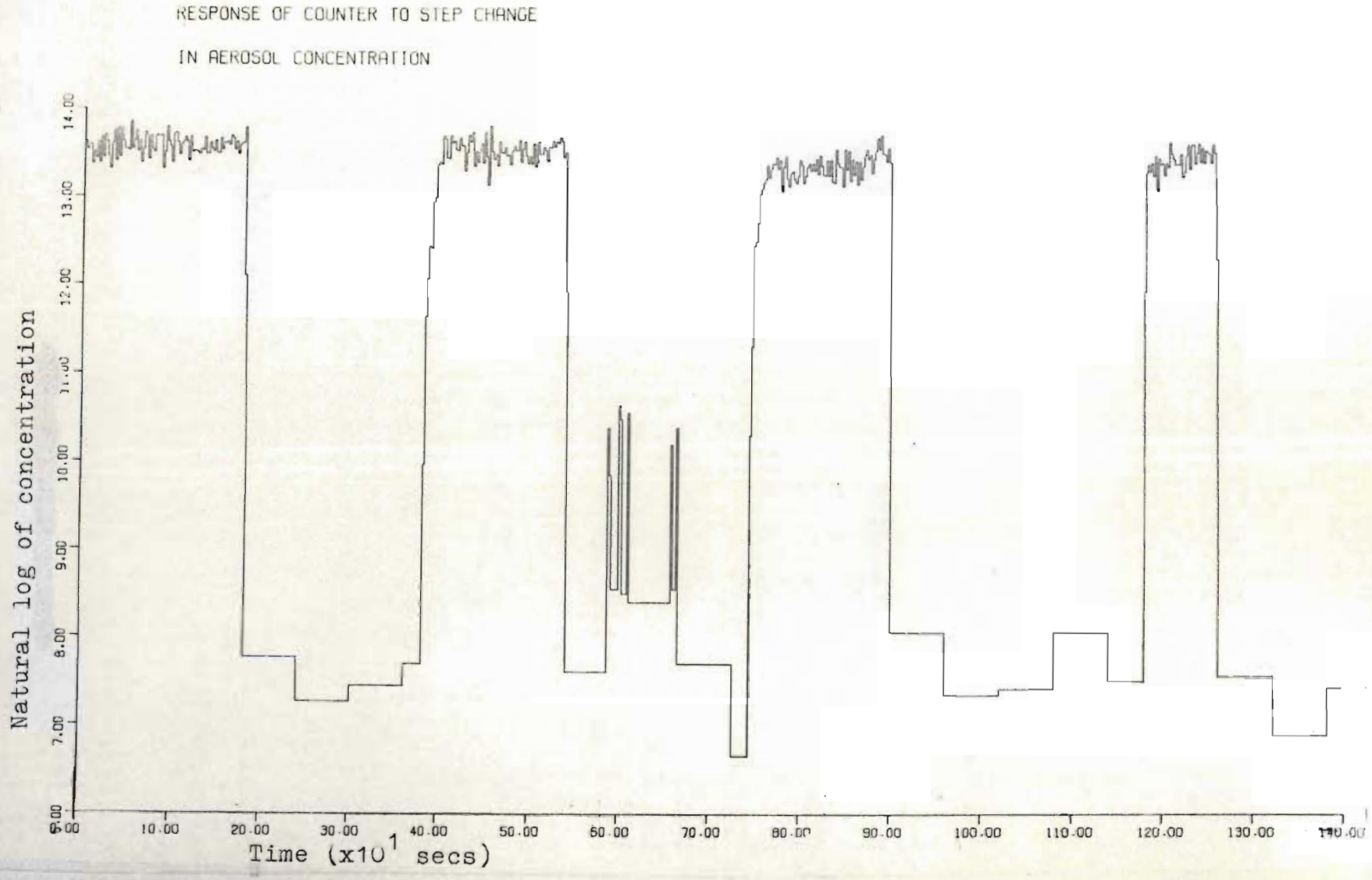

igure 4.8: Dynamic response of the fluorescent particle counter to step changes in tracer concentration concentration

In principle there should be no lower limit to the concentration which can be determined with an instrument capable of counting single particles. In practice however photomultiplier tubes are inherently noisy devices and with the instrument running but with no aerosol to be sampled a background counting rate of about 10 pulses/minute was observed. This was the lowest rate achieved after optimising the optical and electronic systems. By taking the lowest reliable counting rate as three times the background counting rate (a rule of thumb from the electronics field), and from equation 4.2, the lowest detectable concentration is therefore 600 particles/m^3.

By comparison Goldberg's instrument apparently had a noise count rate of 1,2 pulses/minute and a viewing window of 100 μs. This would have resulted in lowest and highest detectable concentrations on the same basis of roughly 300 and 8×10^6 particles/m^3 respectively. As Goldberg gives no calibration for his instrument and does not deal formally with upper and lower detection limits these figures are somewhat speculative. Goldberg does claim a lower detection limit of 100 particles/m^3 but this is

doubtful since this concentration appears to coincide with the noise level he quotes.

In concluding the laboratory characterisation of the fluorescent particle counter it is useful to summarise its operating characteristics:

1) Aerosol transmission efficiency:
better than 90%.

2) Calibration equation:
$A = 4{,}21\ B^{1{,}45}$

3) Highest detectable concentration:
4×10^5 particles/m^3.

4) Lowest detectable concentration:
600 particles/m^3.

5) Response to step changes in concentration:
less than 2 seconds.

6) Minimum time resolution:
2 seconds.

4.3 Field Characterisation

The final test of any new instrument must be to take measurements in the enviroment for which it was designed and to compare the data with previous measurements for a similar environment. Thus by conducting a field test of the fluorescent particle counter the dispersion of fluorescent pigment in the atmosphere could be measured. From this data the atmospheric dispersion parameters were estimated and compared with published information. In this section the actual field test is described. The analysis of the data is described in subsequent chapters.

As has already been mentioned, section 4.1, the site chosen for the field test was the top of a large water reservoir located near the Dept. of

Chemical Engineering. Although this site was rather far from ideal it provided the opportunity to test the equipment at a location not far from where the instrument could easily be serviced and kept under close scrutiny by the existing staff. Figure 4.9 is a contour map showing the location of the site.

The aerosol generator and dectector were laid out about 20m apart with the line joining the two oriented for the north easterly wind, one of the main winds for the Durban area. The other main wind in Durban is the south-westerly but this wind usually brings rain. The nozzle of the aerosol generator was set up about 2,1m above ground level and pointing upwards, giving an effective source height of about 2,7m.

Wind azimuth and elevation angles were measured near the source with a Gelman-Gill bivane set up 2,7m above ground level. Mean hourly wind speeds were obtained from a Lamprecht anemometer also mounted 2,7m above ground level and near the source. The fluorescent particle counter

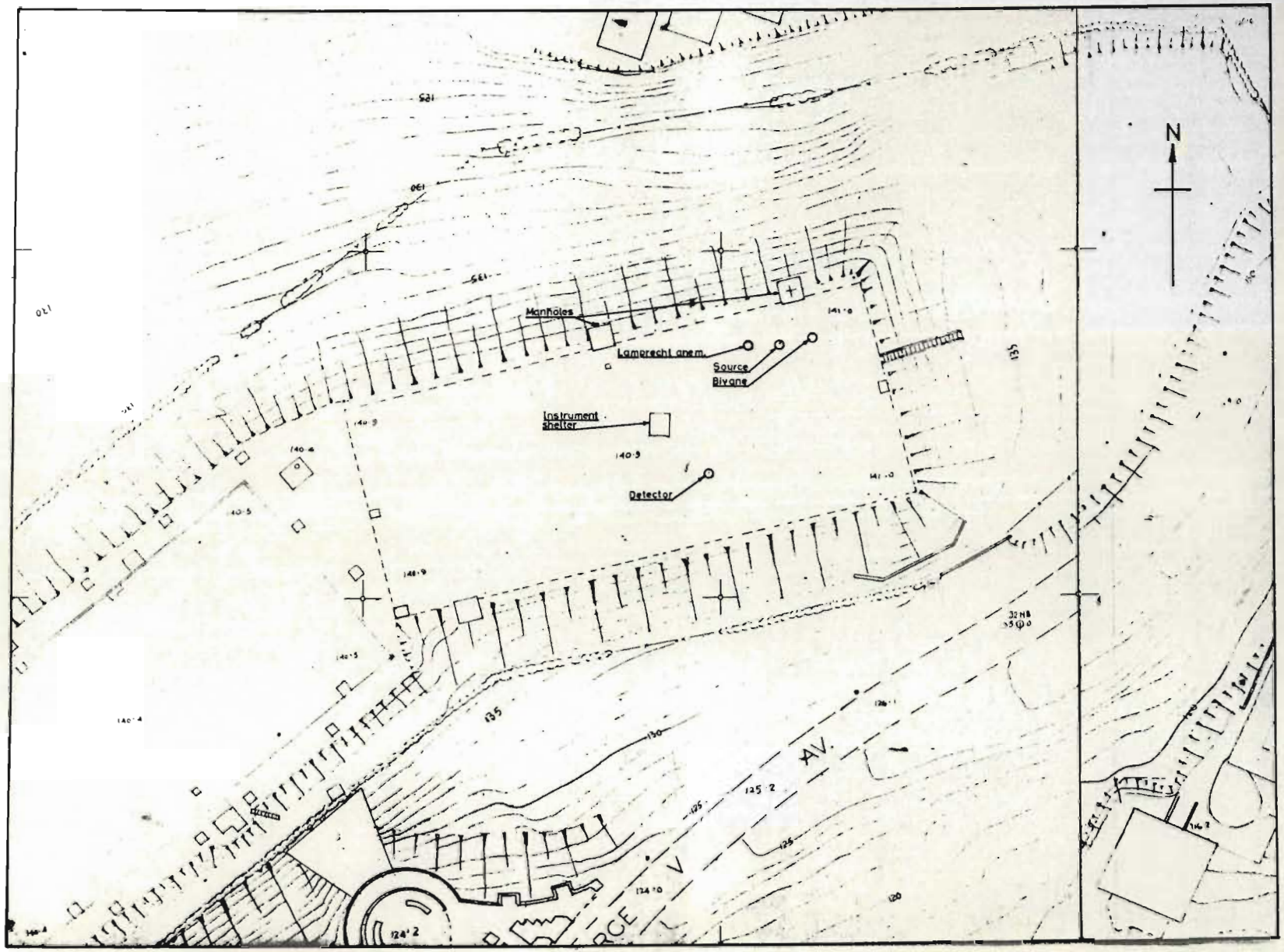

Figure 4.9: Contour map showing the reservoir on top of which the field trial of the fluorescent particle counter was undertaken

was mounted down-wind of the aerosol generator with the sampling probe located about 1,5m above ground level. There was no specific reason for the choice of these heights other than that they corresponded with readily available equipment on which to mount the various instruments.

The bivane provides two analogue signals proportional to the azimuth and elevation angles respectively. These signals were recorded on a 12-point recorder re-arranged as a two-channel device with six alternate points for each channel. The recorder printed one point every five seconds and six points per minute for each channel. To recover this information in digital form a special digitiser was devised which is shown in figure 4.10. A pointer is moved across the chart by means of a light non-elastic cord attached to a knob on a three turn potentiometer. An analogue signal can thus be obtained which is proportional to the position of the pointer and which was fed to the computer

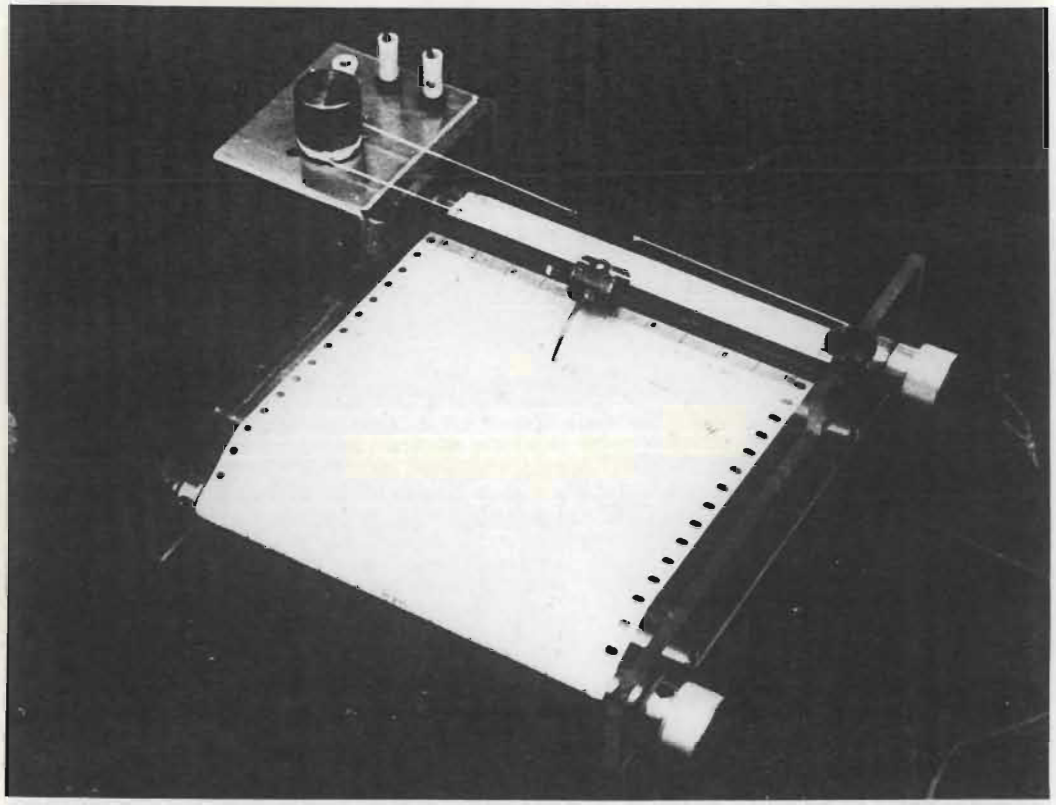

Figure 4.10: View of the device developed to digitise the wind direction information from the bivane which was recorded by means of a conventional twelve point chart recorder

via its analogue-to-digital converter. Software was written to enable the computer to store the value of the next point at the push of a button. Using a three turn potentiometer the accuracy was reckoned to be better than 2% of full scale.

Lamprecht anemometers record wind run on their own standard chart and so an average wind speed is obtained by measuring the slope of the wind-run line.

Using this arrangement the fluorescent particle counter was operated for a total of about 41 hours in three separate experiments giving about 37 hours of useful data. The variables which were fixed for the duration of these tests were as follows:

a) Orientation of the dispersion axis: $27,5^{o}$ from true north.

b) Tracer release rate: about $7,3 \times 10^{5}$ particles /s

c) Distance from source to detector: about 20m.

d) Height of source above ground level: 2,7m.

e) Height of detector above ground level: 1,5m.

The data obtained were all averaged over a period of one minute and then plotted as azimuth, elevation and concentration as a function of time. These graphs are all included in appendix C. Azimuth and elevation angles are measured with respect to the disperion axis and the horizontal respectively. Positive elevation angles indicate an updraft.

A particularly significant piece of data which demonstrates the importance of real-time measurements is the graph marked run 1:1060 to 1075 minutes in appendix C reproduced as

figure 4.11 This piece of data was recorded in the early hours of the morning when the wind speed was imperceptibly low. The atmosphere was probably stable, although no measurements were taken to verify this. The plume of tracer can clearly be seen to meander over the counter first from south-west to the south-east and then back again.

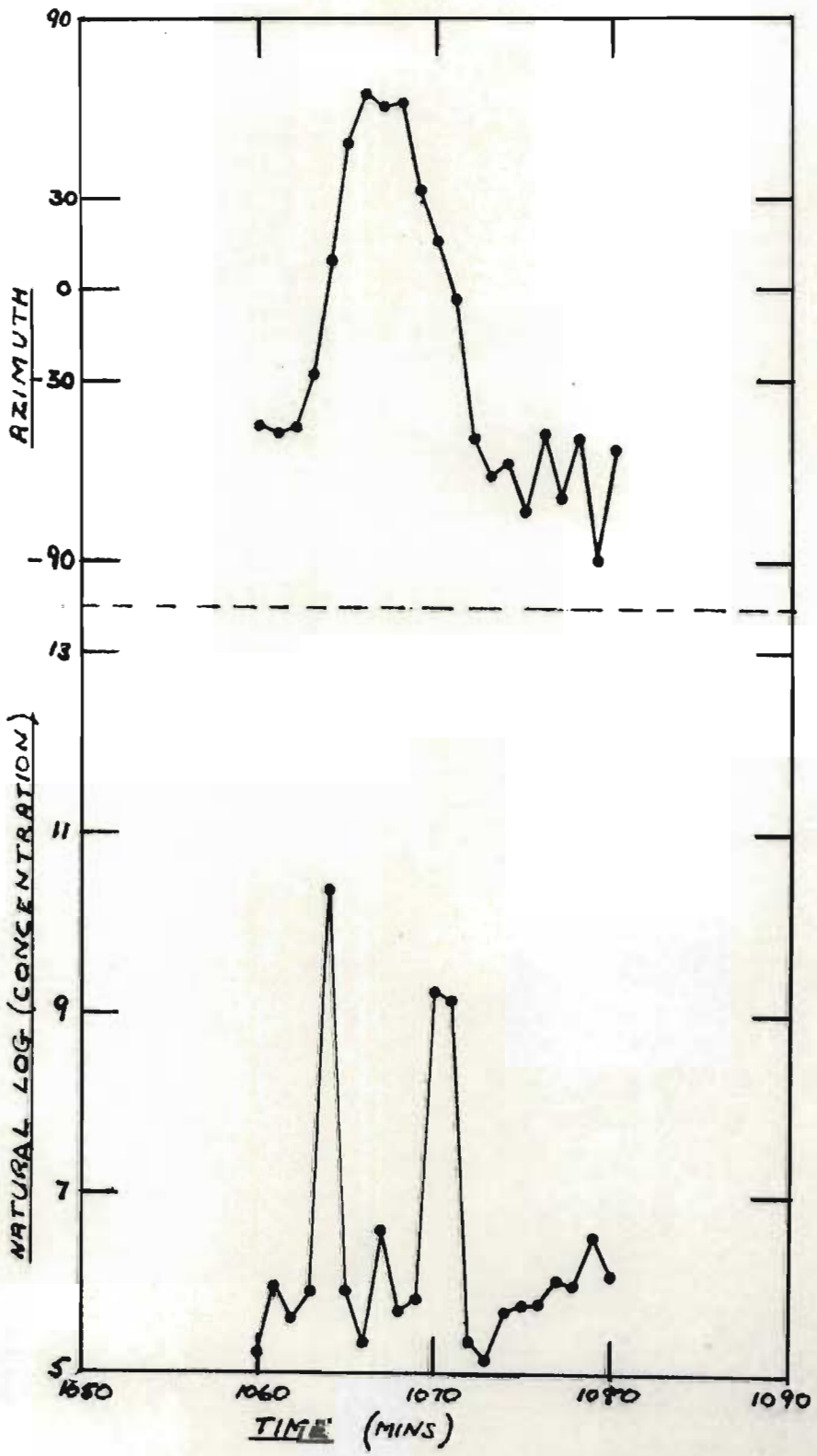

Figure 4.11: Recording of tracer concentration taken well before dawn under conditions of a stable atmosphere and extremely low wind velocity, showing clearly the plume meandering across the counter and back again.

CHAPTER FIVE: THE THEORY OF ATMOSPHERIC DISPERSION AS APPLIED TO REAL-TIME MEASUREMENTS

5.1 Introduction

As has already been mentioned in the foregoing chapters the first test of the fluorescent particle counter was its calibration in the laboratory. The second test of the counter was a field test in which real atmospheric dispersion data were accumulated with a view to extracting atmospheric dispersion parameters for comparison with the published results of other workers.

In order to extract the dispersion parameters, or eddy diffusivities, from a set of measurements it is necessary to apply a theory and find the parameters which yield the best approximation between theory and measurement. In the present work the measurements were taken with a single instrument and were taken in real-time, which means that the time varying, or fluctuating nature of concentration in the atmospheric dispersion process was actually measured. As the existing models were steady-state in nature and required time-mean concentrations measured at a number of locations these were not considered suitable for the present work.

Although most of the atmospheric dispersion work reported in the literature deals with the steady-state nature of the process there has been some theoretical work reported on the fluctuating nature of dispersion.

Two authors in particular who have considered this problem are Gifford (22,23) and Csanady (10). Both authors have considered the dispersion process as one of the plume spreading uniformly about the plume centreline which itself meanders about some fixed reference path, usually the mean wind direction. Whilst in principle this approach seems reasonable a practical problem arises in that it is difficult to separate fluctuations in concentrations into those which occur as a result of the spreading of the plume and those which occur as a result of the plume meandering.

For the purpose of this work therefore an alternative model was proposed which in essence is the K-theory model for a continuous point source adapted for a wind which is considered to fluctuate in direction. The plume is regarded as being made up of segments which travel in straight lines from the source, the direction of each line being the current wind direction at the source.

In this chapter Gifford's approach to the problem of modelling fluctuating concentrations in atmospheric dispersion is outlined. An alternative model is proposed, and as a test of its validity is applied to some experimental results published by Ramsdell and Hinds (54). The application of this model to the measurements made with the fluorescent particle counter is dealt with in chapter 6.

5.2 Approach by Gifford and Csanady

Gifford (22), and in a later development Csanady (10), took the view that the fluctuating concentrations which are a feature of atmospheric diffusion occur as a result of the plume meandering about a mean plume centreline which could be taken as the mean wind direction. Gifford then showed that the variances of the concentration distributions σ_y^2 and σ_z^2 in the horizontal and vertical directions respectively from the gaussian plume formula could each be seen as the sum of two components; the variance of the concentration distribution about the plume centreline and the variance of meander of the instantaneous plume centreline about the mean plume centreline. Gifford's view results in the following form for the mean concentration downwind of a continuous point source:

$$\overline{\chi} = \frac{Q}{2\pi u \sigma_z (\sigma_y^2 + \sigma_c^2)^{\frac{1}{2}}} \exp\left[-\frac{1}{2}\left\{\frac{y^2}{(\sigma_y^2+\sigma_c^2)} + \frac{z^2}{\sigma_z^2}\right\}\right] \qquad (5.1)$$

where σ_c^2 is the variance of plume meander in the horizontal plane, and where meander in the vertical plane has been ignored for the purpose of the ensuing discussion, but can nevertheless be treated in the same way.

Neither Gifford nor Csanady gave any suggestions as to how σ_c^2 could be measured experimentally. As it was not considered possible to measure plume meander using the measurement of fluctuating concentration at a single point, as was done in this work, an alternative model is proposed.

5.3 A Fluctuating Wind Dispersion Model

An alternative to Gifford's view of a meandering plume is to view the plume as comprised of a succession of segments each travelling along its own path from the source. Each path is assumed to be approximately straight and to take the instantaneous wind direction at the moment the segment leaves the source. Within each plume segment diffusion is assumed to take place uniformly about the centre of the segment. This view of a meandering plume is consistent with the author's own observations of, and with Pasquill's (48) qualitative description of a "looping plume".

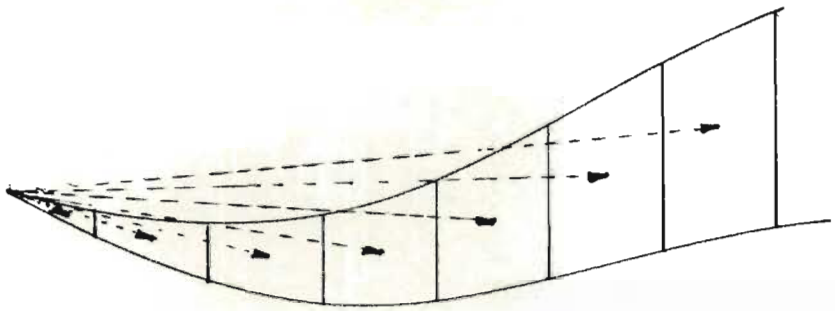

For the purpose of this discussion diffusion is assumed to take place within each segment according to the K-theory model of a continuous point source:

$$\chi = \frac{Q}{4\pi x (K_y K_z)^{\frac{1}{2}}} \exp\left[-\frac{u}{4x}\left(\frac{y^2}{K_y} + \frac{z^2}{K_z}\right)\right] \qquad (5.2)$$

where K_y and K_z are the eddy diffusivities in the horizontal and vertical planes respectively.

Suppose now that a sampler is located at a horizontal distance S from a tracer source and at azimuth and elevation angles of θ_s and ψ_s respectively measured at the tracer source. Suppose that a wind is blowing from source to sampler with a mean velocity u, and that the instantaneous path which it follows has an azimuth angle of θ in relation to the same tracer source. The angle between the line joining the source to the sampler and the instantaneous wind direction can therefore be written:

$$\alpha = \theta - \theta_s \qquad \text{(5.3)}$$

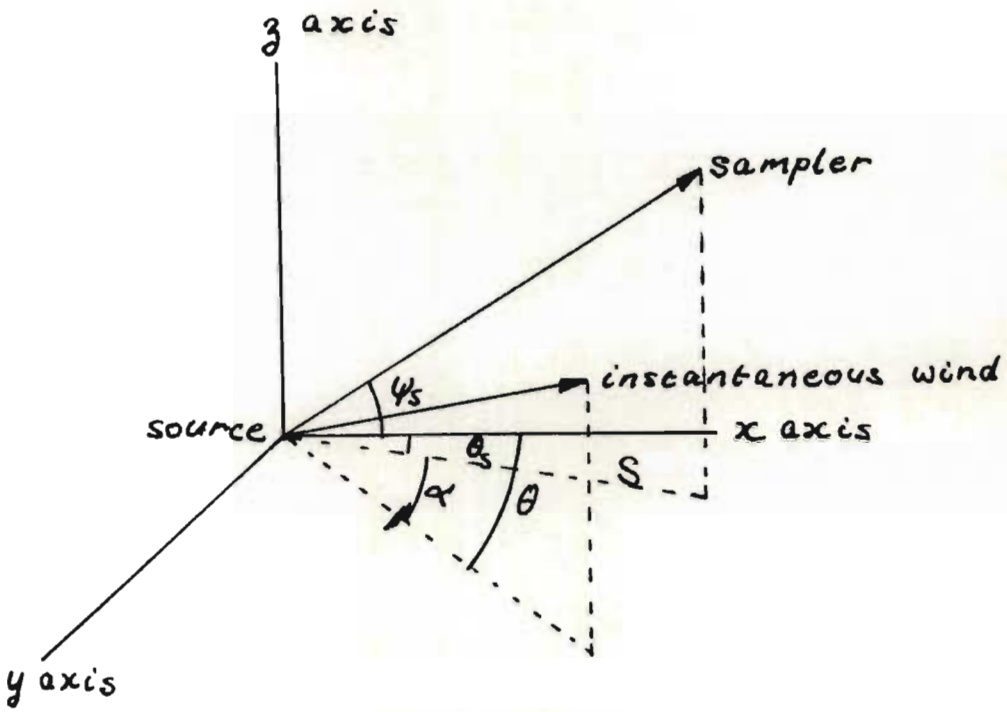

The transformations from rectangular to polar coordinates for the sampling point relative to the instantaneous wind direction are then:

$$\left.\begin{aligned} x &= S \cos \alpha \\ y &= S \sin \alpha \\ z &= S \tan \psi_s \end{aligned}\right\} \qquad \text{(5.4)}$$

Substituting the transformations 5.4 into equation 5.2 yields an equation for the instantaneous concentration at the sampling point for a given instantaneous wind direction θ:

$$\chi = \frac{Q}{4\pi S \cos\alpha \left(K_y K_z\right)^{\frac{1}{2}}} \exp\left[-\frac{uS}{4\cos\alpha}\left(\frac{\sin^2\alpha}{K_y} + \frac{\tan^2\psi_s}{K_z}\right)\right] \qquad (5.5)$$

The mean concentration at the sampler is calculated by integrating over all possible wind directions:

$$\overline{\chi} = \int_{-\pi/2}^{\pi/2} \chi(\theta)\, p(\theta)\, d\theta \qquad \text{(5.6)}$$

where $p(\theta)$ is the probability density of θ.

Measurements of wind azimuth taken during the course of this work and plotted on probability axes in figure 5.1 suggest that $p(\theta)$ is normally distributed, an assumption supported by Pasquill (48). Substituting equation 5.5 into 5.6, and introducing a normal distribution for $p(\theta)$ yields the following equation for the mean concentration at the sampling point:

$$\overline{\chi} = \int_{\bar{\theta}-\frac{\pi}{2}}^{\bar{\theta}+\frac{\pi}{2}} \frac{Q}{2^{\frac{5}{2}}\,\gamma^{\frac{3}{2}}\,\sigma_\theta\, S \cos\alpha \left(K_y K_z\right)^{\frac{1}{2}}} \times \exp\left[-\frac{uS}{4\cos\alpha}\left(\frac{\sin^2\alpha}{K_y} + \frac{\tan^2\psi_s}{K_z}\right) - \frac{(\theta-\bar{\theta})^2}{2\sigma_\theta}\right] d\theta \qquad \text{(5.7)}$$

where $\bar{\theta}$ is the mean wind azimuth and σ_θ is the standard deviation of wind azimuth.

Thus the seemingly difficult task of measuring the variance of plume meander σ_c in Gifford's model of fluctuating concentration is replaced by a measurement of the variance of wind azimuth σ_θ.

The explanation of fluctuating concentrations in terms of a fluctuating wind alone is however subject to certain limitations. As individual plume segments are assumed to follow straight line trajectories this view is only valid for travel times much shorter than the Lagrangian integral time scale (85). Furthermore the use of the K-theory, which accounts for diffusion due to concentration differences and not for diffusion due to turbulence, is least valid for short time averages of narrow plumes near the source (86). In the present work therefore the fluctuating wind model is used merely as a way of reducing the data from the fluorescent particle counter in order to obtain a "feel" for the measurements it yields, and to obtain some measure of comparison of these measurements with other work.

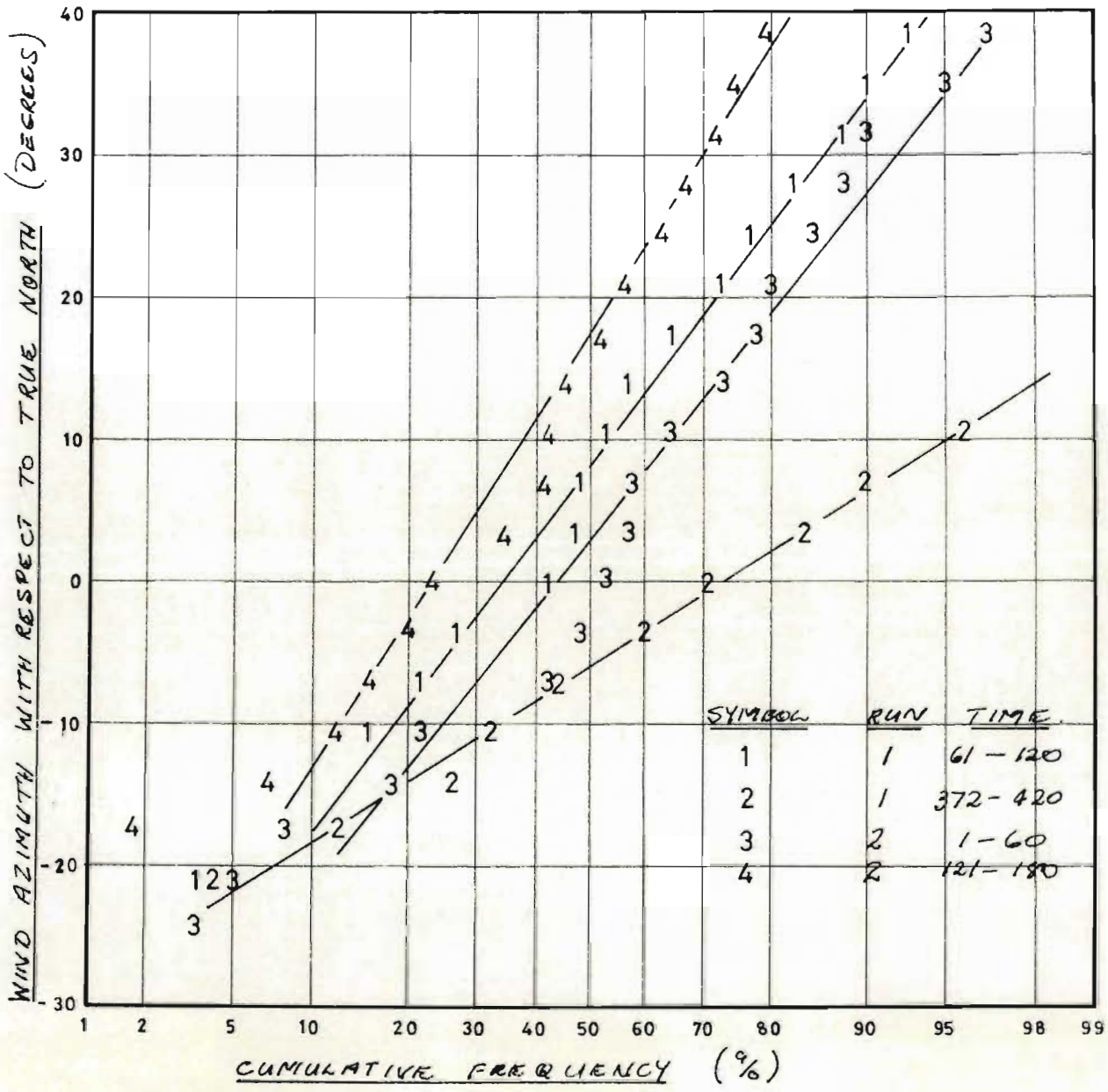

Figure 5.1: Samples of the cummulative frequency of wind direction recorded during the field trial of the fluorescent particle counter

5.4 Test of the Validity of the Fluctuating Wind Model

In early attempts to characterise fluctuating concentrations in the dispersion process (10, 22, 23, 26, 54, 58, 66) the concept of the ratio of the peak concentration to the mean concentration measured at a sampling location was developed and is commonly referred to simply as the peak-to-mean ratio. Arising from some very detailed measurements of fluctuating concentrations (43, 44, 45) Ramsdell and Hinds (54) have reported the variation of peak-to-mean ratio with distance measured perpendicular to the plume centreline in the horizontal plane. Their result with a sampling time for the peak one twentieth of the sampling time for the mean concentration is reproduced in figure 5.2.

In order to compare with the work of Ramsdell and Hinds the proposed model was developed to yield an equivalent peak-to-mean ratio. For a given location downwind of a source the peak concentration will occur when the wind blows directly towards the sampler, or in other words when $\theta = \theta_s$ and $\alpha = 0$ giving:

$$\chi_{peak} = \frac{Q}{4\pi S (K_y K_z)^{\frac{1}{2}}} \exp\left[- \frac{uS \tan^2 \psi_s}{4 K_z} \right] \qquad (5.8)$$

The peak-to-mean ratio is obtained by dividing equation 5.8 by equation 5.7 , the mean concentration, and the variation with cross-wind distance by varying the value of α in equation 5.7 . In examining this comparison it is important to note that Ramsdell and Hinds measured σ_y, the standard deviation of the cross-wind distribution as an angle measured from the source and their results suggest that this angle was not dissimilar to σ_θ , the standard deviation of fluctuations in the wind azimuth. Thus for the purpose of comparison the values of parameters used in the fluctuating wind model in order to calculate peak-to-mean ratios are as follows: $\sigma_\theta = 10^\circ$; u , the mean wind velocity, = 4 m/s ; and S , the horizontal distance from source to receptor, = 500 m. These values were picked as representing an approximate average of the measurements reported by Ramsdell and Hinds. The eddy diffusivities K_y and K_z were taken to be equal and were calculated by taking the square root of the product of K_y and K_z calculated from the spreading coefficients σ_y and σ_z for a distance of 500 m, taken from the Pasquill-Gifford curves reported by Seinfeld (64). Ramsdell and Hinds reported their results, shown in figure 5.2 , as a series of geometric means with a range of one standard deviation on either side of each mean.

Although the correspondence between the fluctuating model and Ramsdell and Hinds' results appears good near the centreline of the plume the correspondence deteriorates with distance from the centreline. This deterioration can probably be attributed to two main reasons:

1) the fluctuating wind model does not take into account the finite time required to sample the peak concentration. Ramsdell and Hinds show clearly from their experiments that the peak-to-mean ratio is increasingly sensitive to the ratio of time required to sample the peak to time required to sample the mean, as the distance from the plume centreline increases.
2) the cross-wind distance y is defined in the model as the distance from the mean wind direction whereas Ramsdell and Hinds defined y as the distance from the mean plume centreline. Furthermore Ramsdell and Hinds suggest that the centre of the mean plume did not always coincide with the mean wind direction, thus the two definitions are not necessarily equivalent.

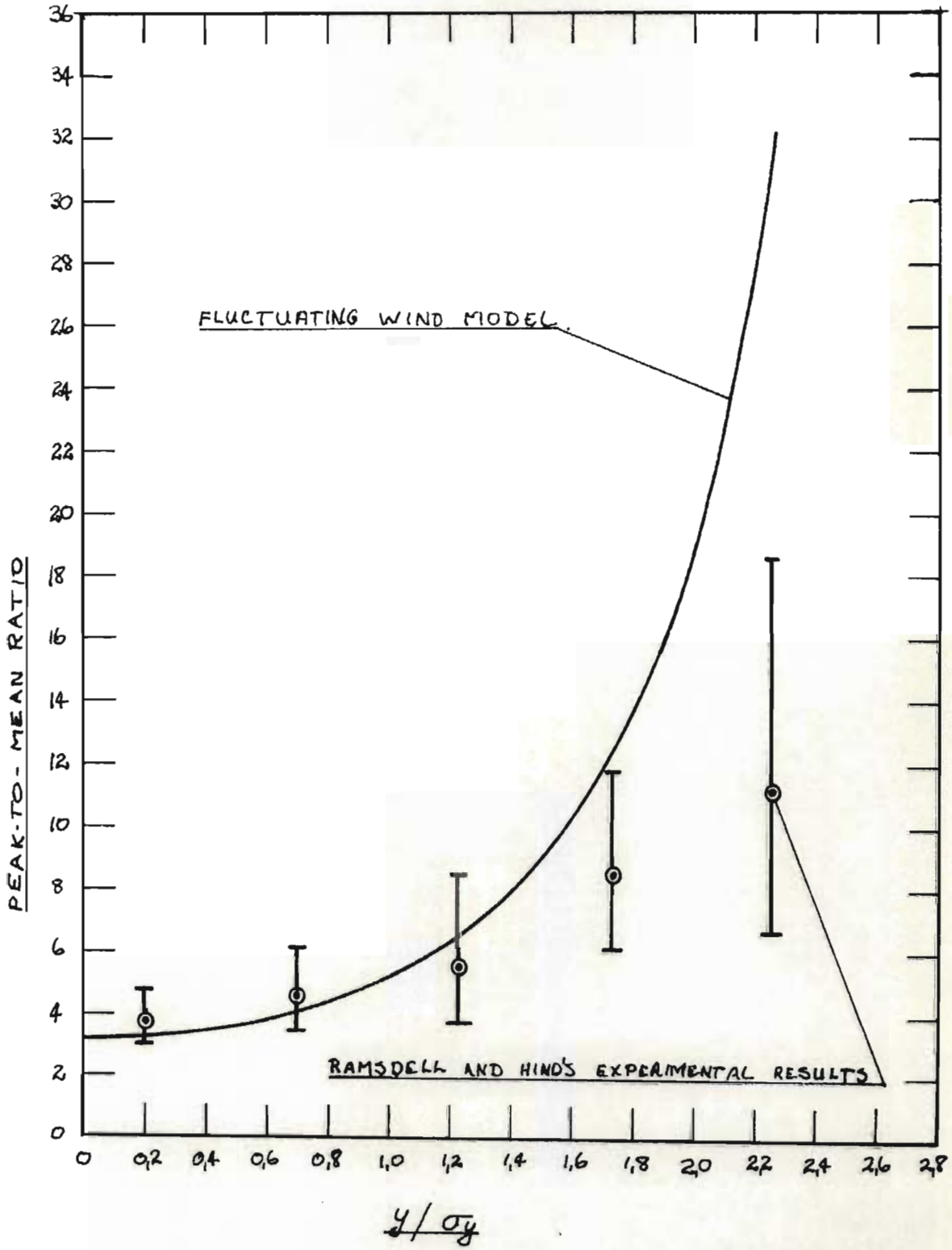

Figure 5.2: Variation of the peak-to-mean ratio with cross-wind distance as predicted by the fluctuating wind dispersion model, compared with measurements reported by Ramsdell and Hinds (54).

CHAPTER SIX : ANALYSIS OF DATA FROM FIELD TRIALS

6.1 Introduction

In chapter six the data collected from the field trial (described in chapter four) of the fluorescent particle counter is analysed with the object of estimating the eddy diffusivities. To do this the K-theory model of atmospheric diffusion from a continuous point source (64) was modified as existing models were not considered appropriate for the type of measurements taken during the course of this work.

The eddy diffusivities are estimated by fitting the modified model to the data accumulated, and then, to complete the characterisation of the fluorescent particle counter, the diffusivities thus estimated are compared with data published by other workers.

6.2 Screening of the Data

The primary data from three field trials of the fluorescent particle counter are included in appendix C. This data has been edited only in so far as periods during which the equipment was known to be malfunctioning have been eliminated from the record. Although the counter was capable of resolving concentration measurements to periods of as short as two seconds the amount of data which results is enormous, and it would not have been possible to process this data efficiently on the available computer. Each data point given in appendix C is therefore an average for a period of one minute.

To make the task of analysis easier the data record has been divided into one hour sets each set comprising 60 data points. The data sets were then screened for suitability by plotting the concentration against azimuth. Broadly speaking the model to be used for the analysis, equation 5.5, suggests that concentration varies with azimuth and any data sets which did not exhibit this behaviour were regarded as

unsuitable for regression. As discussed in section 5.4 the assumption of a meandering plume model implies that the time of travel between source and receptor is much shorter than the Lagrangian integral time scale. Thus of the 37 sets of data collected 13 appeared to exhibit the degree of correlation of motion expected under the above assumption, and were submitted for regression. The balance of the data sets did not show any apparent correlation between concentration and wind azimuth and this behaviour is consistent with an unstable atmosphere and a reasonably strong wind, conditions under which turbulence within the plume is well developed and is likely to be the dominant cause of concentration fluctuations over plume meander.

6.3 Fitting the Model to the Data

The model, equation 5.5, makes it possible to predict the concentrations which will be measured at a sampler for a given set of wind azimuths and eddy diffusivities. Thus the best fit of model to data can be obtained by varying the diffusivities until the

difference between predicted and measured concentrations is minimised. The diffusivities which yield the minimum are then regarded as the best estimates of the eddy diffusivities for the given set of data.

To accomplish the fitting of the model to the data a non-linear regression package developed by Imperial Chemical Industries Ltd. (52) was used. This package makes use of the Nelder and Mead simplex search (29) assisted by a quadratic fitting procedure, the combination being claimed to converge more rapidly and reliably than the unassisted simplex method. This package also gives statistical information about the goodness-of-fit and errors of estimation of the parameters which is particularly useful when screening a number of models.

6.4 Results of the Fitting Procedure

The results from fitting the fluctuating wind model, equation 5.5 , to the selected data are recorded in detail in the tables in appendix D. Apart from estimating the eddy diffusivities K_y and K_z it was also found necessary to estimate the tracer release rate Q and the tables in appendix D embody the results of choosing different combinations of parameters for estimation.

However rigorous the development of a model to describe a particular process the quality or reliability of the parameters which can be estimated by fitting the model to process data is very dependent on the complexity of the model and on the type of data to which it is fitted. For example if there is a strong interaction between the parameters in a model the estimates of each parameter are likely to be poor unless there is some feature of the data which makes it possible to break the interaction.

Thus on inspecting equation 5.5 closely it will be seen that K_y and K_z interact strongly, and in fact for a single concentration there are no unique values of K_y and K_z which will yield a solution to the dispersion equation as is demonstrated in figure 6.1 . Furthermore on inspecting the regression results in appendix D it is evident that while most of the estimates for K_y are statistically significant none of the estimates for K_z are significant. For this reason the eddy diffusivities were made equal thus simplifying the model and bringing about a substantial improvement in the statistical significance of the regression. This simplification must however be seen for what it really is, and that is numerical convenience, for in practice K_y is almost always greater than K_z..

The second problem encountered in the fitting procedure was concerned with Q , the release rate of tracer. Normally Q would have been carefully measured and the value inserted as a fixed value into the regression. However doing this caused one or other of the eddy diffusivities to become abnormally large or to violate a constraint, and frequently the routine

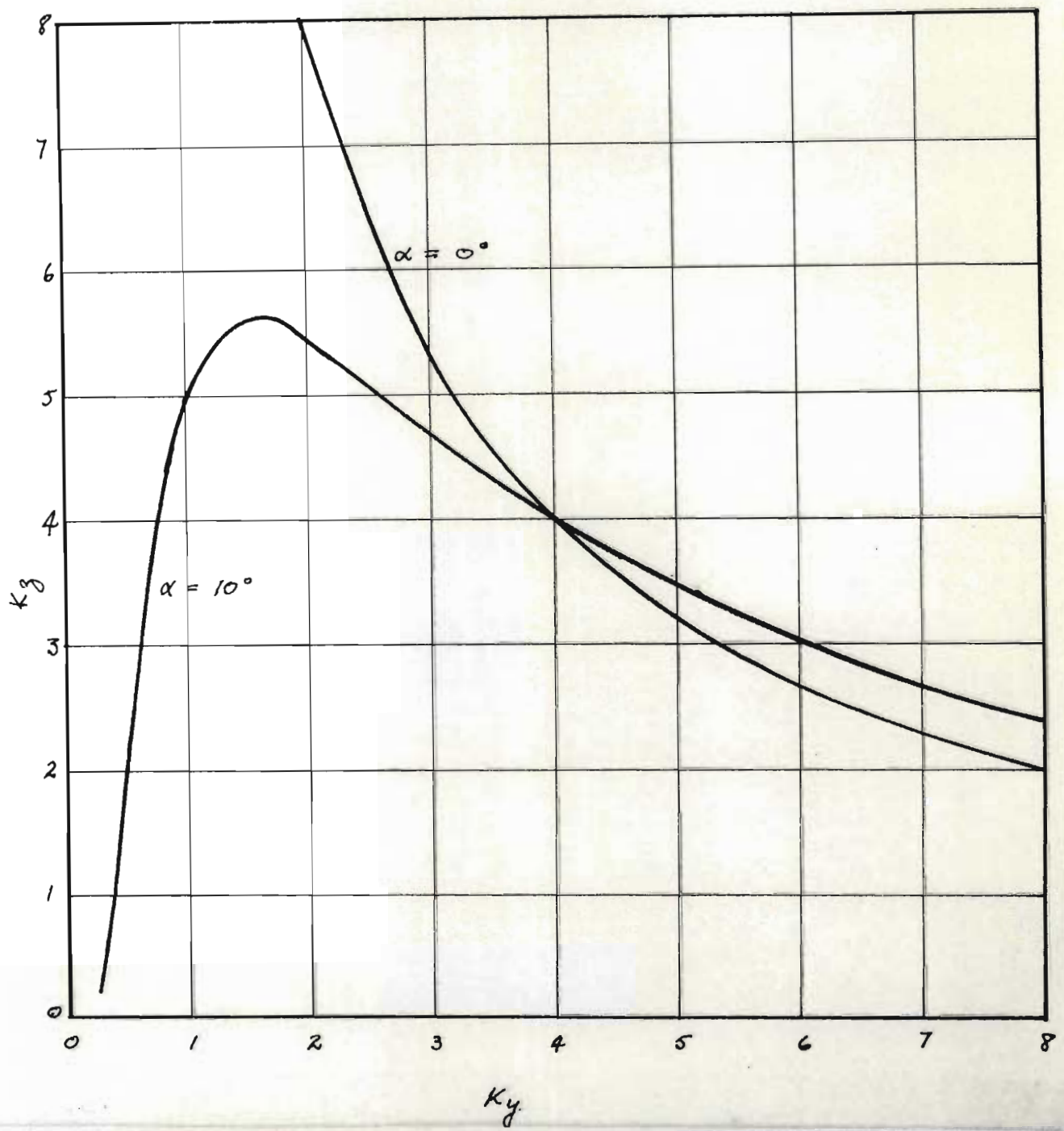

Figure 6.1: The range and interaction of the values of K_y and K_z which will solve the fluctuating wind dispersion model for a given set of the dependent and independent variables

did not coverge at all as shown in appendix D. Entering Q into the regression as a parameter to be estimated brought about a significant improvement in the result.

From this improvement in results it has been concluded that the measured values of Q are probably not reliable and this could have been due to the unreliable operation of the dispersion apparatus. During the course of the field work the pigment was found to settle in certain of the pipelines leading to blockages which had to be cleared from time to time. The fact that blockages were never a problem in the laboratory is probably due to the fact that a much lower concentration of pigment was used in the dispersion apparatus, and furthermore, the apparatus was required to operate for much shorter periods of time.

The best set of fitted parameters has been recorded in table 6.1.

6.5 Comparison with Other Work

By comparing the parameters estimated from the data collected with equivalent parameters published by other workers a measure of confidence could be developed in the fluorescent particle counter as a means of measuring atmospheric dispersion. Such a comparison was found to be problematic in that firstly

Table 6.1: The best set of eddy diffusivities estimated by fitting the fluctuating wind dispersion model to the data collected during the field trial of the fluorescent particle counter

Field Test	Time	Fitted Parameters		Wind velocity (m/s)
		Q(particles)	K(m^2/s)	
1	61 -120	1,64 x10^7	6,04	4,1
1	121 -180	2,95 x10^7	6,98	5,1
1	181 -240	2,83 x10^7	6,95	6,0
1	241 -300	2,02 x10^7	9,57	5,9
1	301 -360	1,03 x10^7	11,02	6,1
1	901 -960	0,97 x10^7	2,08	3,7
1	961 -1020	0,39 x10^7	6,69	2,7
1	1141 -1200	0,51 x10^7	8,03	4,4
2	121 -180	1,09 x10^7	8,57	3,8
3	601 -660	1,92 x10^7	4,61	2,5
3	661 -720	1,15 x10^7	1,84	3,2

much of the reported work deals with the measurement of the spreading coefficients in the guassian plume model and not the eddy diffusivities in the K-theory model which was the subject of this work. Secondly most of the reported work relates to distances of the order of hundreds and thousands of metres whereas this work was carried out over a distance of 19,5m making it necessary to extrapolate the reported data backwards with some loss of accuracy.

Before embarking on the comparisons the equivalence between the spreading coefficients and the eddy diffusivities is as follows:

$$\sigma_y^2 \equiv \frac{2 K_y x}{u} \qquad \text{(6.1)}$$

6.5.1 Comparison with the Work of Venter (79,80)

Venter and his co-workers measured atmospheric dispersion over distances of between 157m and 915m on the Transvaal Highveld in South Africa. His results enabled him to correlate the Sutton

dispersion parameters with atmospheric stability. He reports the following correlations :

$$n = 0{,}04 \frac{dT}{dz} + 0{,}37 \qquad \text{(6.2)}$$

$$C_y = 0{,}57n + 0{,}106 \qquad \text{(6.3)}$$

$$C_z = 0{,}38n + 0{,}112 \qquad \text{(6.4)}$$

where $\frac{dT}{dz}$ is the vertical temperature gradient

and n is the index in the equation :

$$2\sigma_i^2 = C_i^2 x^{2-n} \quad i = y, z \qquad \text{(6.5)}$$

Equation 6.5 and the equivalence between K_y and σ_y given by equation 6.1 leads to the following result for K_y

$$K_y = \frac{C_y^2 x^{1-n} u}{4} \qquad \text{(6.6)}$$

Table 6.2 lists the form of K_y for different stability classes, and for x = 19,53m.

Table 6.2 : Values of n and C_y for different stability classes. Taken from Venter (79,80)

Stability Class	dT/dz	n	C_y	K_y
Stable	0,5	0,57	0,43	$K_y = 0.166\ u$
Neutral	0	0,37	0,32	$K_y = 0,166\ u$
Unstable	-0,5	0,17	0,20	$K_y = 0.118\ u$

The comparison between the equivalent K_y from Venter's work and the K_y measured in this work is shown in figure 6.2 as a function of wind velocity. Clearly K_y estimated in this study exceeds the K_y derived from Venter's work by up to six times. Venter does make the point in his paper however that his results really only apply to neutral atmospheric conditions, and cautions against the use of his results for other stability conditions.

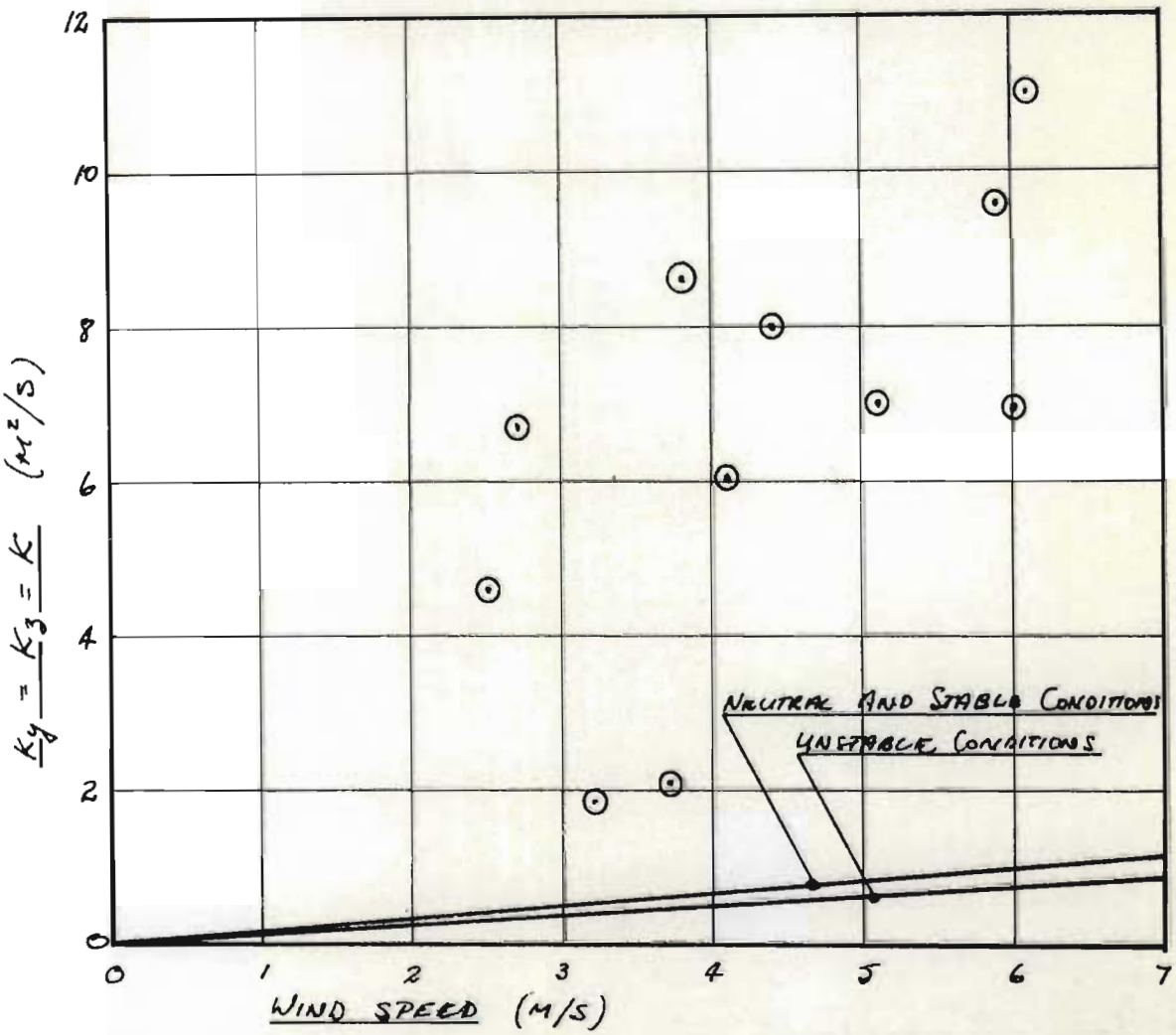

Figure 6.2: **Eddy diffusivities** estimated from the field trial data compared with **eddy diffusivities derived from** the work by Venter, Halliday and Prinsloo (79). ⊙ - data from this study.

6.5.2 Comparison with the Work of Singer et al (66,67,68).

In 1966 Singer, Frizzola and Smith published formulae to enable the spreading coefficients to be estimated from non-ideal meteorological data. The formulae are published for two broad atmospheric stability conditions, namely stable and unstable. Since the magnitude of σ_z is usually similar but slightly less than the magnitude of σ_y it is convenient to consider only σ_y in this discussion. The equations given by Singer et al follow :

$$\sigma_y = 0{,}15\,\sigma_\theta\, x^{0{,}71} \qquad \text{stable case -(6.7)}$$

$$\sigma_y = 0{,}045\,\sigma_\theta\, x^{0{,}86} \qquad \text{unstable case -(6.8)}$$

Crude approximations for σ_θ are given as :

$$\sigma_\theta = 2^\circ \qquad \text{stable case -(6.9)}$$

and

$$\sigma_\theta \Big|_{100} = \frac{23}{u} + 4{,}75 \qquad \text{unstable case -(6.10)}$$

where the subscript indicates that this formula applies only at an elevation of 100m above ground level. The authors also detail the method by which equation 6.10 may be extrapolated to an elevation of 2m above ground level to give :

$$\sigma_\theta\Big|_z = \frac{23}{u} + 12{,}63 \qquad (6.11)$$

Thus for a stable atmosphere equations 6.7, 6.9 and 6.1 may be combined to yield for x = 19,53m

$$K_y = 0{,}16\,u \qquad (6.12)$$

and for an unstable atmosphere equations 6.8, 6.11 and 6.1 may be combined to yield for x = 19,53m.

$$K_y = \left(\frac{13{,}33}{u} + 7{,}32\right)^2 \frac{u}{39{,}06} \qquad (6.13)$$

A table given by J H Seinfeld (64) also enables a different result to be obtained from equations 6.7 and 6.8. This table, reproduced as table 6.3,

gives approximate σ_θ to each atmospheric stability class :

Table 6.3 : Variance of the wind azimuth as a function of stability class. From Seinfeld (64).

STABILITY DESCRIPTION	CLASS	σ_θ (deg)
Extremely unstable	A	25
Moderately unstable	B	20
Slightly unstable	C	15
Neutral	D	10
Slightly stable	E	5
Moderately stable	F	2,5

These figures together with equations 6.7, 6.8 and 6.1 yield the following formulae for K_y :

stability class B : $K_y = 3,44u$ (6.14)

stability class D : $K_y = 0,86u$ (6.15)

stability class F : $K_y = 0,14u$ (6.16)

Equations 6.12 to 6.16 are compared with the data from this study in figure 6.3. Clearly K_y estimated from this study falls within the range of values suggested by Singer et al.

6.5.3 Comparison with the Work of Pasquill-Gifford (64).

Pasquill and Gifford each presented a set of empirical correlations in graphical form for σ_y and σ_z which were reproduced by Seinfeld (64). Although these graphs start at a distance of 100m the correlations for σ_y can, by simple geometry, by extrapolated back to a distance of 20m. Again because σ_z is shown to be generally smaller than σ_y for distances of this order, only σ_y will be considered. These extrapolations together with equation 6.1 yield the formulae for K_y recorded in table 6.4 and are compared

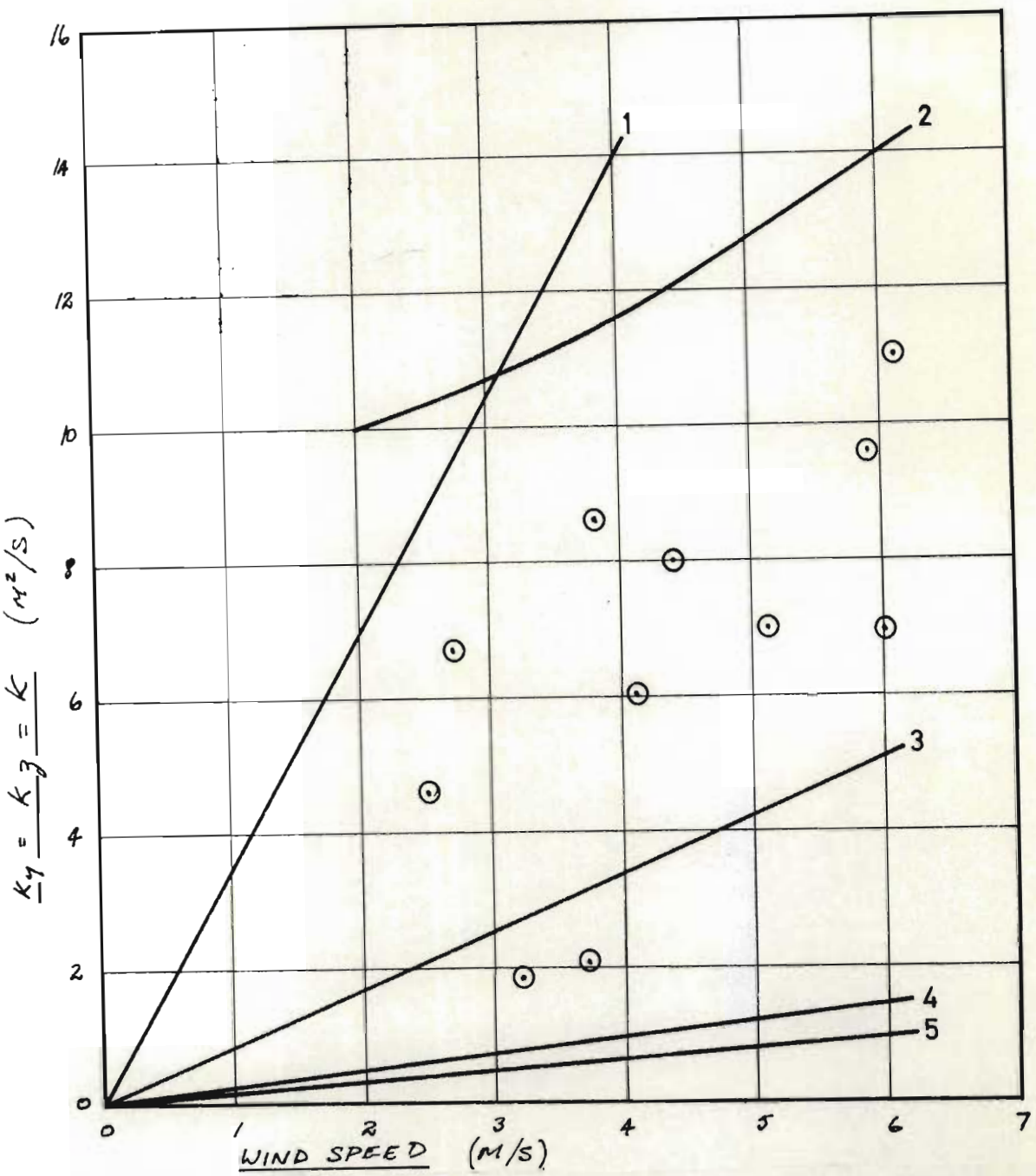

Figure 6.3: **Eddy diffusivities** estimated from the field trial data compared with **diffusivities derived from the** work of Singer and Smith (66,67,68) using their own atmospheric stability criteria, and also using stability criteria attributed to Gifford and reported by Seinfeld (64). With Singer and Smith's stability criteria: 2 - unstable; 5 - stable. With Gifford's stability criteria: 1 - moderately unstable; 3 - neutral; 4 - moderately stable; ⊙ - data from this study.

Table 6.4 : Values of K_y for selected stability classes extrapolated from the Pasquill-Gifford curves (64).

Stability Class	σ_y, extrapolated	K_y
A	6,0	K_y = 0,92 u
B	4.0	K_y = 0,41 u
D	1.95	K_y = 0,097 u
F	0.95	K_y = 0,023 u

with the K_y from this study in figure 6.4. Clearly the K_y from this study are greater than the equivalent values from the Pasquill-Gifford correlations but not by a large margin.

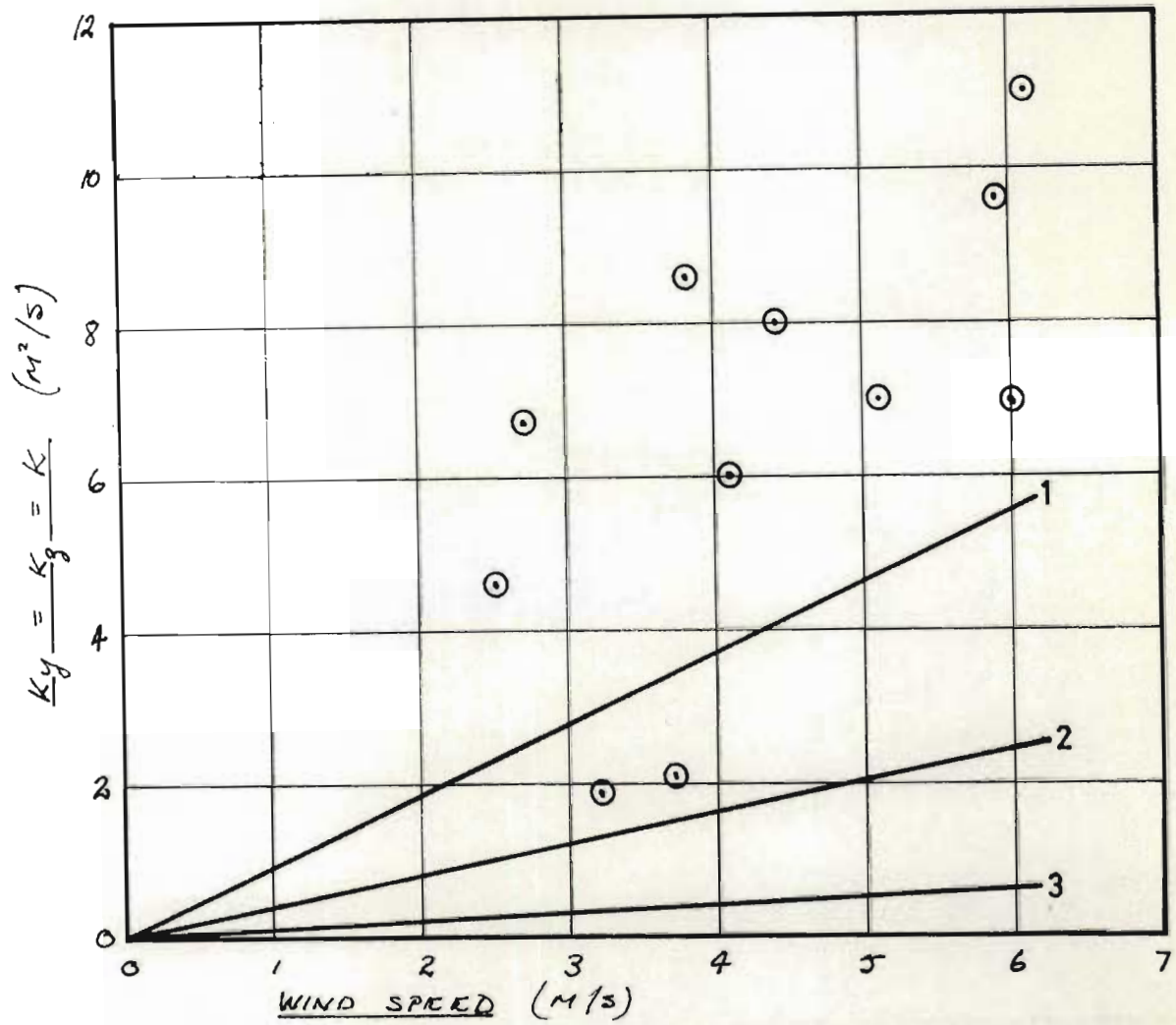

Figure 6.4: **Eddy diffusivities** estimated from the field trial data compared with **diffusivities derived from the** Pasquill-Gifford curves reported by Seinfeld (64). 1 - extremely unstable; 2 - moderately unstable; 3 - neutral; ⊙ - data from this study.

CHAPTER SEVEN: CONCLUSION

With the conventional method of measuring atmospheric dispersion, that is by means of time-mean samples, it is virtually impossible to obtain information about the temporal variation in concentration and, in addition, it is difficult to obtain meaningful data at very low wind speeds under stable atmospheric conditions. To overcome these shortcomings a new instrument has been developed which measures the concentration of a particular tracer (fluorescent pigment) in the atmosphere continuously and automatically, and records the information in real-time.

In principle the new instrument operates by continuously irradiating with ultra-violet light a stream of sampled air which is drawn into the instrument, and simultaneously monitoring the stream for any fluorescence of a yellow colour which may emanate from particles of FP2267 present in the air. Each particle which is detected is counted and the total number of particles occurring in consecutive two second intervals is recorded on tape.

The new instrument as built can assess concentrations of

fluorescent particles in the atmosphere in the range $6,0x10^2$ to $4x10^5$ per m^3, and can operate unattended for periods in excess of twelve hours. As the data collected by the new instrument is recorded on tape it is a simple matter to transfer this information to a computer, thus eliminating the need for a tedious manual counting operation, and making it possible to devote greater effort to the analysis of the data.

The new instrument was calibrated in the laboratory in a specially developed rig comprising a large bore pipe (150mm I.D.) through which a large volume of air was drawn. The tracer was injected continuously at the entrance to the pipe and then sampled at some distance downstream. The performance of the rig itself was checked by measuring the velocity and concentration profiles across the pipe and these were found to conform to the expected profiles for fully developed turbulent flow. In addition a measurment of the number density of the fluorescent pigment was found to agree closely with the result given by Leighton et al (32).

To calibrate the fluorescent particle counter some 68 samples were taken and the number of light pulses counted by

the instrument correlated with the actual concentration of particles in the sample by the formula:

$$A = 4{,}21\ B^{1{,}45}$$

where A is the concentration (particles/m^3) and B the electronic counting rate (pulses/minute).

The correlation between the electronic count and the actual concentration did not turn out to be linear as might have been expected owing probably to the interference by electronic noise at low counting rates, and to the possible coincidence of more than one particle in the view volume at high counting rates.

Although very similar in concept to an instrument described in the literature by Goldberg (25) the present instrument does not have the optical complexity of Goldberg's instrument. Beyond the physical similarity it is very difficult to draw any comparison with Goldberg's instrument regarding its performance as Goldberg did not report a rigorous calibration nor has he reported the use of his instrument in any atmospheric dispersion work. Goldberg does however claim a lower detection limit of 100 particles/m^3, but this is doubtful as it appears to coincide with the background noise level he quotes. At three times the background noise level Goldberg's lower detection limit is therefore more probably in the region of 300 particles/m^3.

As a final test of the fluorescent particle counter it was tested in the field by actually measuring atmospheric dispersion over a distance of about 20 meters. The site chosen for this field test was not ideal being on the crest of a hill and therefore subject to a lot of turbulence, nevertheless the data collected made it possible to estimate the atmospheric dispersion parameters. Out of about 41 hours of operation some 37 hours of useful data was collected.

As there are practical difficulties associated with the use of Gifford (22) and Csanady's (10) fluctuating plume models the K-theory model of dispersion from a continuous point source was modified strictly for the purpose of this work. Essentially a plume is regarded as comprised of segments each of which travels in a straight line from the source parallel with the instantaneous wind direction at the source. As a test of the model the profile of peak-to-mean concentration across the wind was computed and was found to have a shape similar to that actually measured and published by Ramsdell and Hinds (54).

The modified dispersion model was fitted to 13 sets of data selected from the total of 37 sets of data accumulated from the fluorescent particle counter. The parameters estimated were the eddy diffusivities K_y and K_z. Unfortunately as the dispersion model is written K_y and K_z

interact very strongly and can therefore not be estimated independently in this way, a fact supported by the statistics of the regression. A much more precise estimate was therefore obtained by equating the eddy diffusivities and estimating a single diffusivity. Improved results were also obtained by estimating the tracer release rate by regression instead of fixing this parameter at the set point on the aerosol generator. Problems were experienced with the aerosol generator during the field trial and the actual release rate may well have been less than the set point release rate.

Finally the estimated values for the eddy diffusivities were compared with values extrapolated from work published by Venter (79,80), Singer (66,67,68) and Pasquill-Gifford (64). Although there is a fairly considerable lack of agreement between the results from each of these workers their results were found to be within an order of magnitude of the results from the present work.

In conclusion the fluorescent particle counter should make it possible to study the fluctuating nature of atmospheric dispersion in greater detail than was previously possible, and will also make it possible to study dispersion under stable atmospheric conditions more successfully.

REFERENCES

1) Abramowitz M. and Stegun I.A. - " Handbook of Mathematical Functions", Dover Publications Inc. New York (1964)

2) Badzioch S. - "Collection of Gas-Borne Dust Particles by Means of an Aspirated Sampling Nozzle", Brit. J. Appl. Phys. 10, 26 (1959)

3) Bierly K.W. and Gill G.C. - "A Technique for Measuring Atmospheric Diffusion", J. Appl. Meteor. 2, 145 (1963)

4) Bierly E.W. and Hewson E.W. - "Atmospheric Diffusion Studies near a Lake Shore", J. Appl. Meteor. 2 , 390 (1963)

5) Braham R.R., Seely B.K. and Crozier W.D. - " A Technique for Tagging and Tracing Air Parcels", Amer. Geophysical Union, Trans. 33, 825 (1952)

6) Brown R.M., et al. - "Diffusion Measurements in the 10-100km Range", J. Appl. Met. 11, 323 (1972)

7) Clemons C.A., Cockman A.I. and Saltzman C.E. - "Concentration and Ultrasensitive Chromatographic Determination of Sulphur Hexafluoride for Application to Meterological Tracing", Environ. Science and Technol. 2, 551 (1968)

8) Cluck J.W., Adams W.S. and Moroz W.T. - " A Portable Battery Operated Airborn Particle Counter and Size Analyser", ISA Transactions, 12, 208, (1973)

9) Collins F.C. et al. - "A Preliminary Evaluation of Gas Air Tracers", J. Air Poll. Contr. Assoc. 15, 109 (1965)

10) Csanady G.T. - "Dosage Probabilities and Area Coverage from Instantaneous Point Sources at Ground Level", Atmos. Environ. 3, 25 (1969)

11) Davies O.I. and Goldsmith P.L. - "Statistical Methods in Research and Production", Longman Group Ltd. (1976)

11a) Davidson B. and Halitsky J. - "A Method of Estimating the Field of Instantaneous Ground Concentration from Tower Bivane Data", J. Air Poll. Contr. Assoc. 7 , 316 (1958)

12) Drivas P.J and Shair F.H. - "A Tracer Study of Pollutant Transport and Dispersion in the Los Angeles Area", Atmos. Environ. 8, 1155 (1974)

13) Drivas P.J. and Shair F.H. - "Probing the Air Flow within the Wake Downwind of a Building by means of a Tracer Technique", Atmos. Environ. 8, 1165 (1974)

14) Droessler E.G. et al. - "A Stratospheric Air Tracer Experiment Using Zinc Sulfide", J. Appl. Meteor. 6, 373 (1967)

15) Dumbauld R.K. - "Meteorological Tracer Techniques for Atmospheric Diffusion Studies", J. Appl. Meteor. 1, 437 (1962)

16) Brochure No. P001/fP70 + Supplement No. P.001S/a72. - "Photomultiplier Tubes". E.M.I. Electronics Ltd., Electron Tube Division, 243 Blyth Rd., Hayes, Middlesex UB3 1HJ, England.

17) Fisher B.E.A. - "The Long Range Transport of Sulphur Dioxide", Atmos Environ. 9,1063 (1975)

18) Forestall W. and Shapiro A.H. - "Momentum and Mass Transfer in Coaxial Gas Jets", J. Appl. Mech. 17, 399 (1950)

19) Fuquay J.J. et al. - "Results of Recent Field Programs in Atmospheric Diffusion", J. Appl. Meteor. 2, 122 (1963)

20) Fuquay J.J. et al. - "Prediction of Environmental Exposures from Sources Near the Ground Based on Hanford Experimental Data", J.Appl. Meteor. 3, 761 (1964)

21) Gallant A.R. - "Nonlinear Regression", The American Statistician 29, 73 (1975)

22) Gifford P. - "Statistical Properties of a Fluctuating Plume Dispersion Model", Advances in Geophysics 6, 117 (1959)

23) Gifford F. - "Peak to Average Concentration Ratios According to a Fluctuating Plume Dispersion Model", Int. J. Air Poll. 3, 253 (1960)

24) Gifford F.A. - "Diffusion in the Diabatic Surface Layer", J. of Geophysical Res. 67, 3207 (1962)

25) Goldberg L.J. - "Application of the Microaerofluorometer to the Study of Dispersion of a Fluorescent Aerosol into a Selected Atmosphere", J. Appl. Meteor. 7, 68 (1968)

26) Gosline C.A. - "Dispersion from Short Stacks", Chem. Eng. Progr. 48, 165 (1952)

27) Hay J.S. and Pasquill F. - "Diffusion Experiments from a Fixed Source at a Height of a Few Hundred Feet in the Atmosphere", J. Fluid. Mech. 2, 299 (1957)

28) Hilst G.R. - "The Dispersion of Stack Gases in Stable Atmospheres", J. Air Poll. Contr. Assoc. 7, 205 (1957)

29) Himmelblau D.M. - "Process Analysis by Statistical Methods", John Wiley & Sons Inc. (1970)

30) Hosey A.D. et al. - "Evaluation of an Aerosol Photometer for Dust Counting and Sizing", Am. Ind. Hyg. Assoc., J. 21, 491 (1960)

31) Kingslake R. (ed) - "Applied Optics and Optical Engineering" Vol. I, Academic Press. (1965)

32) Leighton P.A. et al. - "The Fluorescent Particle Atmospheric Tracer", J. Appl. Meteor. 4, 334 (1965)

33) Levi L.-"Applied Optics: A Guide to Modern Optical System Design", John Wiley & Sons Inc. (1968)

34) Lewis G.P.-"Discussion: Fluorescent Particle Atmospheric Tracer", Atmos. Environ. 7, 659 (1973)

35) Ludwick J.D. - "Atmospheric Diffusion Studies with Fluorescein and Zinc Sulfide Particles as Dual Tracers", J. Geoph. Res. 71, 1553 (1966)

36) Ludwick J.D. and Perkins R.W. - "Liquid Scintillation Techniques Applied to Counting Phosphorescence Emission, Measurement of Trace Quantities of Zinc Sulfide", Anal. Chem. 33, 1230 (1961)

37) Map. Nos. M37C and M37D from University Campus Series, Dept. of Survey, University of Natal, King George V Ave., Durban.

38) Martens A.E. and Keller J.D. - "An Instrument for Sizing and Counting Airborne Particles", Am. Ind. Hyg. Assoc., J. 29, 257 (1968)

39) Martin A. and Barber F.R. - "Further Measurements around Modern Power Stations - I - III", Atmos. Environ. 7, 17 (1973)

40) McElroy J.L. - "A Comparative Study of Urban and Rural Dispersion", J. Appl. Meteor. 8, 19 (1969)

41) Mitchell R.S. - "Discussion: Fluorescent Particle Atmospheric Tracer: Toxicity Hazard", Atmos. Environ. 7, 589 (1973)

42) Murray J.A. and Vaughan L.M. - "Measuring Pesticide Drift at Distances to Four Miles", J. Appl. Meteor. 9, 79 (1970)

43) Nickola P.W. - "Measurements of the Movement, Concentration and Dimensions of Clouds Resulting from Instantaneous Point Sources", J. Appl. Meteor. 10, 962 (1971)

44) Nickola P.W. et al. - "An Inert Gas Tracer System for Monitoring the Real-Time History of a Diffusing Plume or Puff", J. of Appl. Meteor., 9, 621, (1970)

45) Nickola P.W. et al. - "A System for Recording Air Concentration of Zinc Sulfide Fluorescent Pigment on a Real-Time Scale", J. Appl. Meteor. 6,430 (1967)

46) Niemeyer L.E. and Mc Cormick R.A. - "Some results of Multiple-Tracer Diffusion Experiments at Cincinnati", J. Air Poll. Contr. Assoc. 18, 403 (1968)

47) Nordberg G. - "Discussion : Fluorescent Particle Atmospheric Tracer : Toxicity Hazard", Atmos. Environ. 7, 590 (1973)

48) Pasquill F. - "Atmospheric Diffusion", 2nd edn., D. van Nostrand Co. Ltd., London (1974)

49) Perkins W.A. et al. - "A Fluorescent Atmospheric Tracer Technique for Mesometeorological Research", Proc. Second National Air Pollution Symposium, California (1952)

50) Perry J.H. - "The Chemical Engineers Handbook", 4th Edn. Mc Graw-Hill Book Co. (1963)

51) Pooler F. - "A Tracer Study of Dispersion over a City", J. Air Poll. Contr. Assoc. 16, 677 (1966)

52) Porter D.W. - "The Nelder and Mead Simplex Procedure and its Application to Non Linear Least Squares Fitting", Imperial Chemical Industries Report No. A 127, 181 (1968)

53) Pringsheim P. - "Fluorescence and Phosphorescence", Interscience New York (1949)

54) Ramsdell J.V. and Hinds W.T. - "Concentration Fluctuations and Peak-to-Mean Concentration Ratios in Plumes from a Ground-Level Continuous Point Source", Atmos. Environ. 5, 483 (1971)

55) Rankin M.O. - "Zinc Sulphide Particle Detector", U.S. Atomic Energy Commission, HW-55917(1958)

56) Raynor G.S. et al. - "Dispersion and Deposition of Ragweed Pollen from Experimental Sources", J.Appl. Meteor. 9, 885 (1970)

57) Raynor G.S. et al. - "Mesoscale Transport and Dispersion of Airborne Pollens", J. Appl. Meteor 13, 87 (1974)

58) Record F.A. and Cramer H.E. - "Preliminary Analysis of Project Prairie Grass Diffusion Measurements", J. Air Poll. Contr. Assoc. 8, 240 (1958)

59) Roberts O.F.T. - "The Theoretical Scattering of Smoke in a Turbulent Atmosphere", Proc. Roy. Soc. (London A 104, 640 (1923)

60) Robinson E. et al. - "A Meteorological Tracer Technique Using Uranine Dye", J. Meteor. 16, 63 (1959)

61) Saltzman B.E. et al. - "Halogenated Compounds as Gaseous Meteorological Tracers.", Anal. Chem. 38, 753 (1966)

62) Schulz E.J. et al - "A Tracer Technique to Measure Deposition of Stack Emissions", Amer. Ind. Hyg. Assoc. J. 21, 343 (1960)

63) Scriven R.A. and Fisher B.E.A. - "The Long Range Transport of Airborne Material and its Removal by Deposition and Washout - II. The Effect of Turbulent Diffusion", Atmos. Environ. 9, 59 (1975)

64) Seinfeld J.H. - "Air Pollution", McGraw'Hill Book Co. (1975)

65) Sinclair D. - " A New Photometer for Aerosol Particle Size Analysis", J. Air Poll. Contr. Assoc. 17, 105 (1967)

66) Singer I.A. - "The Relationship between Peak and Mean Concentrations", J. Air Poll. Contr. Assoc. 11,336 (1961)

67) Singer I.A. et al. - "A Simplified Method of Estimating Atmospheric Diffusion Parameters", J. Air. Poll. Contr. Assoc. 16, 594 (1966)

68) Singer I.A. and Smith M.E. - "Atmospheric Dispersion at Brookhaven National Laboratory", Air and Water Poll. Int. J. 10, 125 (1966)

69) Spomer L.A. - "Fluorescent Particle Atmospheric Tracers : Toxicity Hazard", Atmos. Environ. 7, 353 (1973)

70) Stampfer J.F. and Anderson J.A. - "Locating the St. Louis Urban Plume at 80 and 120 km and Some of its Characteristics", Atmos. Environ. 9, 301 (1975)

71) Starkey J.R. - "Fluorescent Particle Analyser - Operating Manual", Project No. EL. 399 Atomic Energy Board, Pelindaba, Pretoria, Republic of South Africa.

72) Stewart N.G. et al - "The Atmospheric Diffusion of Gases Discharged from the Chimney of the Harwell Reactor BEPO". Int. J. of Air Poll. 1, 87 (1958)

73) Stewart R.E. - Atmospheric Diffusion of Particulate Matter Released from an Elevated Continous Source", J. Appl. Meteor. 7, 425 (1968).

74) Strauss W. (ed.) - "Air Pollution Control - Part 1", Wiley Interscience (1971)

75) Strom L. - "Transmission Efficiency of Aerosol Sampling Lines", Atmos. Environ. 6, 133 (1972)

76) Toby G.E., Graeme J.G. and Huelsman C.P. - "Operational Amplifiers - Design and Applications", McGraw-Hill Book Co. (1971)

77) Turner D.B. - "A Diffusion Model for an Urban Area", J. Appl. Met. 3, 83 (1964)

78) Van Buijtenen C.J.P. and Clarenburg L.A. - "Phosphorescence Microscopy : A Simple Automatic Counting Device for Phosphorescent Particles", Particle Size Analysis Conference (1966)

79) Venter G.P.N., Halliday E.C. and Prinsloo L.A. - "The Determination of the Sutton Diffusion Parameters for the Highveld of S.A.", Atmos. Environ. 7, 593 (1973)

80) Venter G.P.N. - "'n Ondersoek na die Gebruik van die Sutton Diffusie-Parameters", Report No. APRG/71/2, Council for Scientific and Industrial Research, Pretoria. South Africa.

81) Waldron A.W. - "The Application of an Elevated Line Source Diffusion Formula", J. Appl. Meteor. 2, 740 (1963)

82) Walker E.R. - "A Particulate Diffusion Experiment", J. Appl. Meteor. 4, 614 (1965)

83) Wedin B. et al. - "Comparison of Concentration Measurements of Sulphur Dioxide and Fluorescent Pigment", Advances in Geophysics 6, 425 (1959)

84) Zinky W.R. - "A New Tool for Air Pollution Control : The Aerosol Particle Counter", J. Air Poll. Contr. Assoc. 12, 578 (1962)

85) Hanna S.R. - "Concentration Fluctuations in a Smoke Plume", Atmos. Environ. 18, 1091 (1984)

86) Hanna S.R. (Environmental Research and Technology Inc., 696 Virginia Road, Concord, Massachusetts 01742, U.S.A.): letter to the author dated 18th June (1985).

APPENDIX A: CIRCUIT DIAGRAMS AND TECHNICAL SPECIFICATIONS OF SUBSIDIARY EQUIPMENT USED WITH THE FLUORESCENT PARTICLE COUNTER

A.1. D.C. Power Supply for HBO 200W/2 Mercury Lamp :

The block diagram, figure A.1, shows the power supply to consist essentially of three main parts: the smoothing circuit, the lamp ignition circuit and a current regulator. The detailed circuit diagram is shown in figure A.2. Mains (220 V A.C.) is transformed down to 77 volts and converted to D.C. through a bridge rectifier B1. Smoothing is provided by capacitors C1 and C2 connected in a II network. R1 is a smoothing and ballast resistor and is shown split in two but is actually a single resistor with a centre tap. This was necessary to prevent capacitor C2 from discharging instantaneously through the lamp and hence destroying it. The lamp igniter supplied by the lamp manufacturers, is connected permanently into the circuit and is operated by

push button. The current regulator consisting of transistors T1, T2 and T3 is short circuited at start up by switch S2 which also enables the igniter to be operated and isolates the ammeter. At start up the lamp draws up to 7 amps in order to warm up quickly. As the lamp warms up the internal resistance rises and the current drops to near its normal operating point of 3,5 amps. By switching S2 the regulator and ammeter are activated and the igniter disabled.

The current regulator is an emitter-follower type circuit and makes use of the inherent feed-back control feature of a transistor. By fixing the base potential to the required level a transistor will then control the current through the collector-emitter circuit to equalise the emitter and base potentials. In this regulator T1 is a booster transistor connected as a Darlington pair with each of the power transistors T2 and T3. The control potential is taken from the preset potentiometer P1 and applied to the base of T1.

When the mains power is switched on capacitor C1

appears as a dead short to the rectifier B1 hence resistor R2 was provided as protection. R2 is switched out of circuit by relay L7 as soon as the potential across C1 has built up to 70% of its normal operating level. Relay L2 ensures that the hourmeter only runs while the lamp is actually burning by sensing the potential difference across R1.

The circuit gave trouble-free service but suffered a little thermal drift while warming up, no doubt due to the rather simple design of regulator. The specifications for the circuit, which conform to those laid down by the lamp manufacturer, are :-

No load potential	- 110 volts
Starting potential (minimum)	- 15 volts
Starting current (maximum)	- 7 amps.
Normal operating potential	- 57 volts
Normal operating current	- 3,5 amps.
Igniter potential	- 30 000 volts (R.F.)
Current regulation	- better than 0,1%
Current adjustment	- 3,1 to 3,9 amps.
Power consumption	- 250 watts.
Power requirements	- AC 220 volts $\pm$ 10%

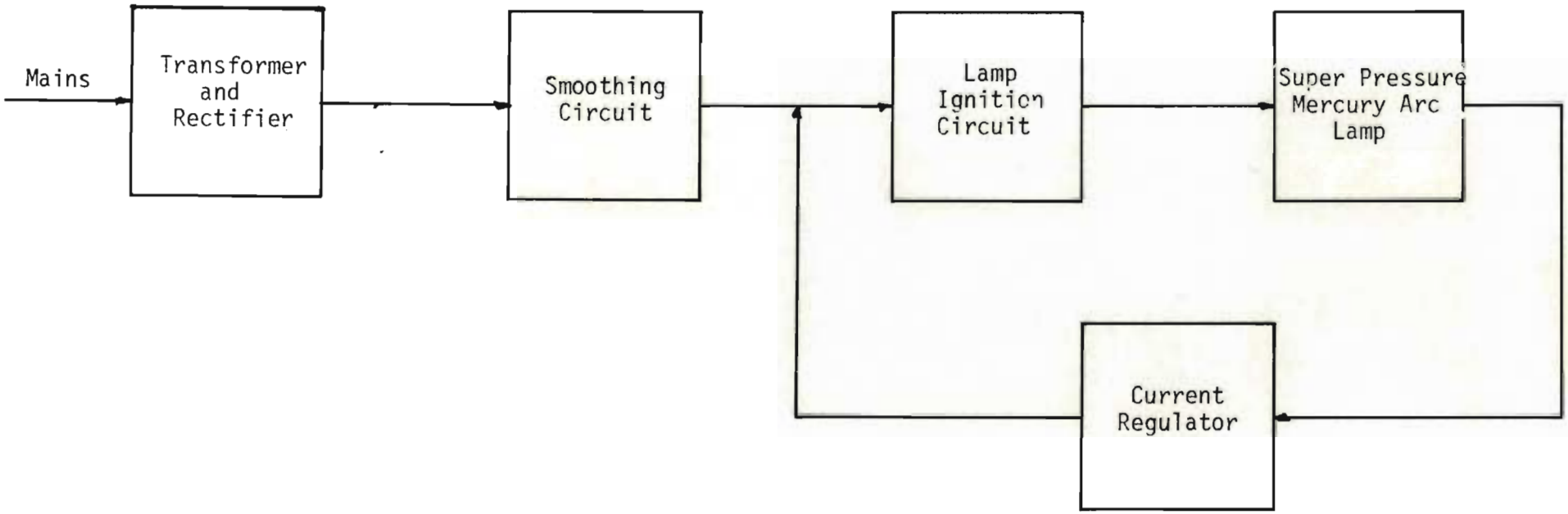

Figure A.1: Block diagram of the D.C. power supply for the HBO 200W/2 high pressure mercury lamp

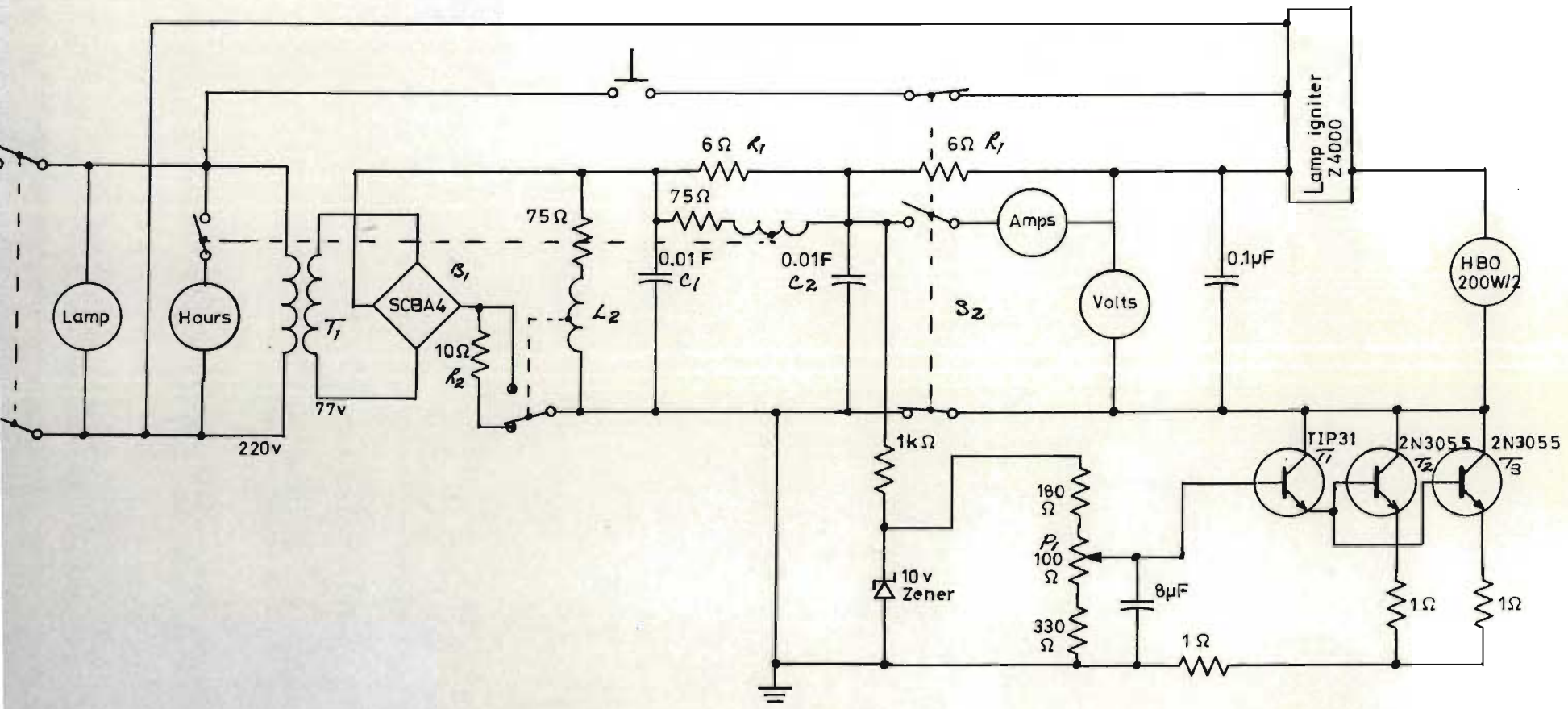

igure A.2: Circuit diagram for the D.C. power supply for the HBO 200W/2 high pressure mercury lamp

A.2 High Voltage Power Supply

The unit used was supplied by EMI and the following specifications accompanied the unit:

Model	PM 25A
Output Voltage	100 to 2500 V
Polarity	Positive or negative w.r.t. chassis by connection of output socket.
Maximum Current	5 mA.
Overload Protection	Current limit at 6 mA, autoreset. Foldback to approx. 2.5 mA on short circuit. Lamp indicates limiting.
Load Regulation	10 ppm from a no load to a full load change.
Line Regulation	10 ppm for a 10% change of mains voltage.
Ripple and Noise	2 mV peak to peak.
Meter	70 mm (2.75 in.). Scale length accuracy 3%.
Mains Supply	200 to 250 V or 100 to 125 V, 48 to 66 Hz. 50 VA @ 240 V rms ac.
Resolution	110 mV (200 volt steps + 3-turn pot.)
Accuracy (with variable control at zero)	1%
Accuracy of fine control	3% of indication
Temperature Coefficient	100 ppm/°C typ.
Drift with time (at constant line, load, and temperature)	50 ppm/hr typ. 100 ppm/day typ.
Output voltage float potential w.r.t. chassis (either terminal)	250 V dc max.
Maximum ambient temp. Working Storage	 45°C 70°C
Net Weight	3.6 Kg (8 lb).
Output connector	Belling Lee L1390 series
Output Lead	UR 70

A.3 Photomultiplier Dynode String

Figure A.3 shows a circuit diagram for the photomultiplier dynode string and the preamplifier. This design was taken from the E.M.I. photomultiplier brochure (ref : P001/fP70) and is described as a "Standard High Gain, High Current" design. All the resistors were 2% hi-stability resistors. It was found necessary to use very high quality polyester capacitors for C1 and C2 to prevent leakage currents.

When light strikes the cathode photoelectrons are emitted which are amplified across the dynodes to the anode which goes negative and draws a current through the anode load resistor. If the duration of the light is very short the resultant voltage pulse is transmitted via the decoupling capacitor to the operational amplifier A1. R2 provides a bias current to the positive side of the amplifier and R3 compensates for the bias voltage introduced by R2. The amplifier A1 is a field effect transistor with very low bias current and fast response.

It is connected as a unity gain voltage follower and successfully isolates the anode circuitry from any subsequent circuitry.

The anode of a photomultiplier may be viewed as a perfect current source, and this poses a problem in the laboratory where most recording equipment is designed to take a voltage signal. The unity gain voltage follower therefore provided an effective way of overcoming this problem.

In order to avoid noise pick-up between the anode and amplifier this whole circuit was sealed into the photomultiplier base. The high voltage was provided by the power supply described in appendix A.2 and the low voltage was provided from the buffer amplifier to be described in appendix A.4. For the purpose of this work the photomultiplier was used as a pulse counter and so the anode was charged to 1200 volts and the cathode grounded. This leads to simpler construction as all objects in contact with the tube envelope are at ground potential.

An antimagnetic shield tied to the cathode potential provided magnetic and electrostatic protection for the tube.

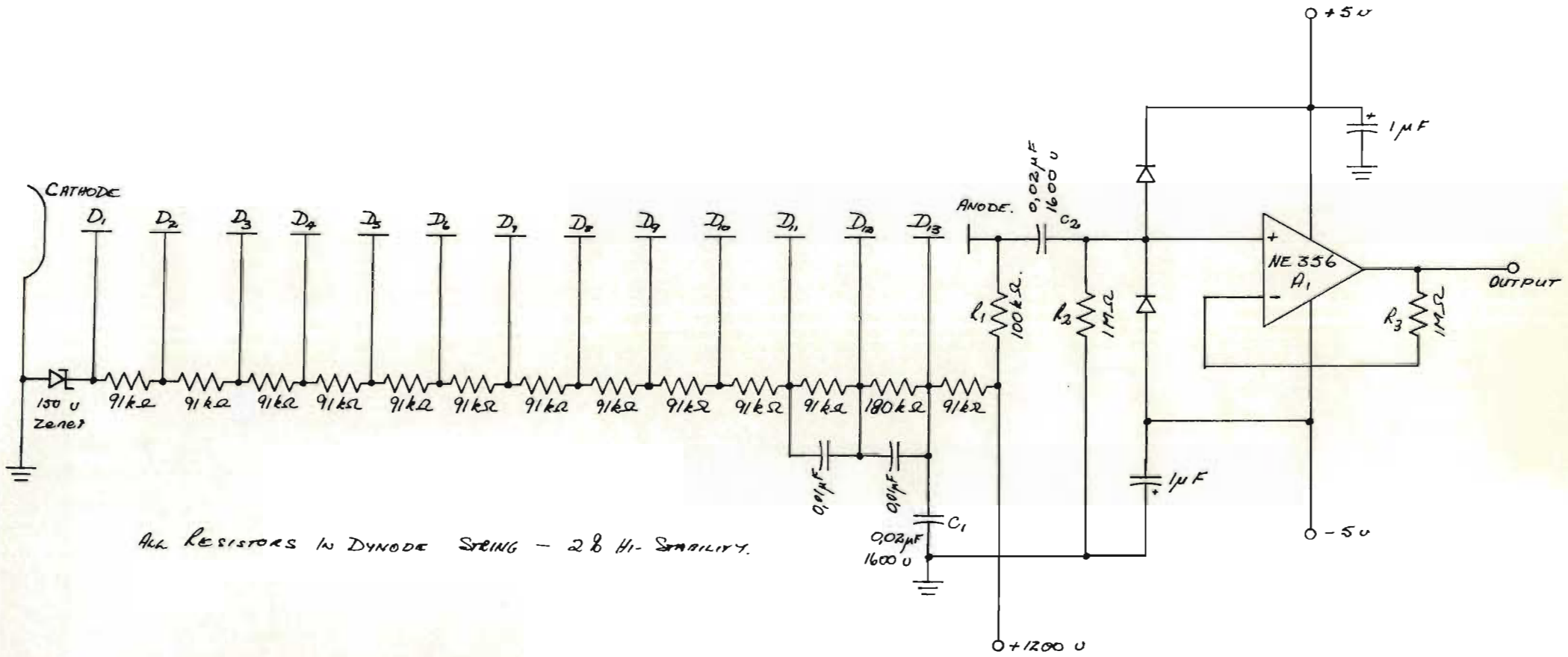

Figure A.3: Circuit diagram for the photomultiplier dynode string and voltage follower

A.4 The Buffer Amplifier

Figure A.4 shows the circuit diagram of the buffer amplifier. R1 and C1 form an integrator with a time constant of 102 μs. This is followed by a unity gain voltage follower A1 which, in turn, is followed by an inverting amplifier A2 with a gain of about 2,6. Amplifier A2 also forms a summing block where a small offset voltage is added in order to cancel the slight offset from all the preceding circuitry.

The smooth output from this amplifier is shown in figure 3.14(d) which shows a typical pulse arising from the passage of a fluorescent particle through the view volume of the FPC.

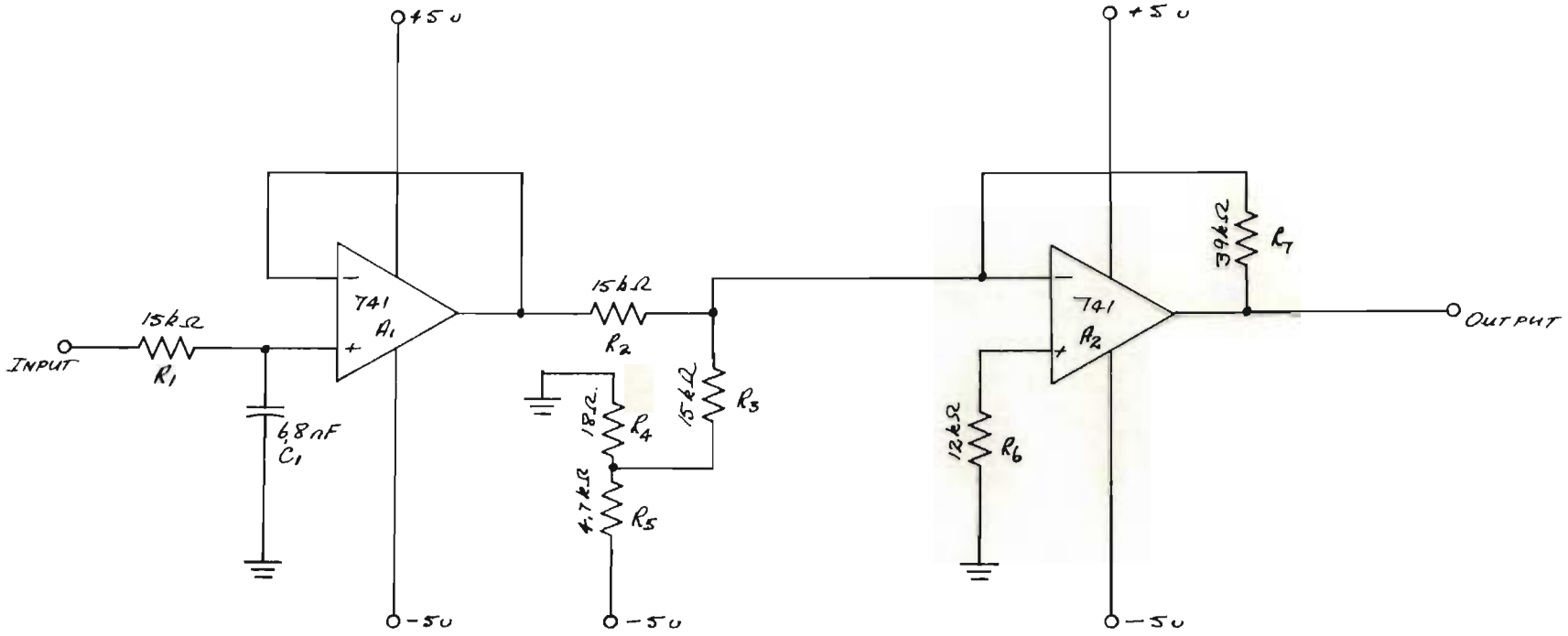

Figure A.4: Circuit diagram for the buffer amplifier

A.5. The Fluorescent Particle Analyser (FPA)

The operation of this unit, which was designed and built by the Atomic Energy Board, has already been outlined in section 3.4.3. The circuits for this unit are complex and will not be reported here, however they may be acquired by writing for report No. I/TN/25/74 on unit No EL.399 from the Atomic Energy Board, Pelindaba, Republic of South Africa.

It is important to note certain modifications which were made to this equipment which are as follows:

a) The output pulse width was increased from 50 µs to 100 µs by replacing R9 at E6 on card C with a 33kΩresistor.

b) The output attenuator in the FPA was removed and placed in the tape recorder.

c) The output impedance of the FPA was set at 2,2kΩwith R8 at E6 on card C.

The instrument specifications are as follows :-

Input impedance	: 1kΩ
Gain range	: 0 - 10 settable on 10-turn potentiometer with an accuracy of 5% of full scale setting.
Maximum pulse counting rate	: 1000 Hz
Minimum pulse size	: 0,2/gain(volts)
Time reference	: Accurate to 3 parts in 10^5 over temperature range $0^{o}C$ to $40^{o}C$.
Pulse height discrimination analysis (PHDA).	: 10 channels - linear spacing, discriminator accuracy - 2% of max. level on all levels.
Timing of PHDA	: Pulse height recorded is the max. during the 1 ms after the lowest threshold is exceeded.

Time discrimination analysis (TDA)	: 30 sequential channels each covering 2 seconds.
Cycle counter	: 1 channel, max. value 1 000.
Output impedance	: 2,2kΩ
Output pulse width	: 100μs.
Output pulse rate	: 2000Hz
Inter-word delay	: 4ms.
Inter-record delay	: approx. 400ms.
Recording time	: Varies with input pulse rate. Typical values for one side of a C.90 cassette: 100Hz 6,7hrs. 1Hz 51,7hrs.
Power requirements	: 200 - 240 volts 50 - 440 Hz 1 amp.
Dimensions	: 200 x 445 x 360mm.

A.6 Tape Recorder

Two modifications were made to this unit:

a) A regulated power supply was provided for the unit, and

b) A potential divider was included in the input stage of the recorder to bring the sensitivity up to 3,5 volts to match the output of the FPA:

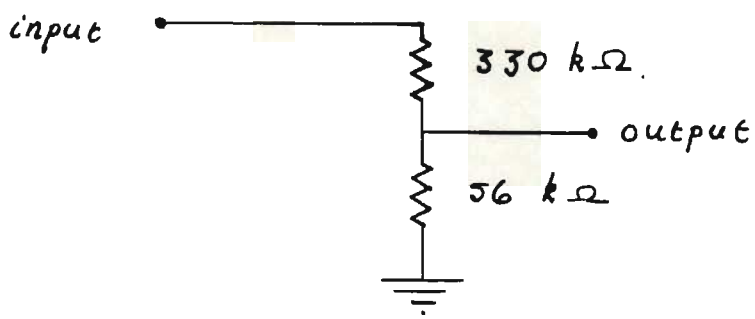

The specifications of the unit are:

Name and model	: Sony Cassette Corder Model TC-115
Power requirements	: AC 200-220 volts
Power consumption	: 5 W
Tape speed	: 48mm/s
Power output	: 1 W

Frequency response	:	80-9000Hz
Input	:	Microphone input sensitivity 0,2 mV
Output	:	Monitor jack load impedance 10kΩ or higher.
Dimensions	:	137 x 62 x 45mm.

A.7 The Tape-Record Decoder

Figure 3.17 gives a block diagram. A schmidt trigger shapes the incoming pulses to square pulses with rise times of less than 1 μs. These are fed direct to the event counter. Word and record interrupts are generated by two dual retriggerable monostables. The word and record monostables have pulse periods of 1 and 20 ms respectively. They are set on by the first incoming pulse and will only reset if no pulses follow within periods of 1 and 20 ms respectively. Each monostable then drives a second monostable to produce an interrupt pulse of the required shape, i.e. rise time less than 1 μs, pulse length greater than 1 μs and pulse height between 3,5 and 6 volts.

APPENDIX B: MAJOR COMPUTER PROGRAMS DEVELOPED FOR THIS PROJECT

The two major programs developed for this project are described in this appendix. The programs were written for the CDC 1700 computer housed in the Department of Chemical Engineering, University of Natal, Durban, South Africa. The CDC 1700 is a real-time machine with digital and analogue inputs and outputs, and an event-counter input. It has a 32k 16-bit word memory and two discs each with approximately 3×10^6 16-bit word storage.

The language used for the software was Fortran IV.

B.1. Program DTAPE

This program has already been outlined in chapter three and the flow diagram is given in figure 3.18. Essentially the program reads and stores tape records from the tape recorder

via the decoder and event counter.

The first step in the program is to set-up the event counters - the two 8-bit event counters $200 and $201 are combined to form a single 16-bit counter entitled $200. The 8-bit counters $202 and $203 are set up as word and record interrupts respectively by loading them with their maximum values, setting the overflow indicators off and enabling the interrupt software.

The program makes use of a permanent disc file in which to store the data. Three parameters are read after setting up the event counter :

a) The experiment number.

b) ISTRT - the point in the file where information transfer is to begin.

c) KREC - the number of records to be transferred.

The program is initiated after the tape recorder is set running. The event counter $200 is read every time a word interrupt is received from $202 and the reading is stored in memory. $202 is reset after each word has been read. Interrupts from $203 cause the computer to transfer the current tape record from memory to file. $203 is reset after each record transfer.

B.2 Program AZIELE

The function of AZIELE was to read and interpret data input via the digitiser and to enter this data at the appropriate place in a file. A flow diagram for this program is given in figure B.1. Because data entry is slow and intermittent three types of error must be taken care of :

a) Entry of the wrong file location parameters.

b) Mistakes in data entry, and

c) Possible computer failure during information transfer.

The first few sectors of the file contain an index for the rest of the file. In sector 31 the file parameters and calibration parameters are stored for the current data set. The contents of this sector are changed only at the start of a new data set.

On initiating the program the current status of the work and the calibration parameters for the digitiser are read from sector 31, and from the index it reads current length of the file.

Four buttons were provided with the digitiser enabling the user to :

a) Accept a new point.

b) Go back one point.

c) Check the calibrations.

d) Terminate the program.

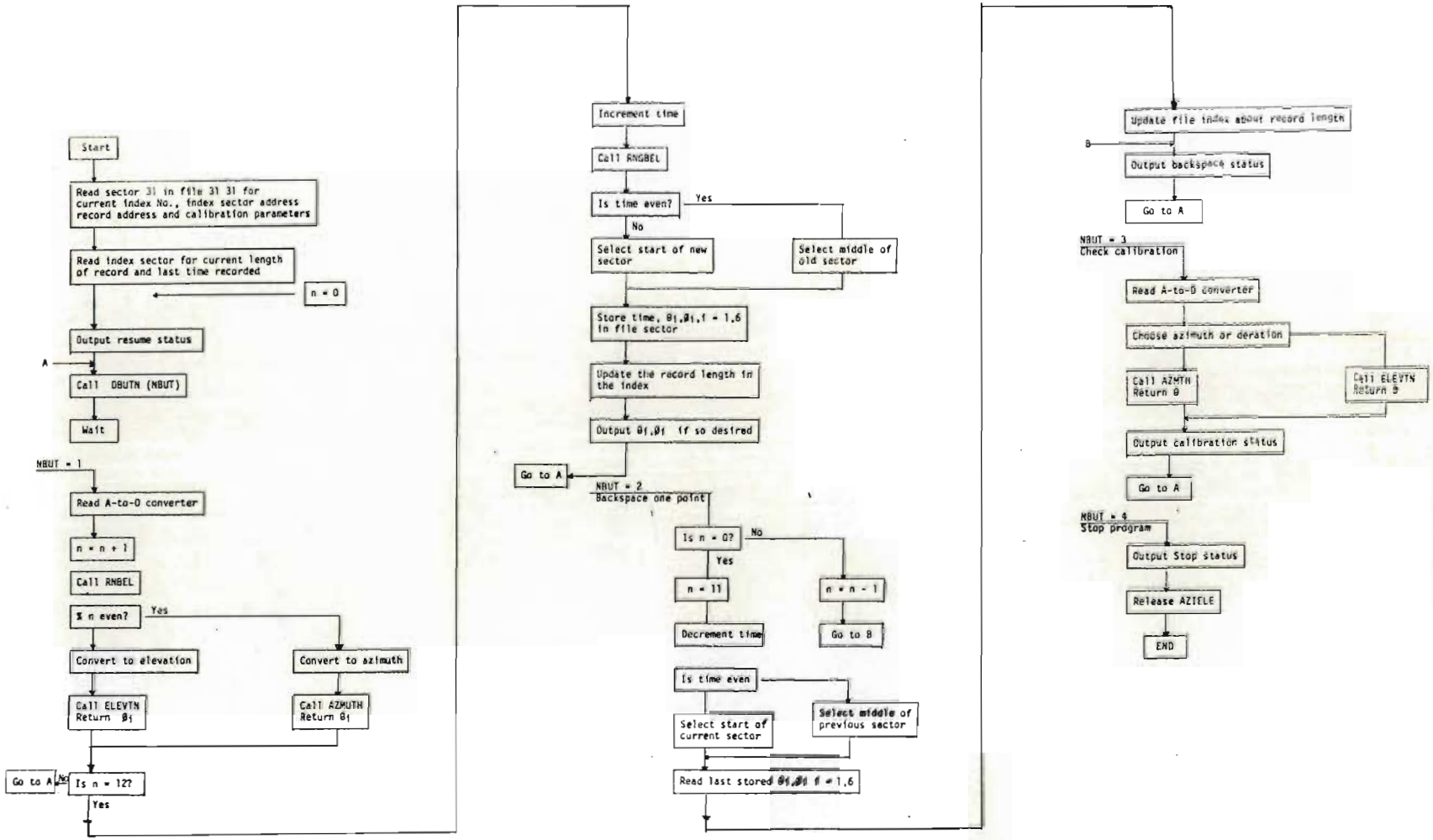

Figure B.1: Flow diagram for the program AZIELE

APPENDIX C : PRIMARY DATA

The following graphs show all the primary data obtained in the dispersion experiments described in chapter 4. To summarise :

a) Wind elevation and azimuth angle was measured with a Gelman-Gill bivane placed near the tracer source.

b) Wind speed (which is shown as hourly averages just below the elevation angle trace in every graph) was obtained from a Lamprecht anemometer placed near the source.

c) The bivane and anemometer were placed 2,7m above ground level. The tracer release nozzle was placed at 2,1m above ground level which, with the bent-over plume, gave an effective source height of 2,7m

d) The fluorescent particle counter intake was sited 20m downwind of the source and 1,5m

above ground level.

e) All readings shown on the traces are averages over one minute.

f) The site was on top of a reservoir adjacent to the Department of Chemical Engineering, University of Natal. There were no obstacles near the dispersion axis except for the instrument shelter which was away to the west of the axis. The ground was level and covered by short grass.

g) The tracer release rate was approximately $6{,}1 \times 10^{7/}s$ for field run 1 and $7{,}3 \times 10^{7/}s$ for field runs 2 and 3.

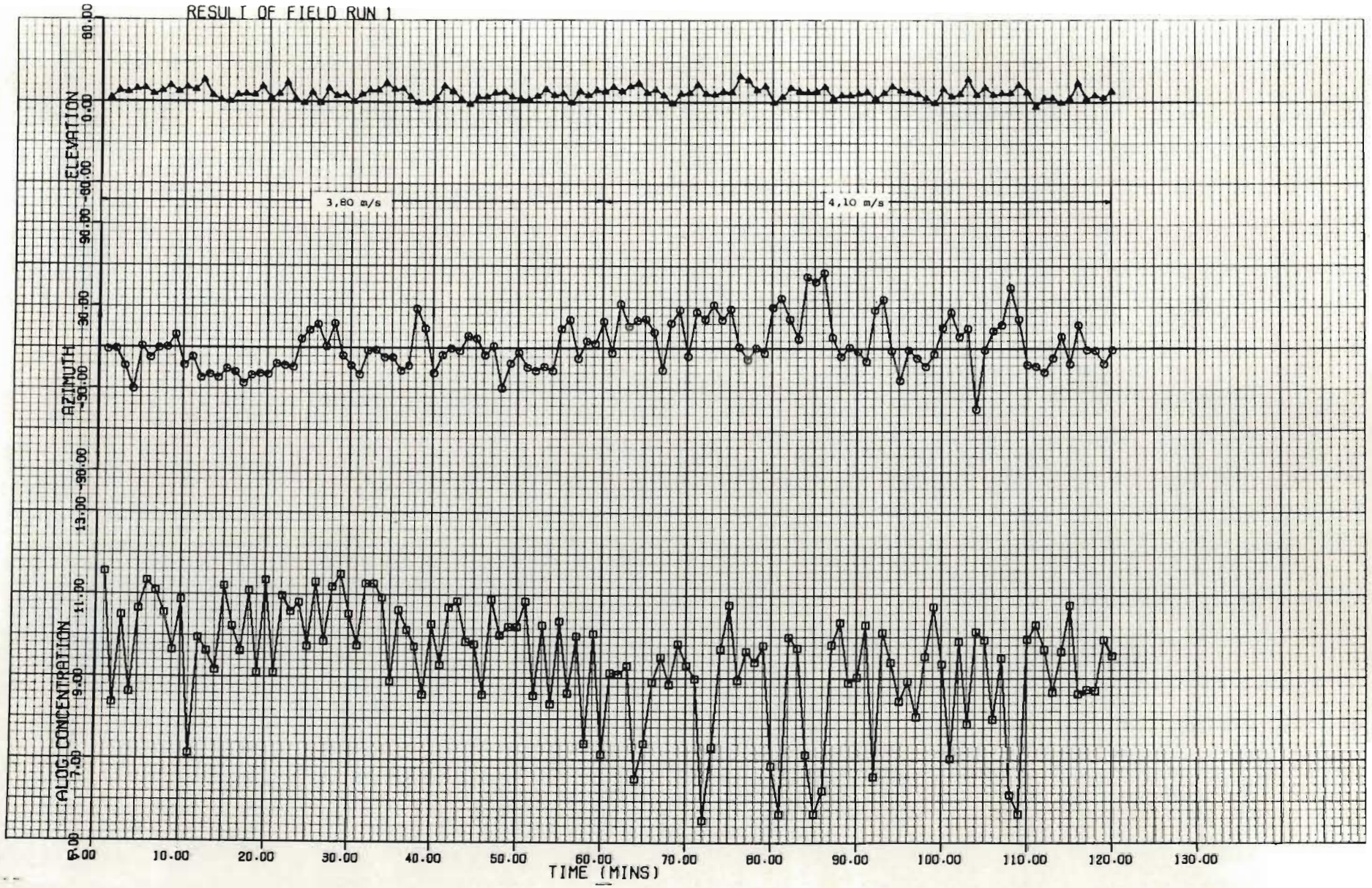

Figure C.1 : Data collected during the field trial of the fluorescent particle counter.
Run 1 ; 0 to 120 minutes

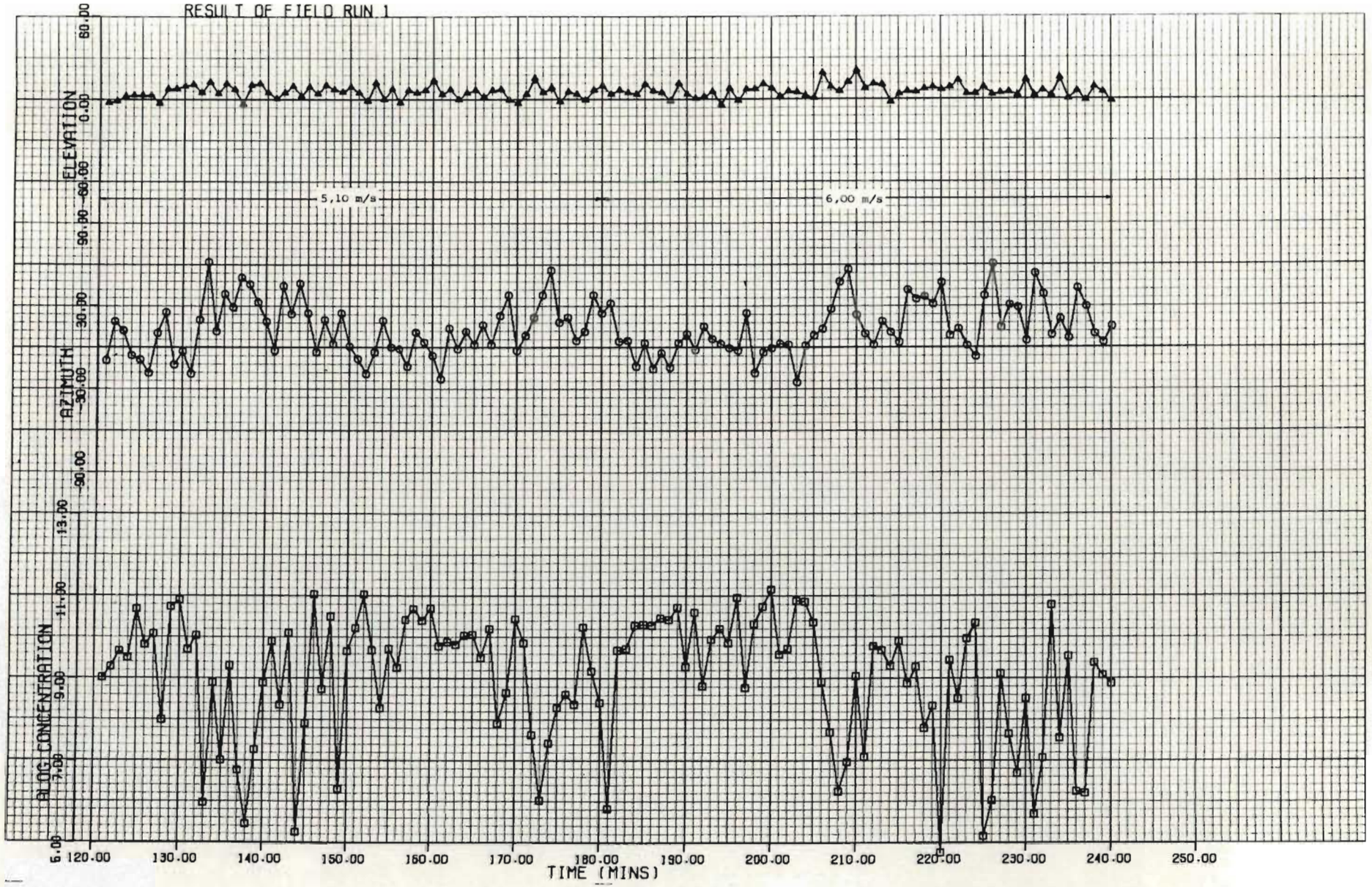

Figure C.2 : Data collected during the field trial of the fluorescent particle counter.
Run 1 ; 120 to 240 minutes

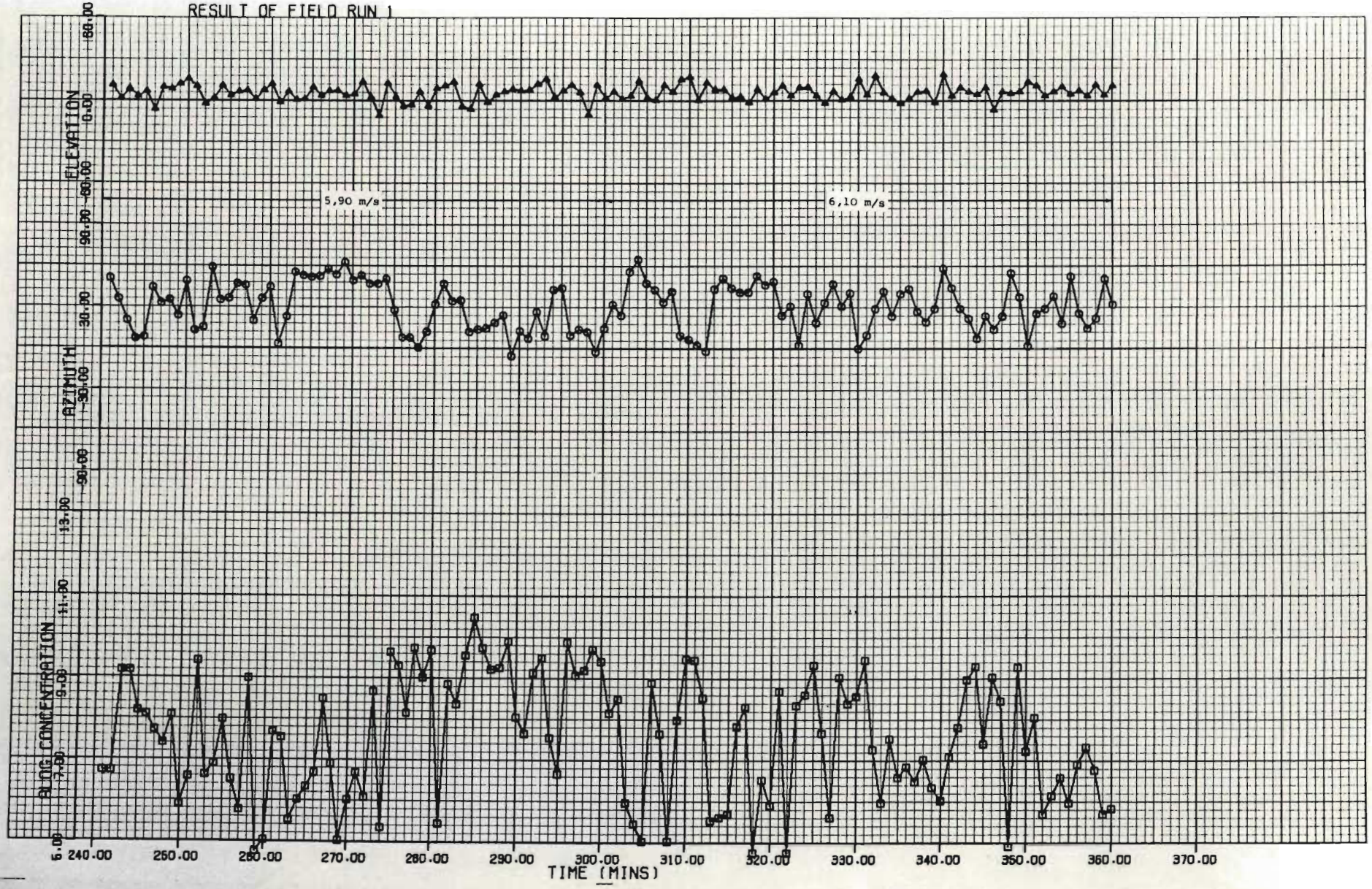

Figure C.3 : Data collected during the field trial of the fluorescent particle counter.
Run 1 ; 240 to 360 minutes

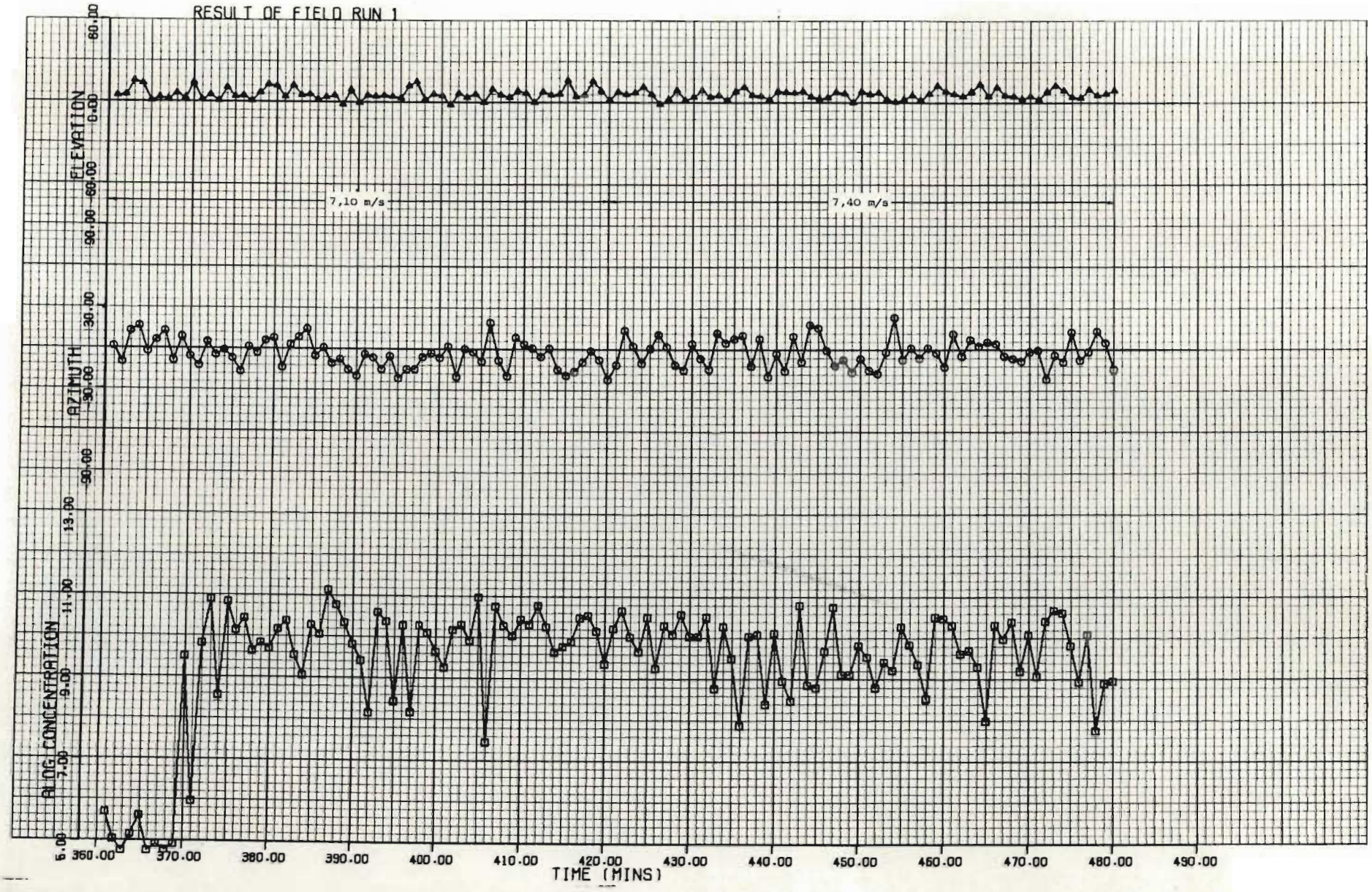

Figure C.4 : Data collected during the field trial of the fluorescent particle counter.
Run 1 ; 360 to 480 minutes

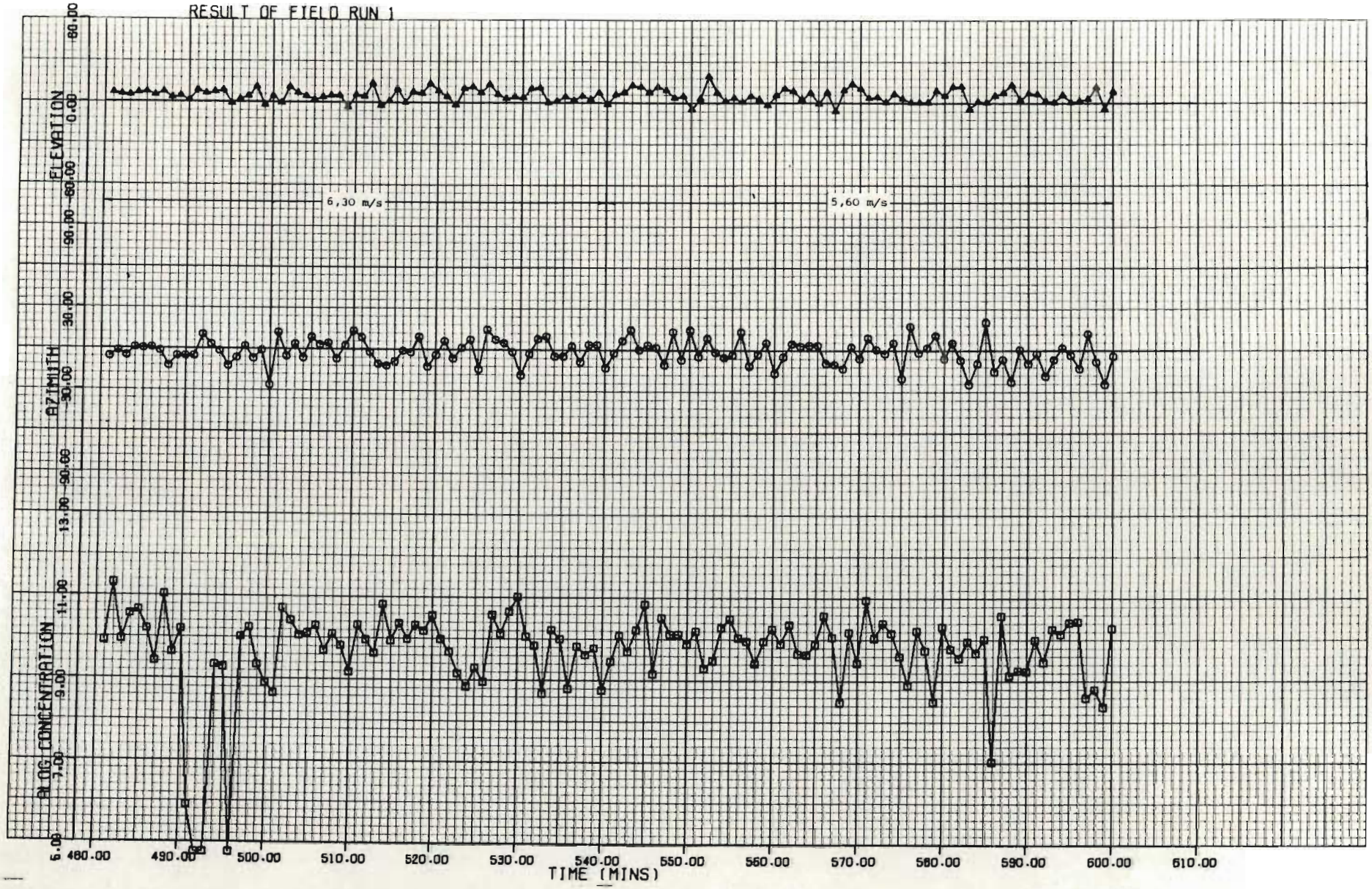

Figure C.5 : Data collected during the field trial of the fluorescent particle counter.
Run 1 ; 480 to 600 minutes

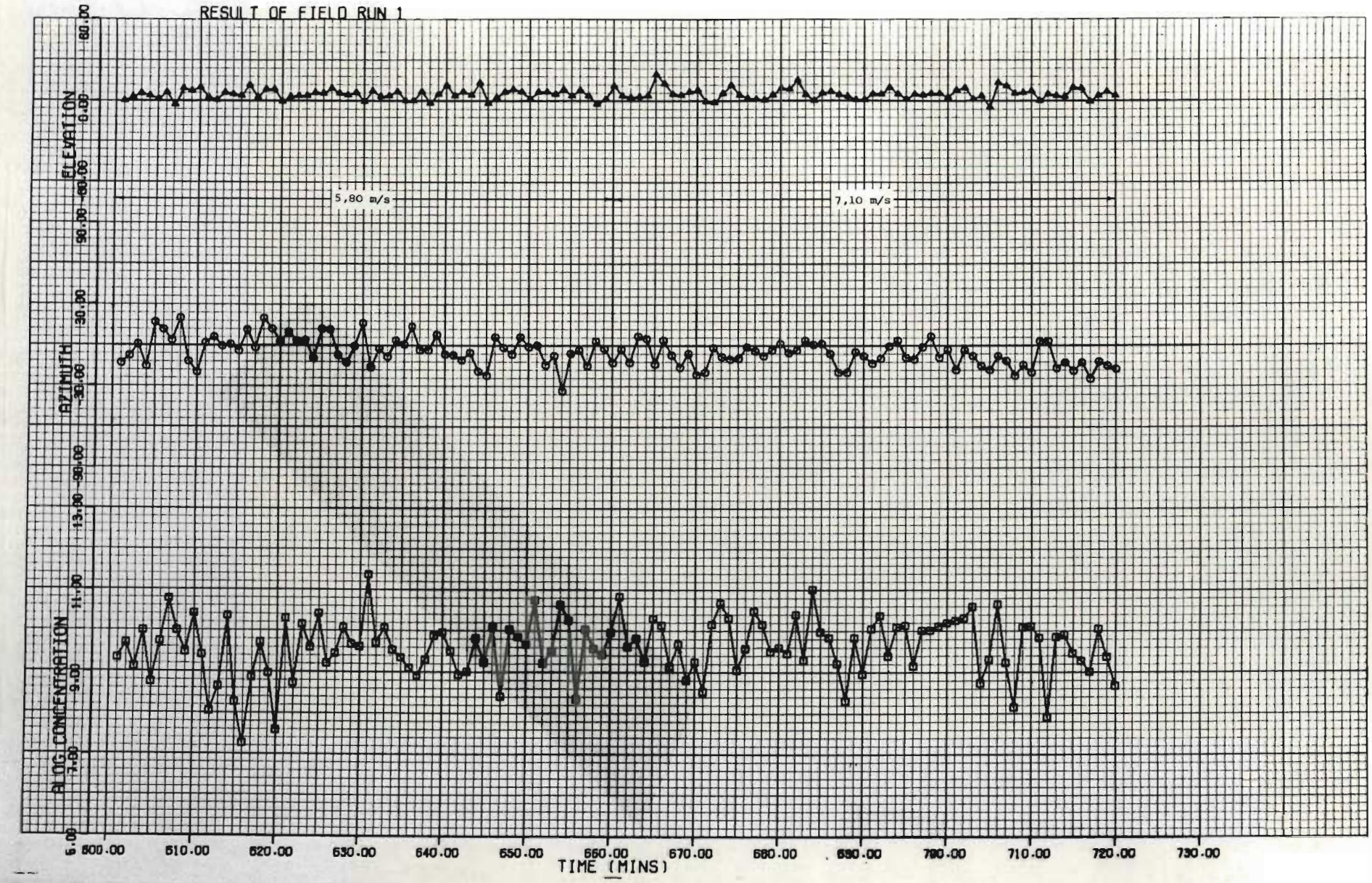

Figure C.6 : Data collected during the field trial of the fluorescent particle counter.
Run 1 ; 600 to 720 minutes

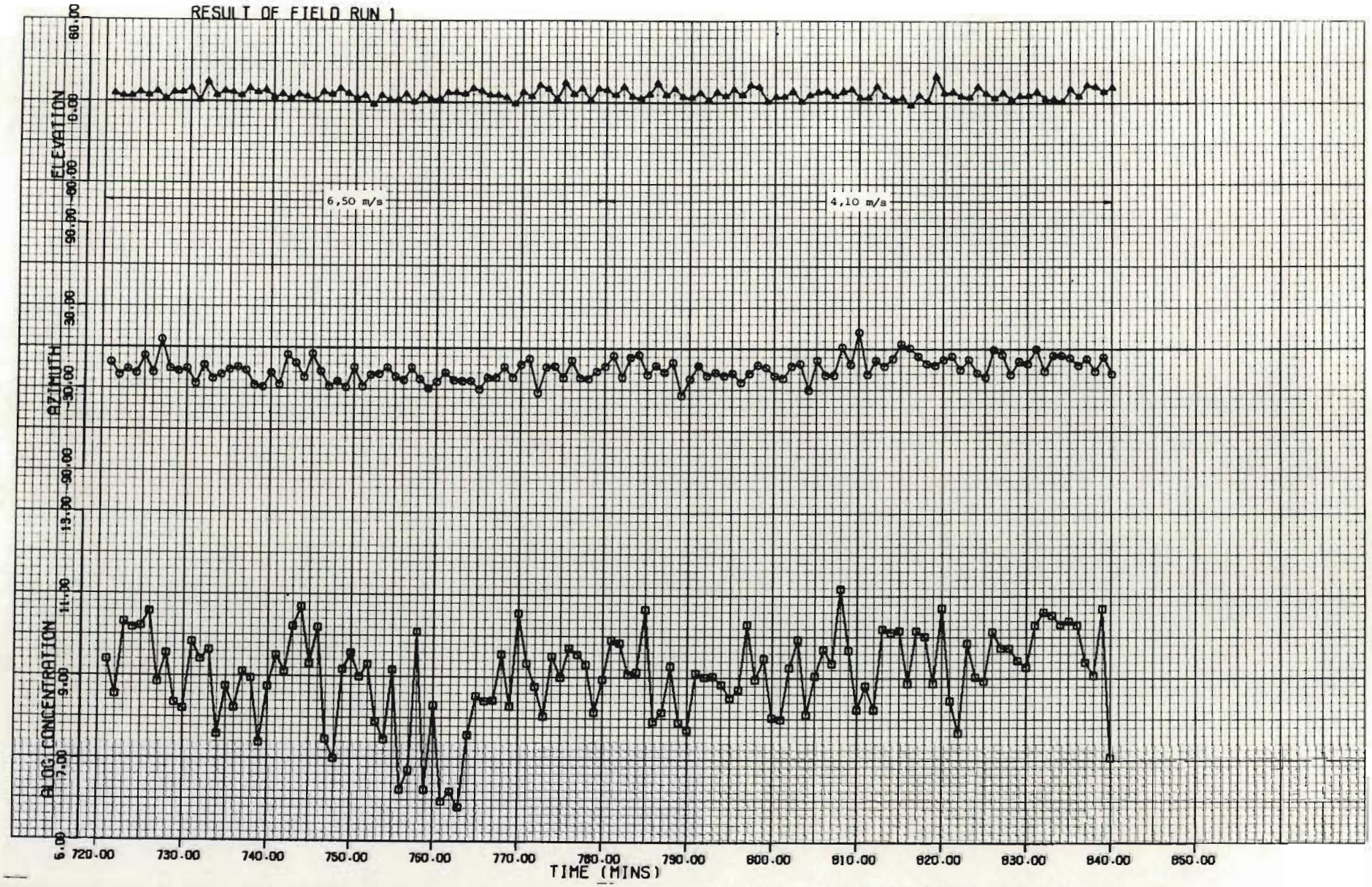

Figure C.7 : Data collected during the field trial of the fluorescent particle counter.
Run 1 ; 720 to 840 minutes

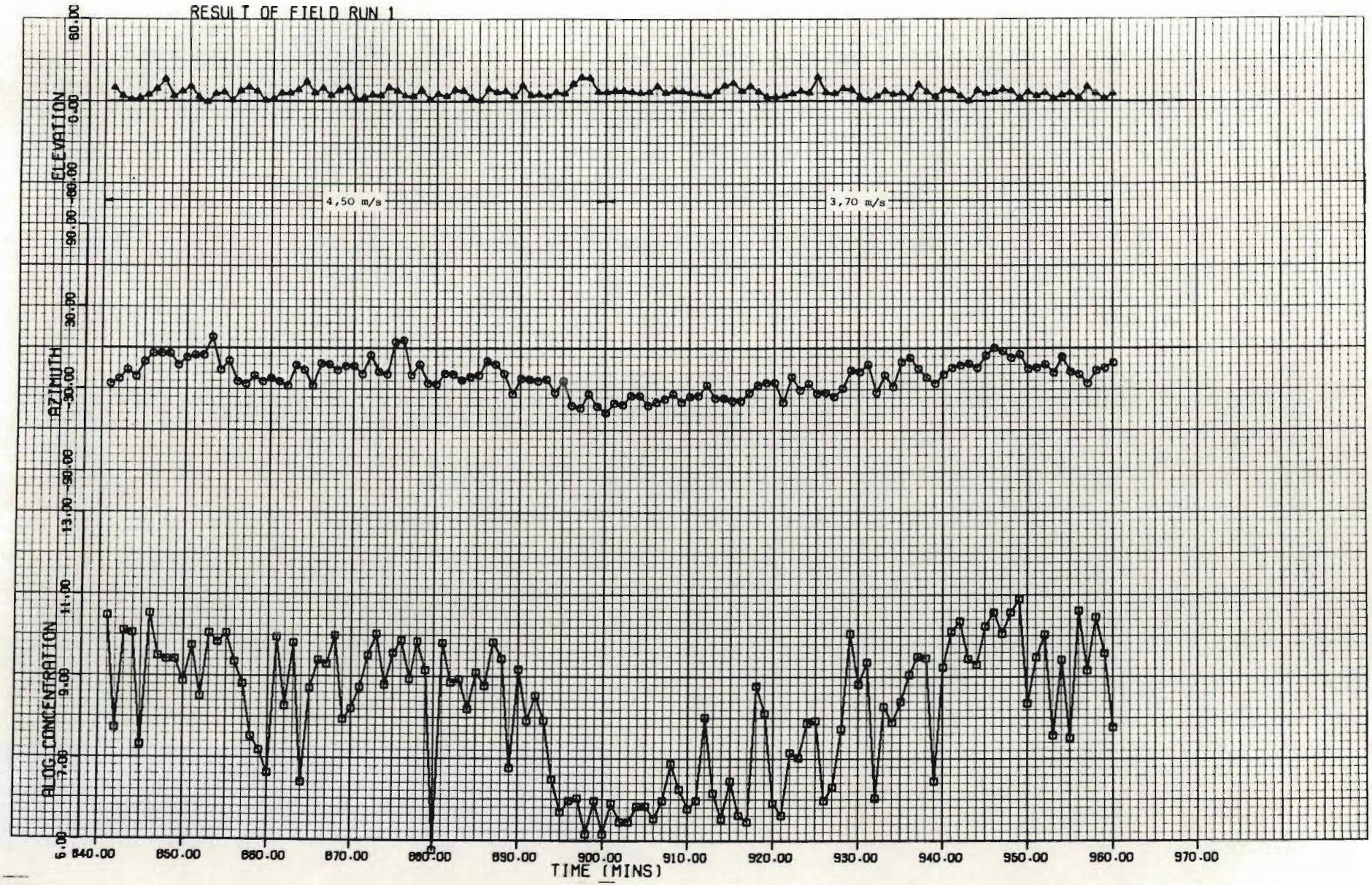

Figure C.8 : Data collected during the field trial of the fluorescent particle counter.
Run 1 ; 840 to 960 minutes

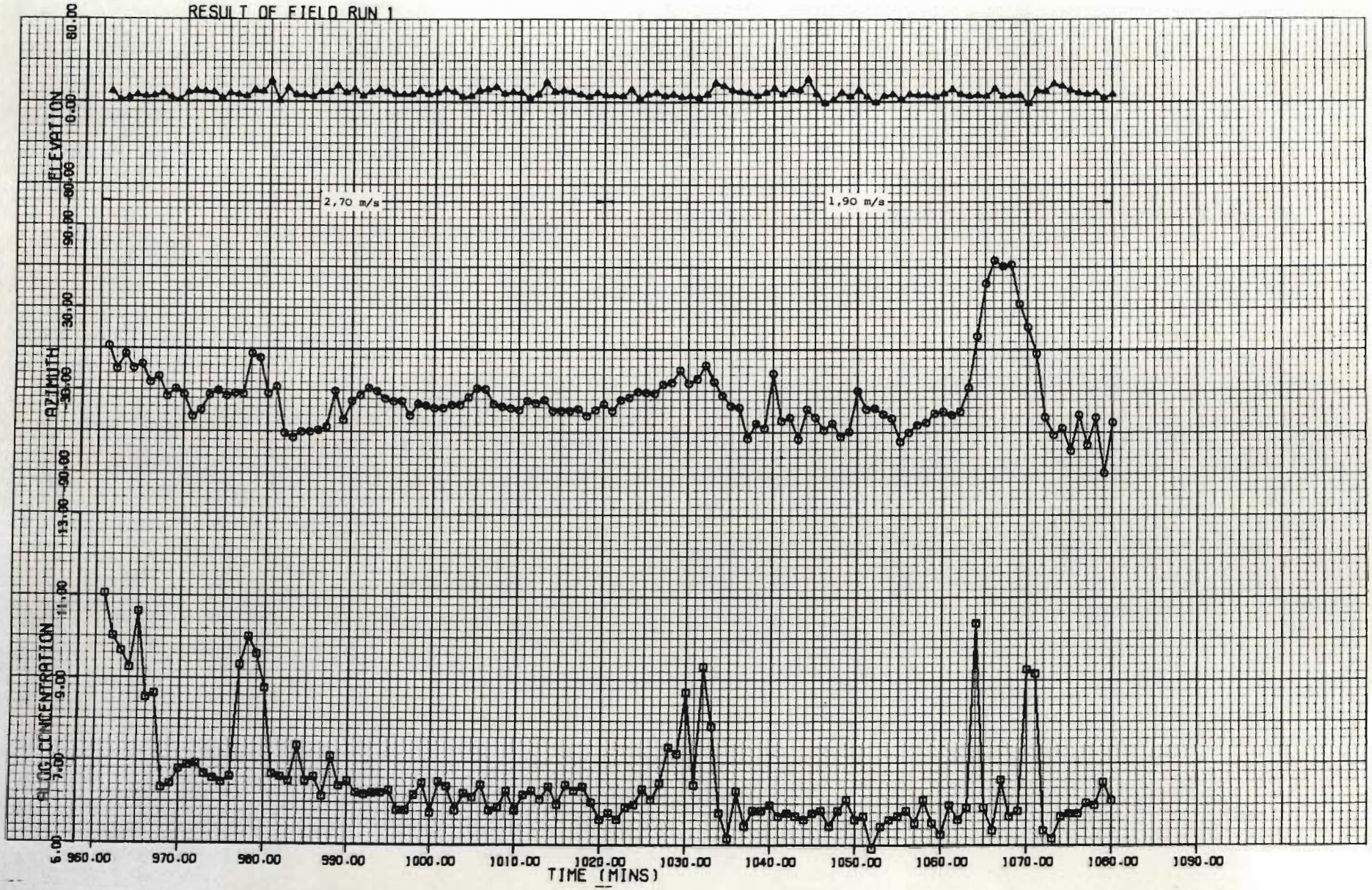

Figure C.9 : Data collected during the field trial of the fluorescent particle counter.
Run 1 ; 960 to 1080 minutes

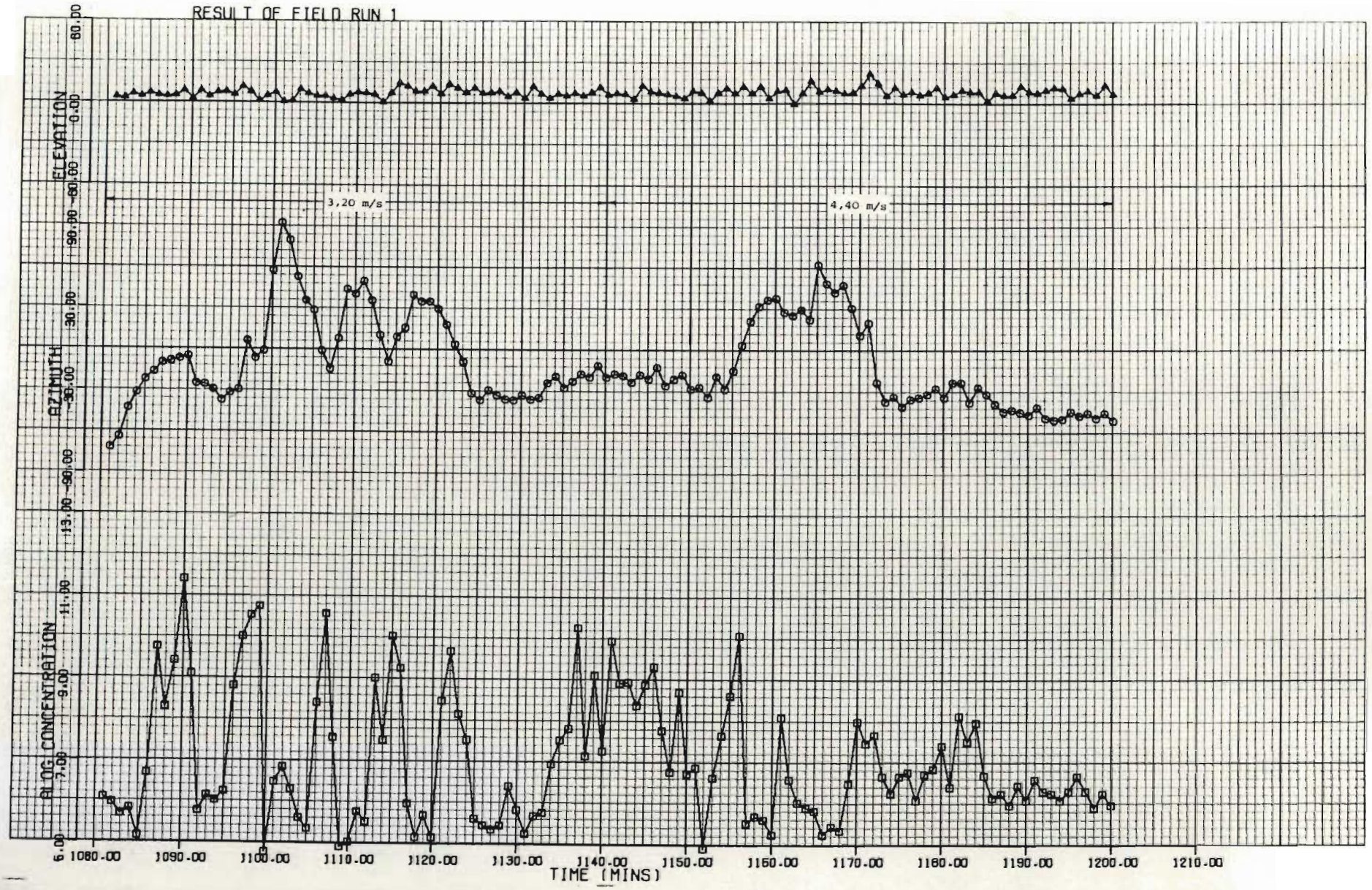

Figure C.10: Data collected during the field trial of the fluorescent particle counter.
Run 1 ; 1080 to 1200 minutes

Figure C.11: Data collected during the field trial of the fluorescent particle counter.
Run 2 : 0 to 120 minutes

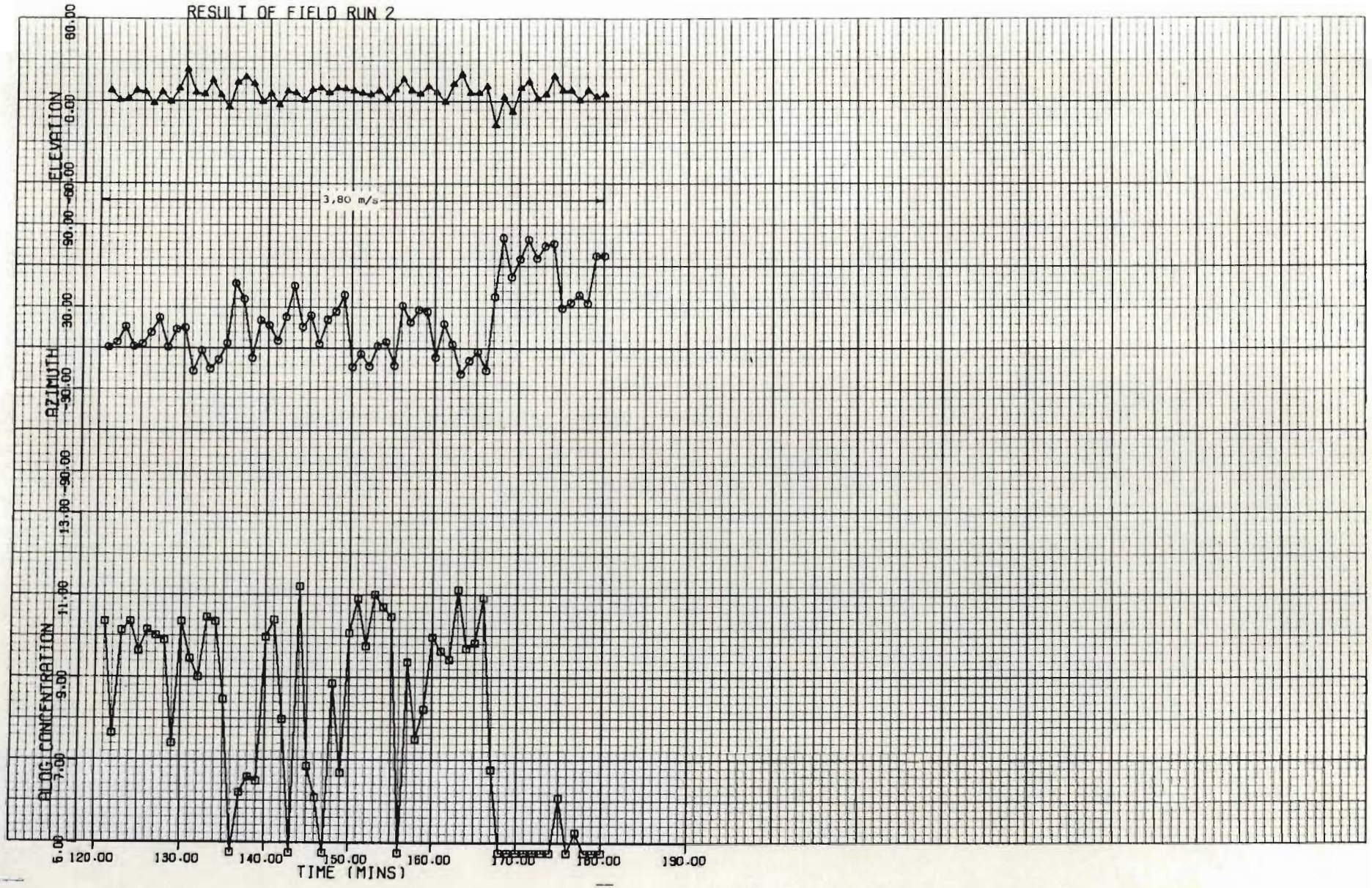

Figure C.12: Data collected during the field trial of the fluorescent particle counter.
Run 2 ; 120 to 180 minutes

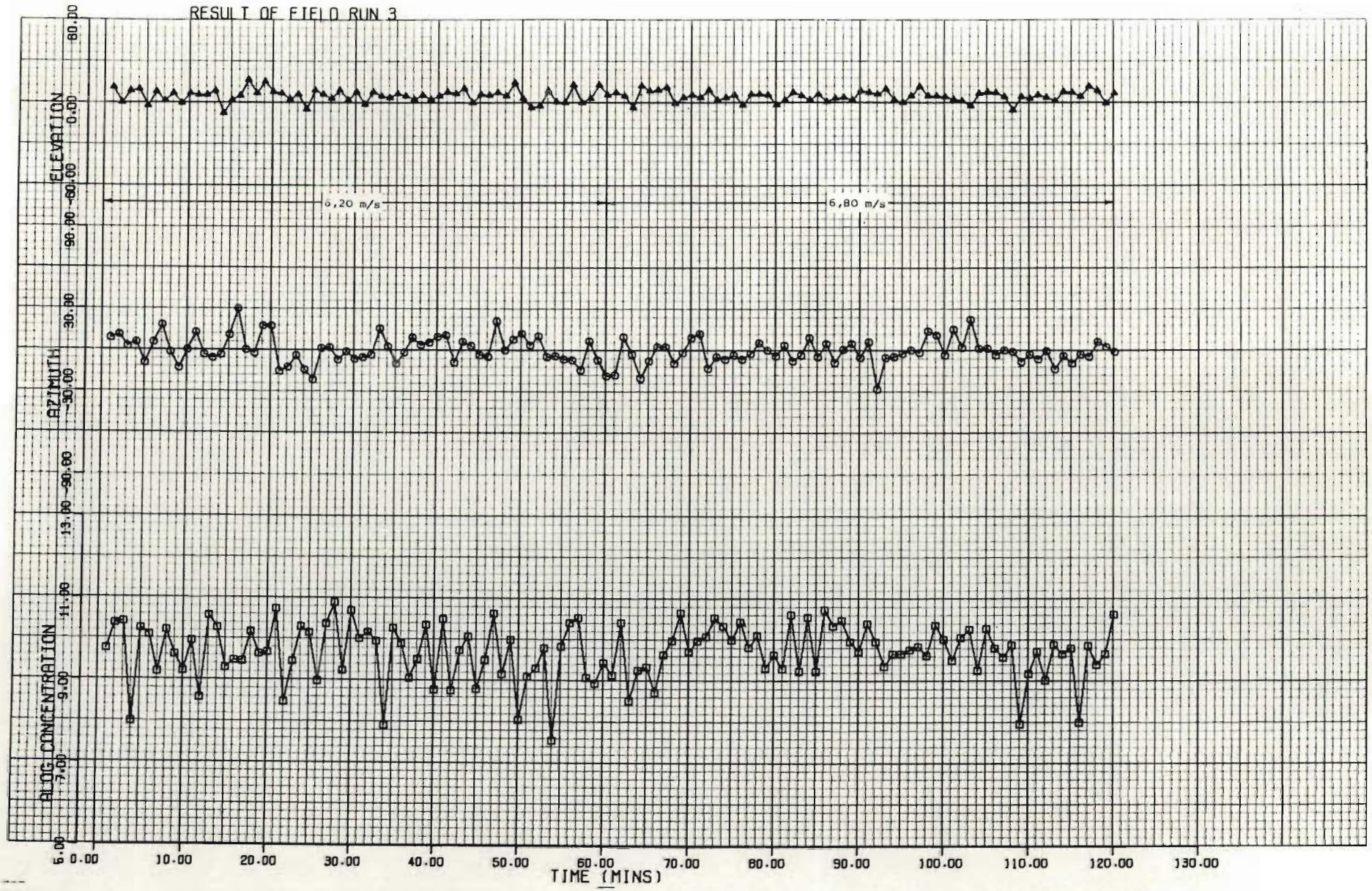

Figure C.13: Data collected during the field trial of the fluorescent particle counter. Run 3 ; 0 to 120 minutes

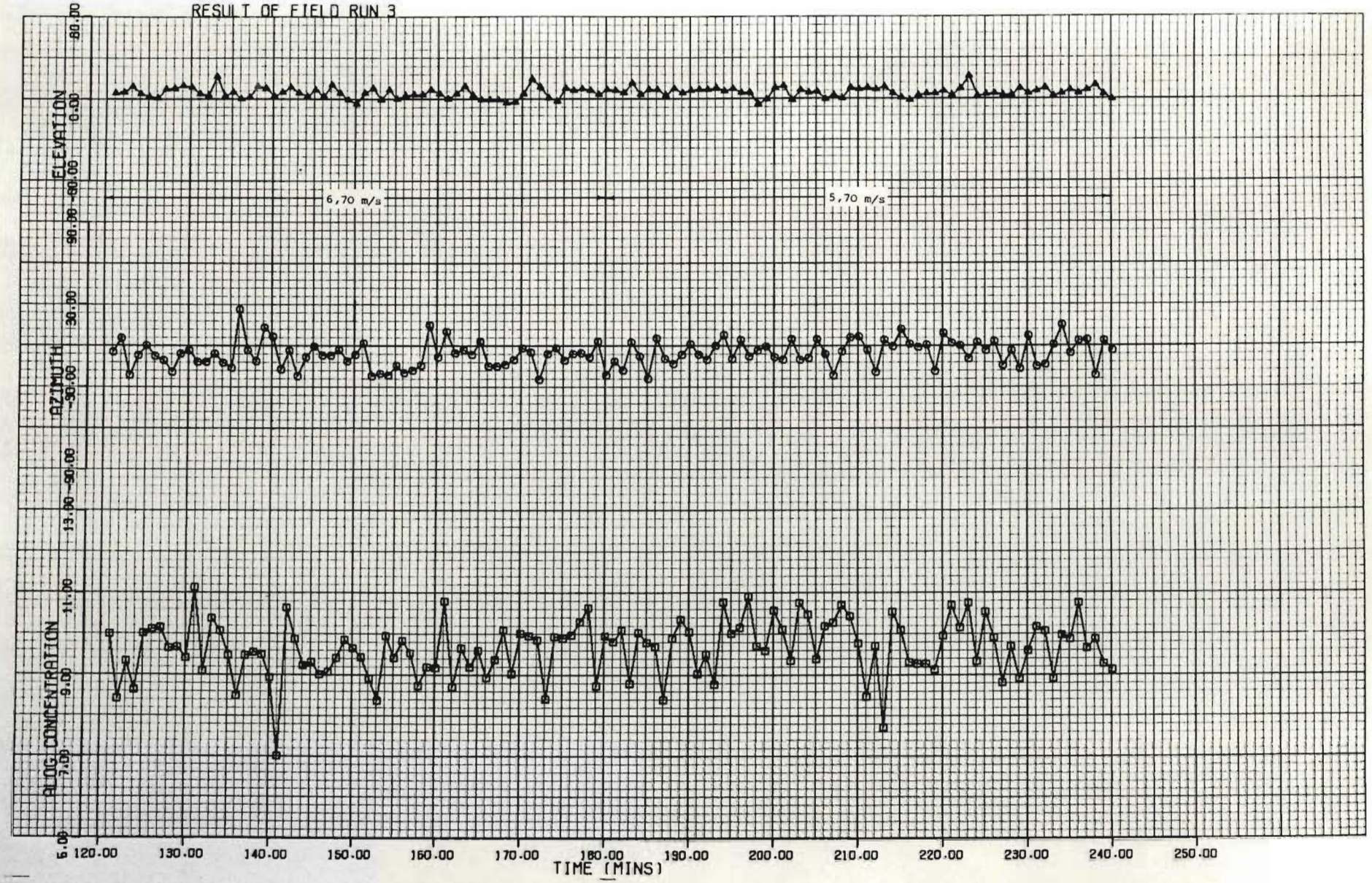

Figure C.14: Data collected during the field trial of the fluorescent particle counter. Run 3 ; 120 to 240 minutes

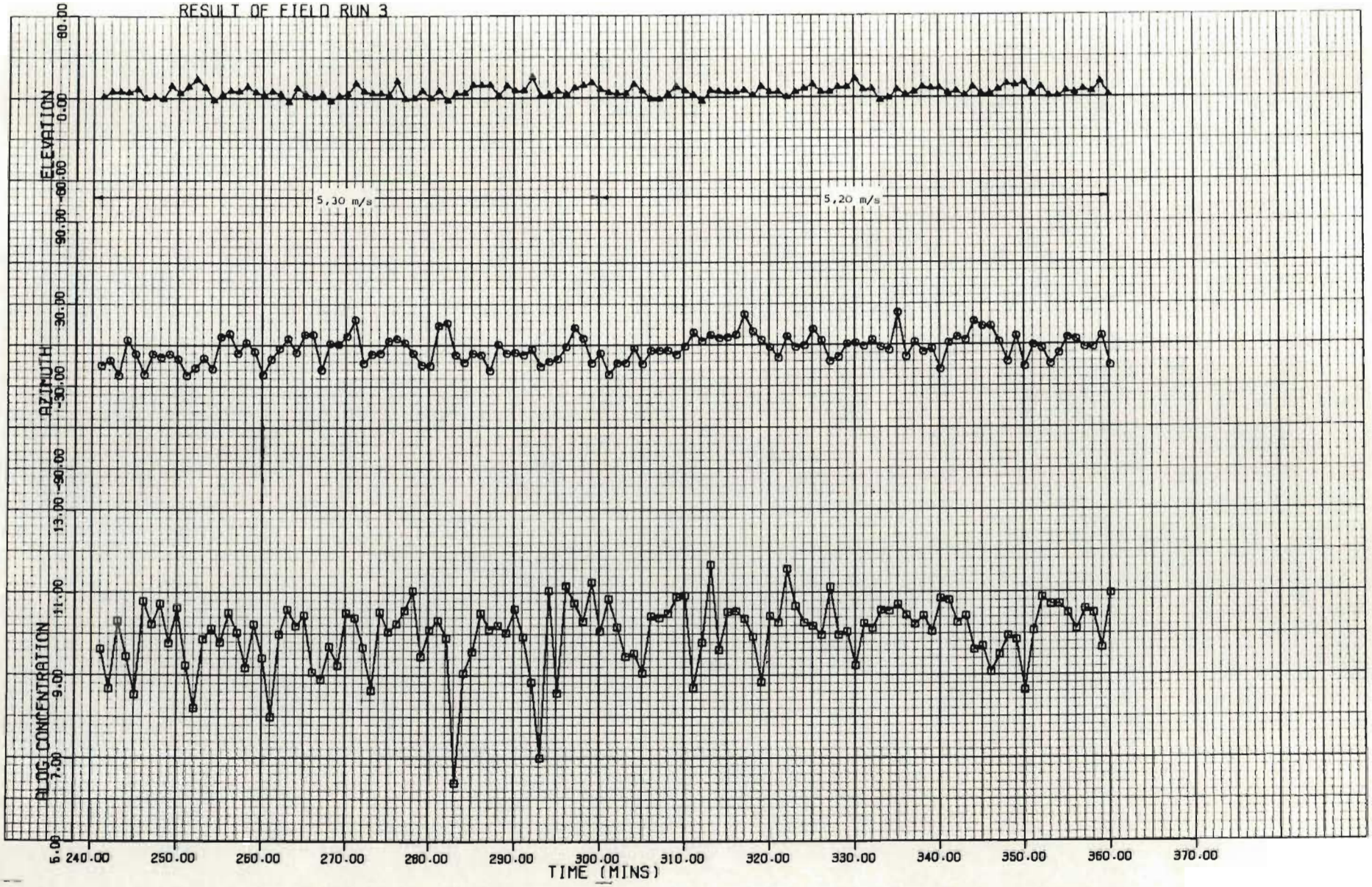

Figure C.15: Data collected during the field trial of the fluorescent particle counter.
Run 3 ; 240 to 360 minutes

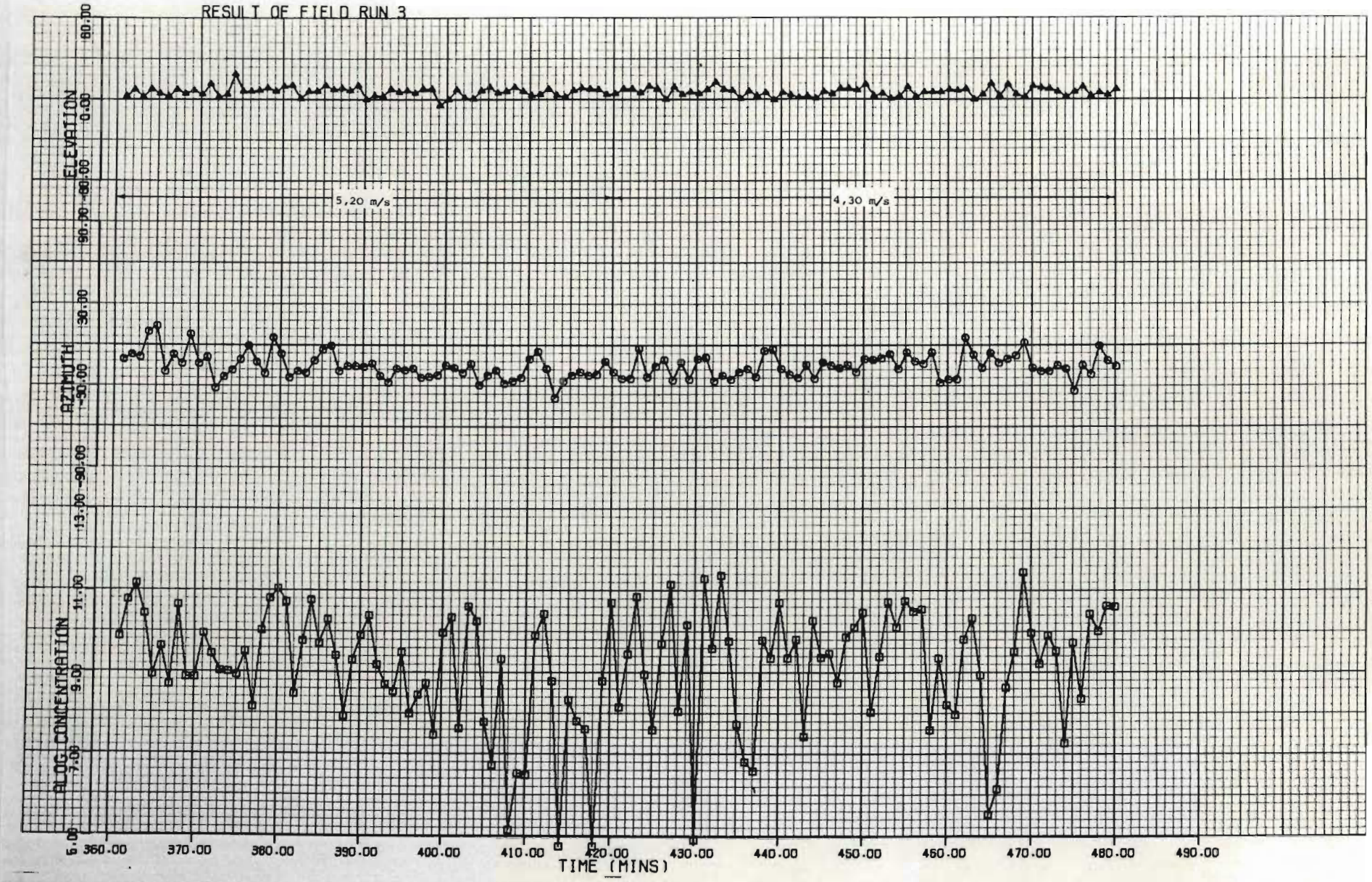

Figure C.16: Data collected during the field trial of the fluorescent particle counter. Run 3 ; 36o to 480 minutes

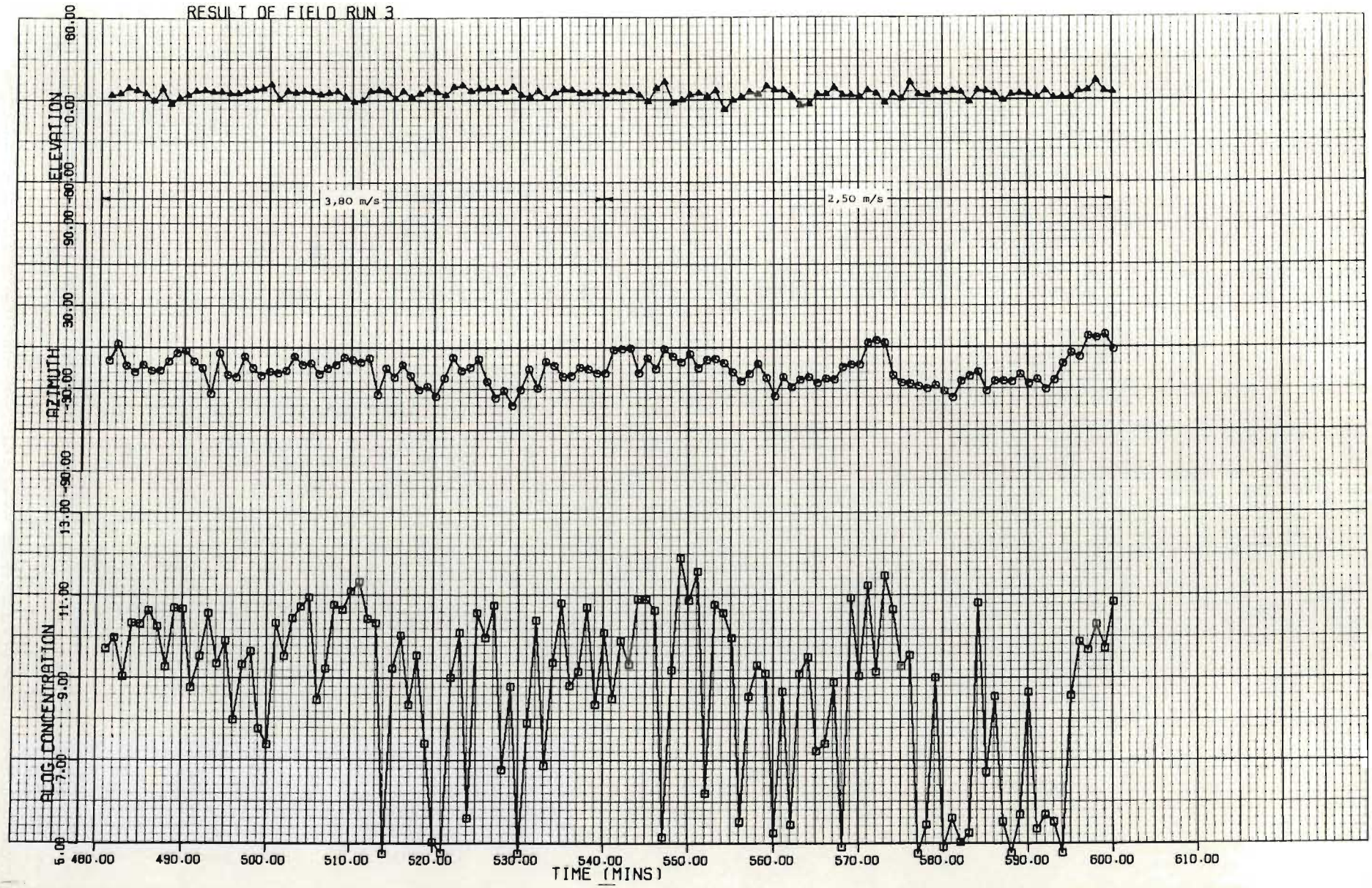

Figure C.17: Data collected during the field trial of the fluorescent particle counter. Run 3 ; 480 to 600 minutes

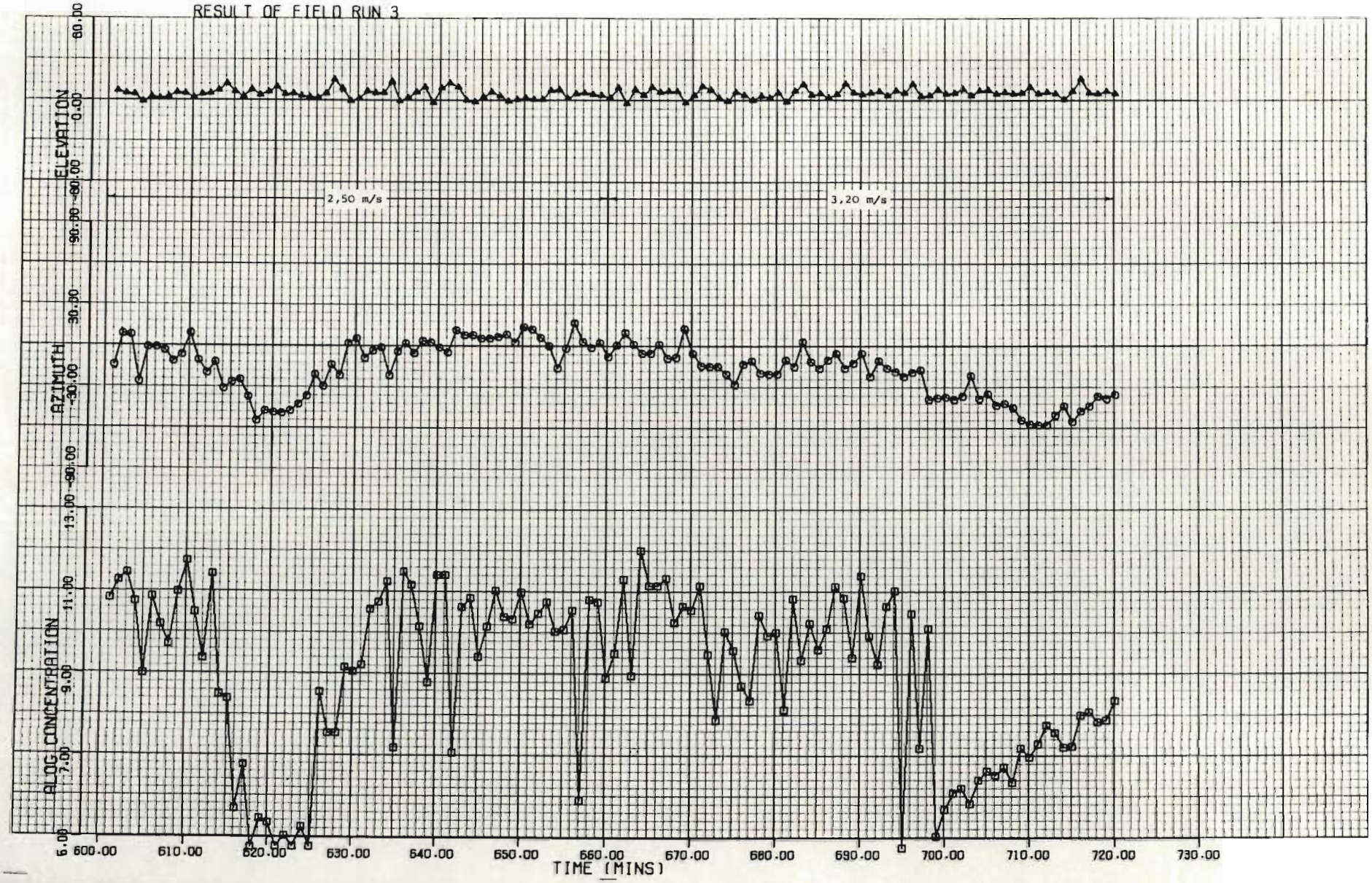

Figure C.18: Data collected during the field trial of the fluorescent particle counter. Run 3 ; 600 to 720 minutes

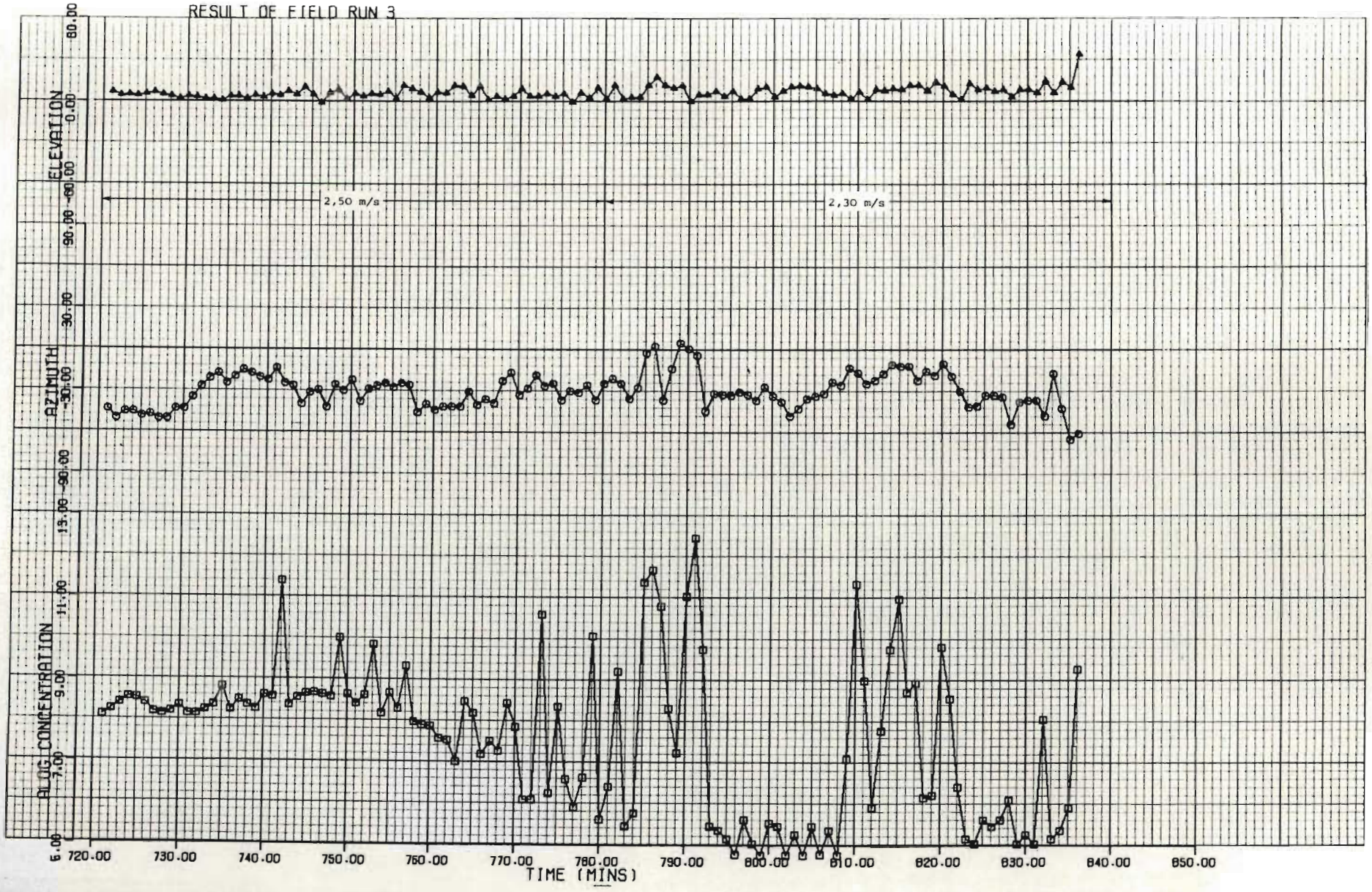

Figure C.19: Data collected during the field trial of the fluorescent particle counter. Run 3 ; 720 to 840 minutes

APPENDIX D: NUMERICAL RESULTS FROM THE REGRESSION ANALYSES

As outlined in Chapter 6 the models used for the purpose of regression were as follows :

(a) $$\chi = \frac{Q}{4\pi S \cos\alpha (K_y K_z)^{\frac{1}{2}}} \exp\left[-\frac{us}{4\cos q}\left(\frac{\sin^2 q}{K_y} + \frac{\tan^2 \mu}{K_z}\right)\right]$$

with Q, K_y and K_z as parameters.

(b) Model (a) but with K_y and K_z only as parameters.

(c) Model (a) but with Q and $K_y = K_z = K$ as parameters.

(d) Model (a) but with $K_y = K_z = K$ as parameter.

Some explanatory notes are necessary for the tables which follow :

1) Student t-test for the parameters is simply the magnitude of the parameter divided by its standard error. For 60 degrees of freedom the value of t at the 99% confidence level is 2,66. All significant parameters are marked with an asterisk.

2) The F-test is given by the mean sum of squares due to the regression divided by the mean sum of squared residuals. The degrees of freedom for regression are taken as equal to the number of parameters estimated and the degrees of freedom for error are taken as the number of points in the regression reduced by the number of parameters. The value of F for 60 degrees of freedom and 1, 2 and 3 parameters are respectively :

$$F\ (1;60) = 7,08$$

$$F\ (2;60) = 4,98$$

$$F\ (3;60) = 4,13$$

and all significant regressions are marked with an asterisk.

3) The "fit" is given by the sum of squares due to regression divided by the total sum of squares.

Table D.1: The selected sets of data submitted for regression analysis

RUN NO.	FIELD TEST	SEQUENTIAL TIME	σ_θ
1	1	61 to 120	19,7°
2	1	121 to 180	19,9°
3	1	181 to 240	19,4°
4	1	241 to 300	18,5°
5	1	301 to 360	16,2°
6	1	901 to 960	11,7°
7	1	961 to 1020	14,0°
8	1	1021 to 1080	33,0°
9	1	1081 to 1140	34,0°
10	1	1141 to 1200	31,2°
11	2	121 to 180	27,2°
12	3	601 to 660	18,3°
13	3	661 to 720	18,1°

Table D.2: Estimates and statistical significance of the three parameters Q, K_y and K_z obtained by fitting the fluctuating wind dispersion model to the selected sets of data

RUN NO.	PARAMETER ESTIMATES			STUDENTS t-TEST FOR THE PARAMETERS			SUM OF SQUARED RESIDUALS	F-TEST FOR THE REGRESSION	FIT %
	Q	Ky	Kz	Q	Ky	Kz			
1	$1,85 \times 10^7$	6,02	7,88	0,92	5,06*	0,41	86,1	6,8*	27
2	$6,54 \times 10^7$	6,78	37,49	0,25	7,57*	0,13	61,6	18,6*	50
3	$2,95 \times 10^7$	6,90	7,67	3,90*	9,45*	0,75	83,0	20,3*	52
4	$1,62 \times 10^7$	9,63	5,54	1,93	8,30	0,95	73,1	19,3*	51
5	$1,56 \times 10^7$	10,79	27,15	0,63	6,96*	0,30	74,7	12,0*	39
6	$5,81 \times 10^7$	1,99	87,49	0,07	12,36*	0,03	44,4	58,9*	76
7	$0,42 \times 10^7$	6,66	8,04	0,76	4,14*	0,35	85,2	4,7*	20
8	unsatisfactory convergence								
9	$0,27 \times 10^7$	15,69	2,08	1,44	3,42*	0,50	187,7	1,1	5
10	$0,93 \times 10^7$	7,89	29,94	0,32	0,67	0,15	55,1	10,1*	35
11	$3,56 \times 10^7$	8,07	99,41	0,08	5,76*	0,04	316,6	13,4*	42
12	$2,22 \times 10^7$	1,83	7,74	0,3	9,10*	0,14	123,6	23,0*	55
13	$5,98 \times 10^7$	4,50	48,5	0,06	6,0*	0,03	141,0	9,7*	34

Table D.3: Estimates and statistical significance of the two parameters K_y and K_z obtained by fitting the fluctuating dispersion model to the selected sets of data

RUN NO.	PARAMETER ESTIMATES		STUDENTS t-TEST FOR THE PARAMETERS		SUM OF SQUARED RESIDUALS	F-TEST FOR THE REGRESSION	FIT %
	Ky	Kz	Ky	Kz			
1	unsatisfactory convergence						
2	6,78	37,09	8,9*	3,8*	61,6	28,4*	50
3	6,86	41,82	8,5*	3,1*	83,4	30,6*	52
4	unsatisfactory convergence						
5	unsatisfactory convergence						
6	unsatisfactory convergence						
7	unsatisfactory convergence						
8	unsatisfactory convergence						
9	unsatisfactory convergence						
10	unsatisfactory convergence						
11	unsatisfactory convergence						
12	unsatisfactory convergence						
13	4,51	57,59	6,1	2,1	14,1	14,8	34

Table D.4: Estimates and statistical significance of the two parameters Q and $K_y = K_z = K$ obtained by fitting the fluctuating wind dispersion model to the selected sets of data

RUN NO.	PARAMETER ESTIMATES		STUDENTS t-TEST FOR THE PARAMETERS		SUM OF SQUARED RESIDUALS	F-TEST FOR THE REGRESSION	FIT %
	Q	K	Q	K			
1	$1,64 \times 10^7$	5,96	5,1*	5,4*	85,9	10,6*	27
2	$2,95 \times 10^7$	6,99	7,3*	8,9*	61,8	28,2*	50
3	$2,83 \times 10^7$	6,90	6,4*	9,2*	83,0	30,9*	52
4	$2,02 \times 10^7$	9,52	6,7*	9,2*	73,4	29,2*	51
5	$1,03 \times 10^7$	11,04	5,9*	7,9*	75,9	17,6*	38
6	$0,97 \times 10^7$	2,12	6,9*	13,3*	49,4	77,8*	73
7	$0,39 \times 10^7$	6,63	6,6*	4,9*	85,2	7,2*	20
8	unsatisfactory convergence						
9	$0,64 \times 10^7$	15,75	3,3*	3,3*	188,4	1,5	5
10	$0,51 \times 10^7$	7,99	7,1*	6,2*	55,4	15,2*	35
11	$1,09 \times 10^7$	8,65	3,0*	7,3*	3,29	18,3	40
12	$1,15 \times 10^7$	1,85	5,0*	7,8*	1,25	34,7*	55
13	$1,92 \times 10^7$	4,61	4,9*	6,5*	1,42	14,5*	34

Table D.5: Estimates and statistical significance of the single parameter $K_y = K_z = K$ obtained by fitting the fluctuating wind dispersion model to the selected sets of data

RUN NO.	PARAMETER ESTIMATES			STUDENTS t-TEST FOR THE PARAMETERS			SUM OF SQUARED RESIDUALS	F-TEST FOR THE REGRESSION	FIT %
	K			K					
1	35,7			4,7*			116,7	0,5	0,85
2	10,88			5,6*			95,4	16,8*	22
3	7,29			0,7			124,2	22,9*	28
4	6,95			10,2*			143,3	0,4	0,7
5	unsatisfactory convergence								
6	unsatisfactory convergence								
7	unsatisfactory convergence								
8	unsatisfactory convergence								
9	unsatisfactory convergence								
10	unsatisfactory convergence								
11	8,02			6,5			515	3,21	5
12	unsatisfactory convergence								
13	unsatisfactory convergence								

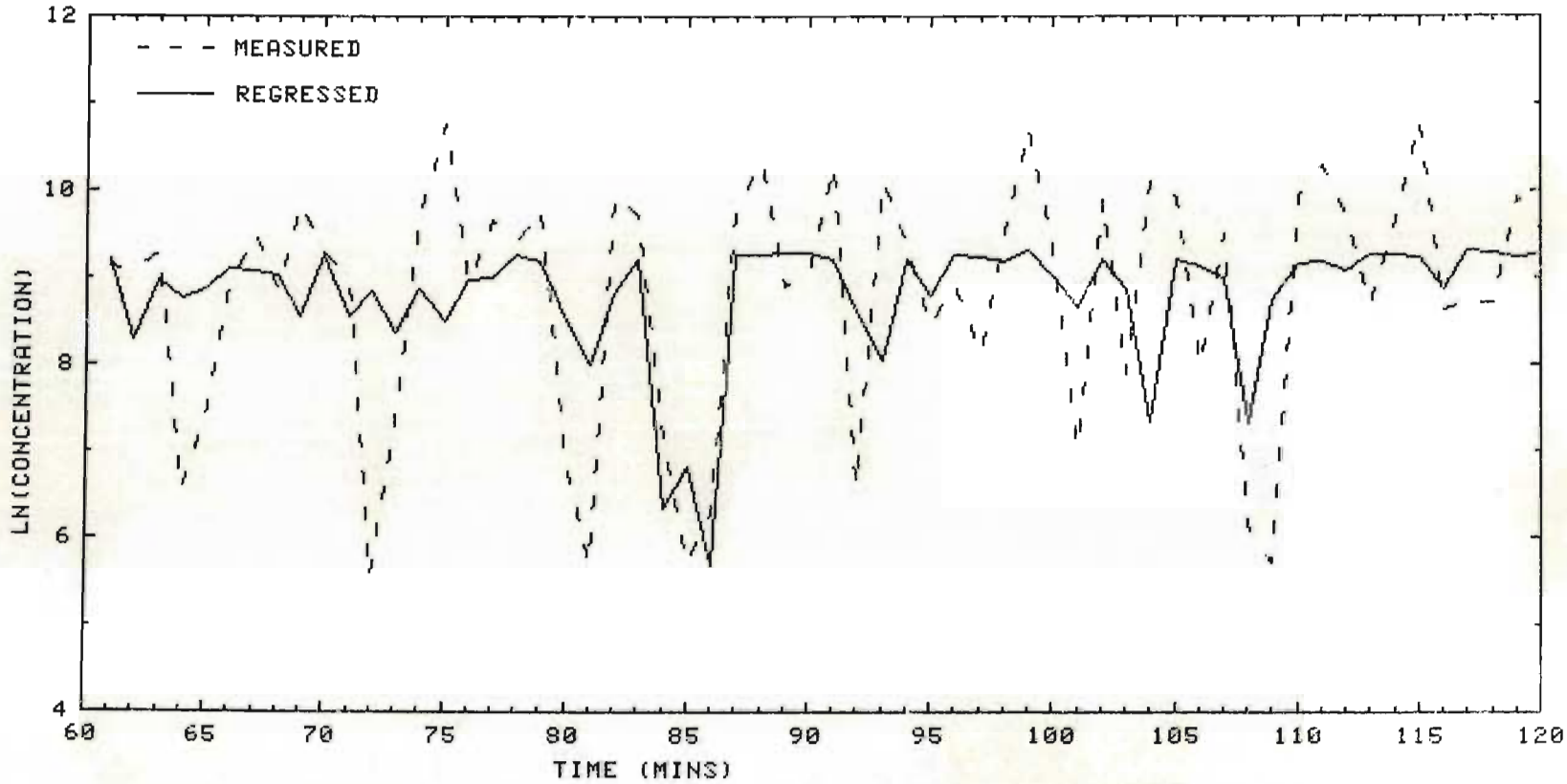

Figure D.1 : The best estimate of the concentration-time history from the fluctuating wind dispersion model compared with the measured history. Run 1 ; 60 to 120 minutes

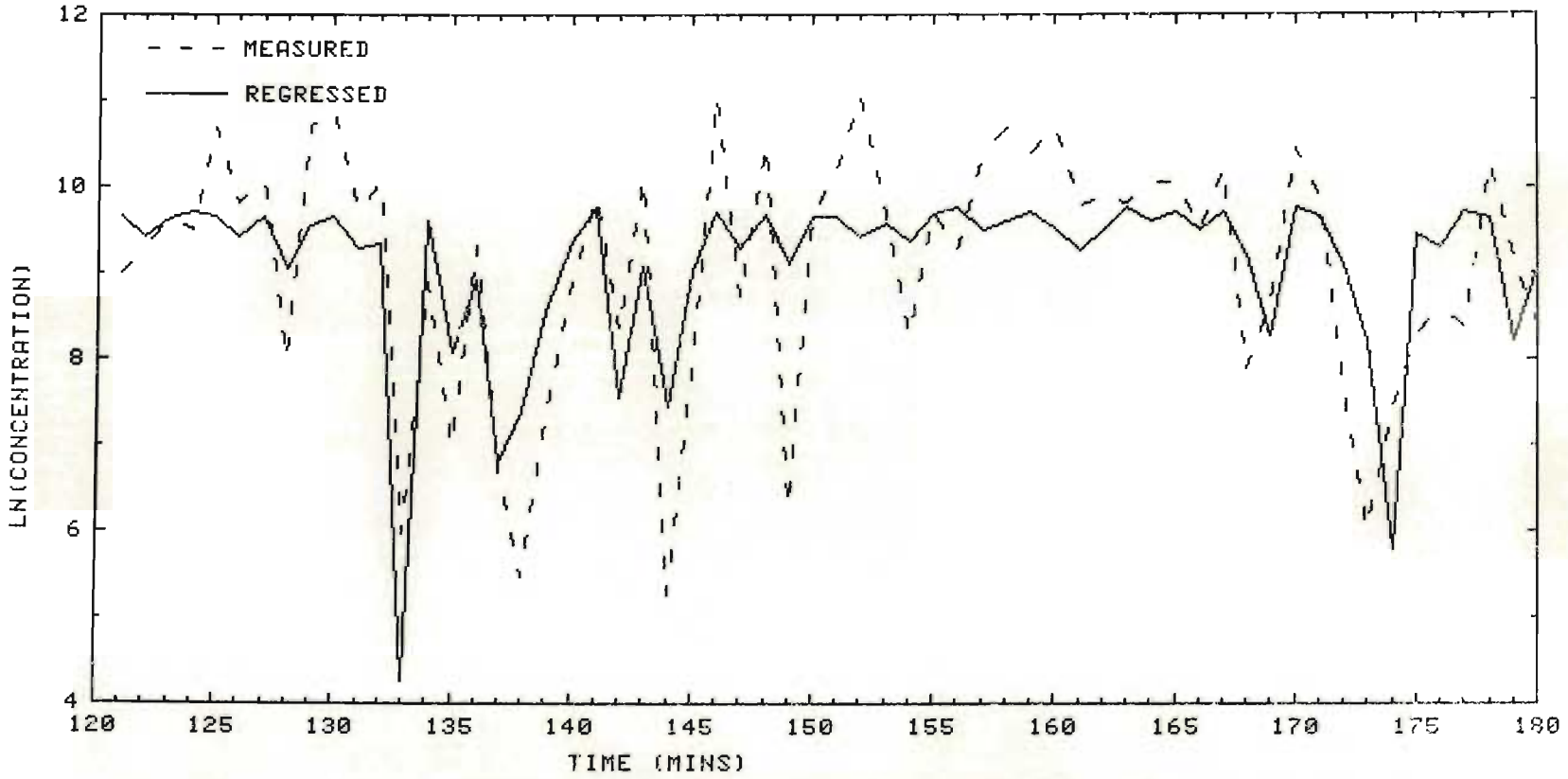

Figure D.2 : The best estimate of the concentration-time history from the fluctuating wind dispersion model compared with the measured history. Run 1 ; 120 to 180 minutes

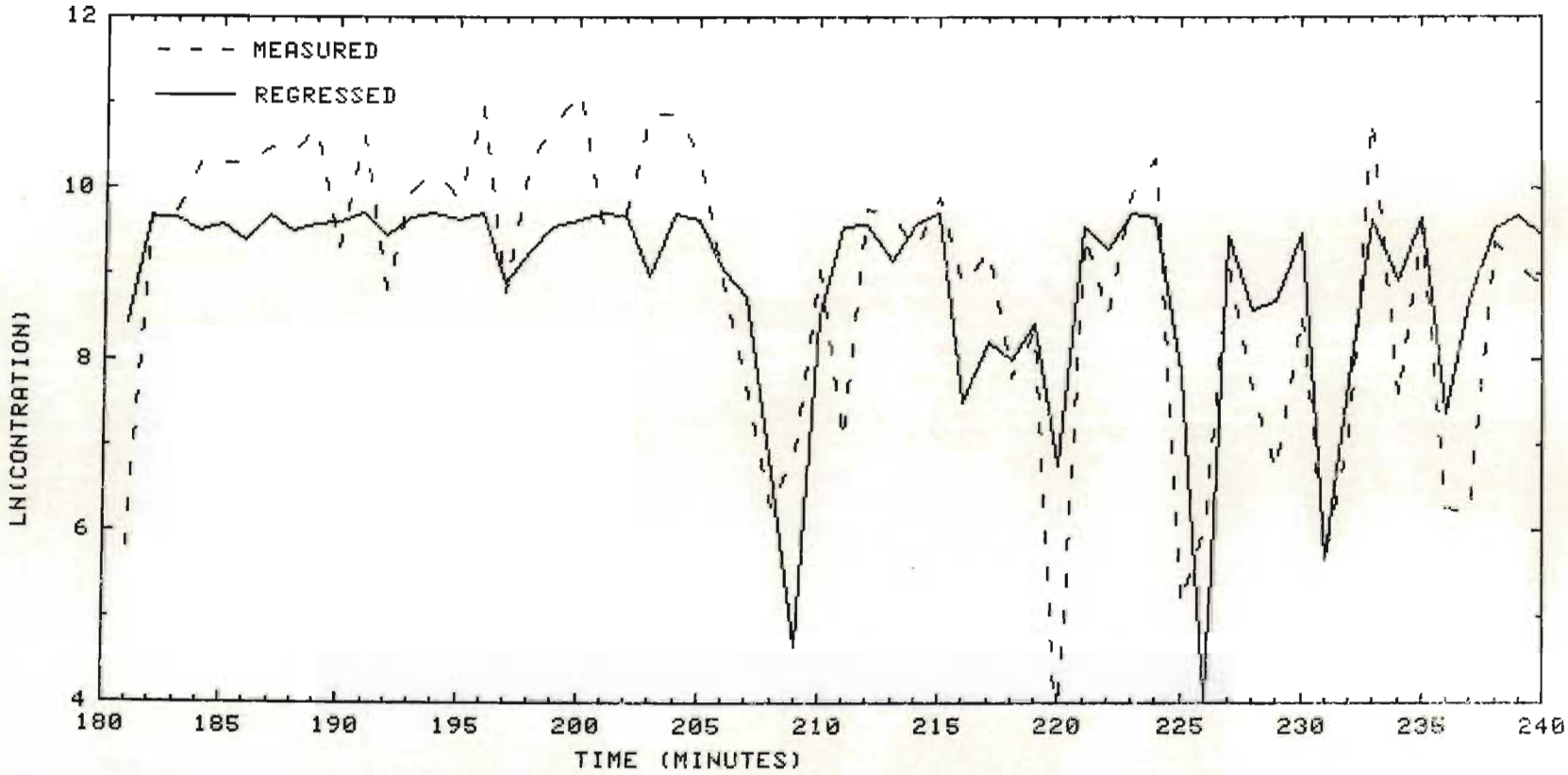

Figure D.3 : The best estimate of the concentration-time history from the fluctuating wind dispersion model compared with the measured history. Run 1 ; 60 to 120 minutes

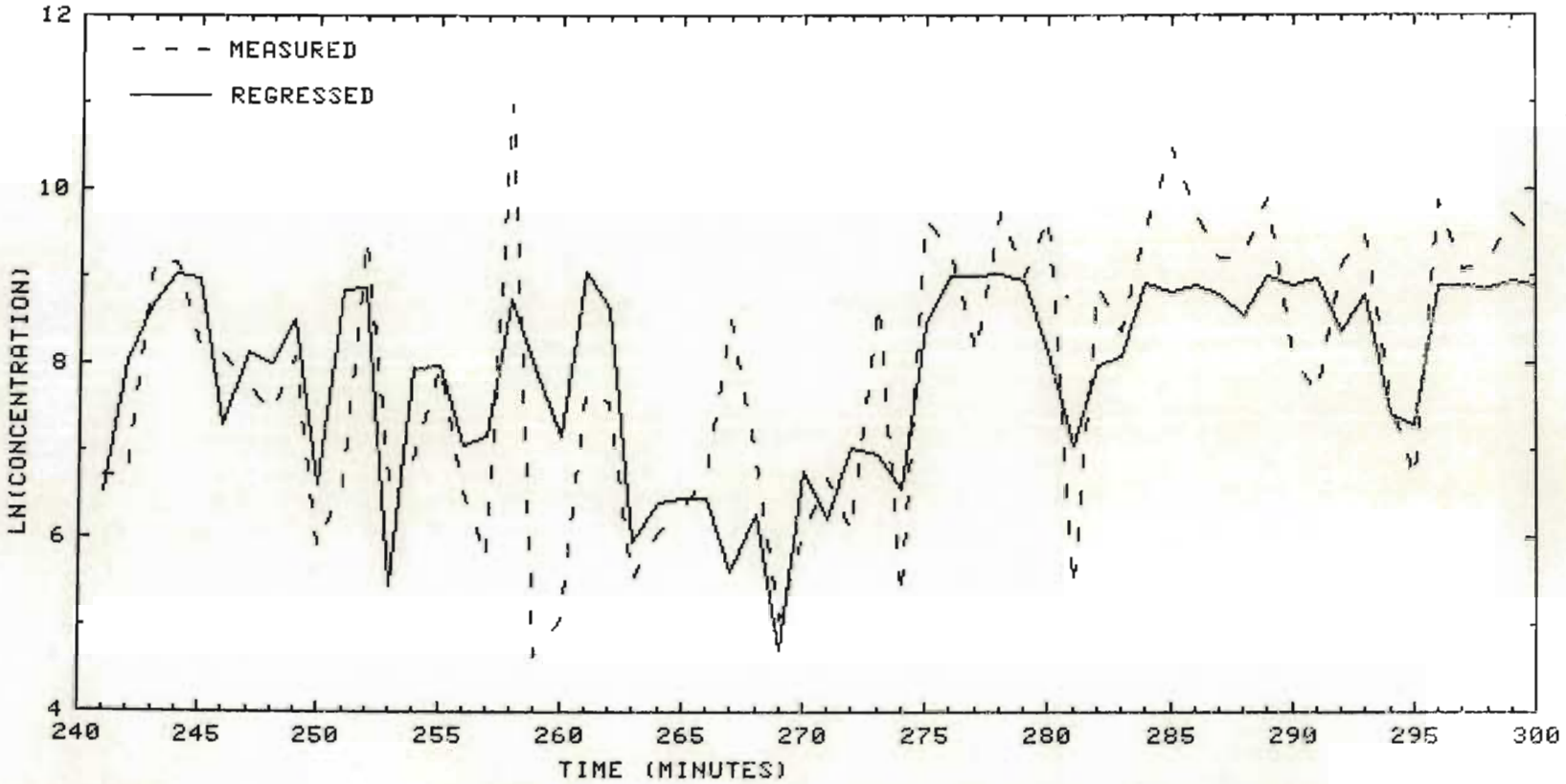

Figure D.4 : The best estimate of the concentration-time history from the fluctuating wind dispersion model compared with the measured history. Run 1 ; 240 to 300 minutes

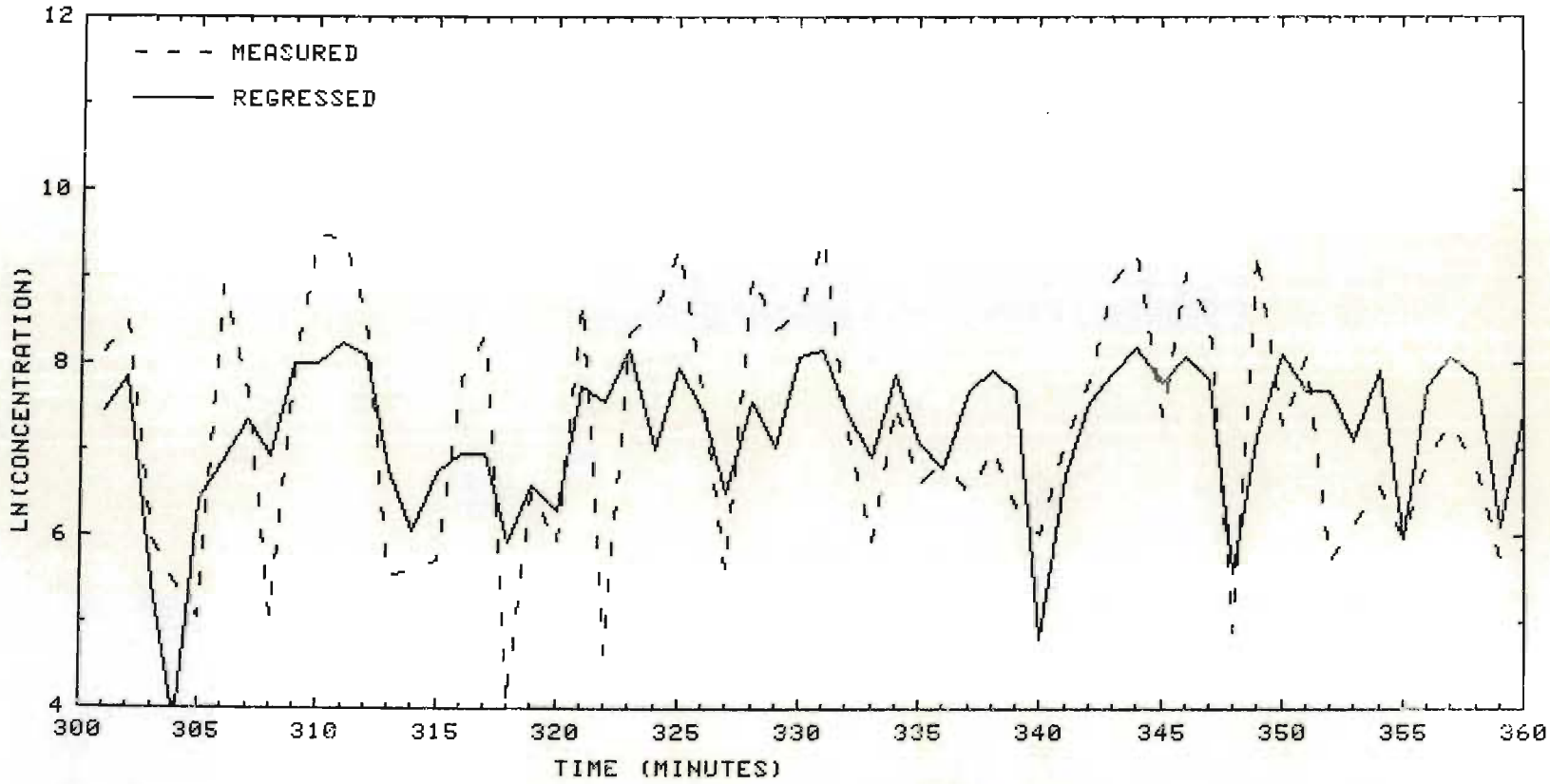

Figure D.5 : The best estimate of the concentration-time history from the fluctuating wind dispersion model compared with the measured history. Run 1 ; 300 to 360 minutes

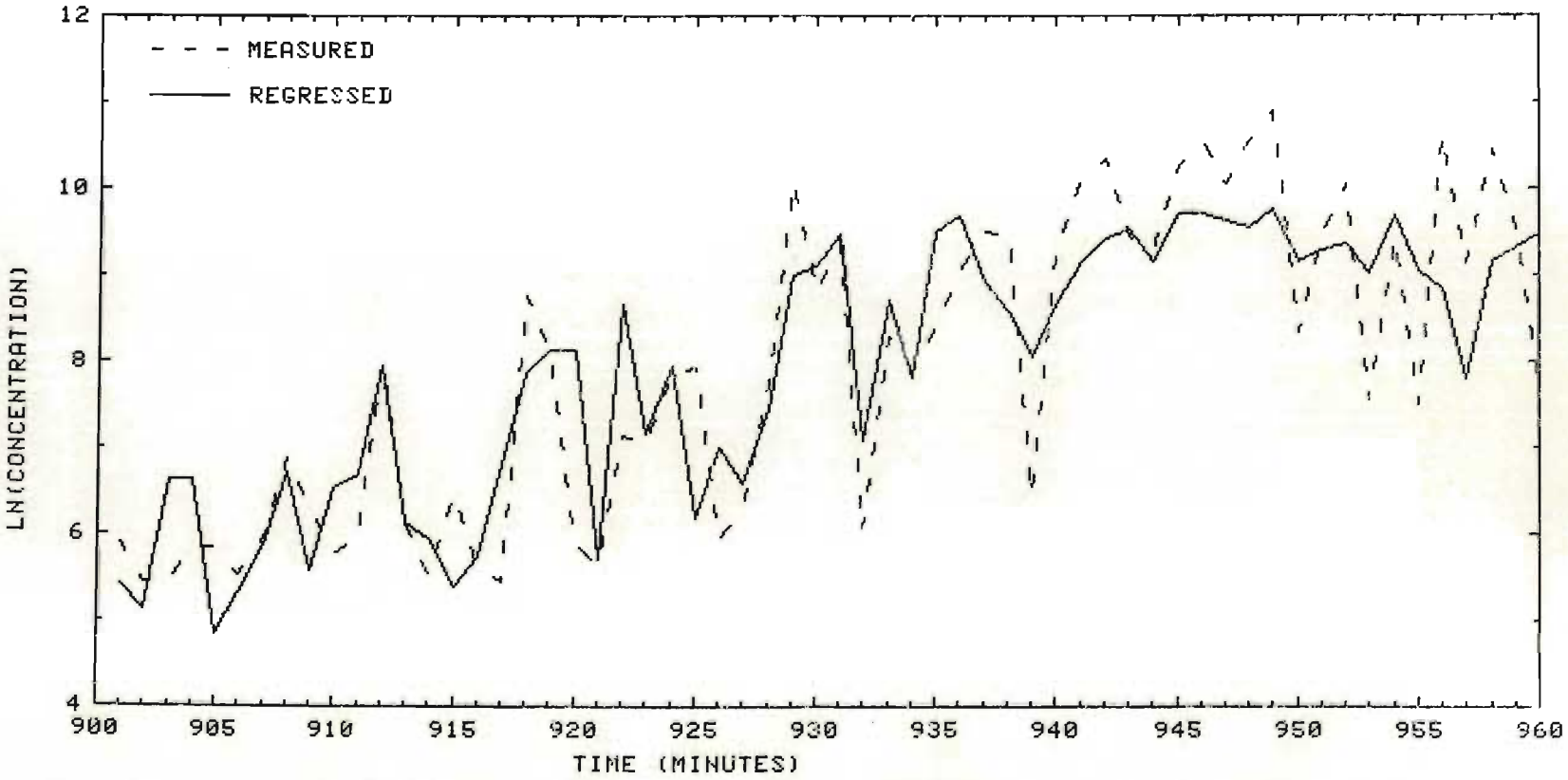

Figure D.6 : The best estimate of the concentration-time history from the fluctuating wind dispersion model compared with the measured history. Run 1 ; 900 to 960 minutes

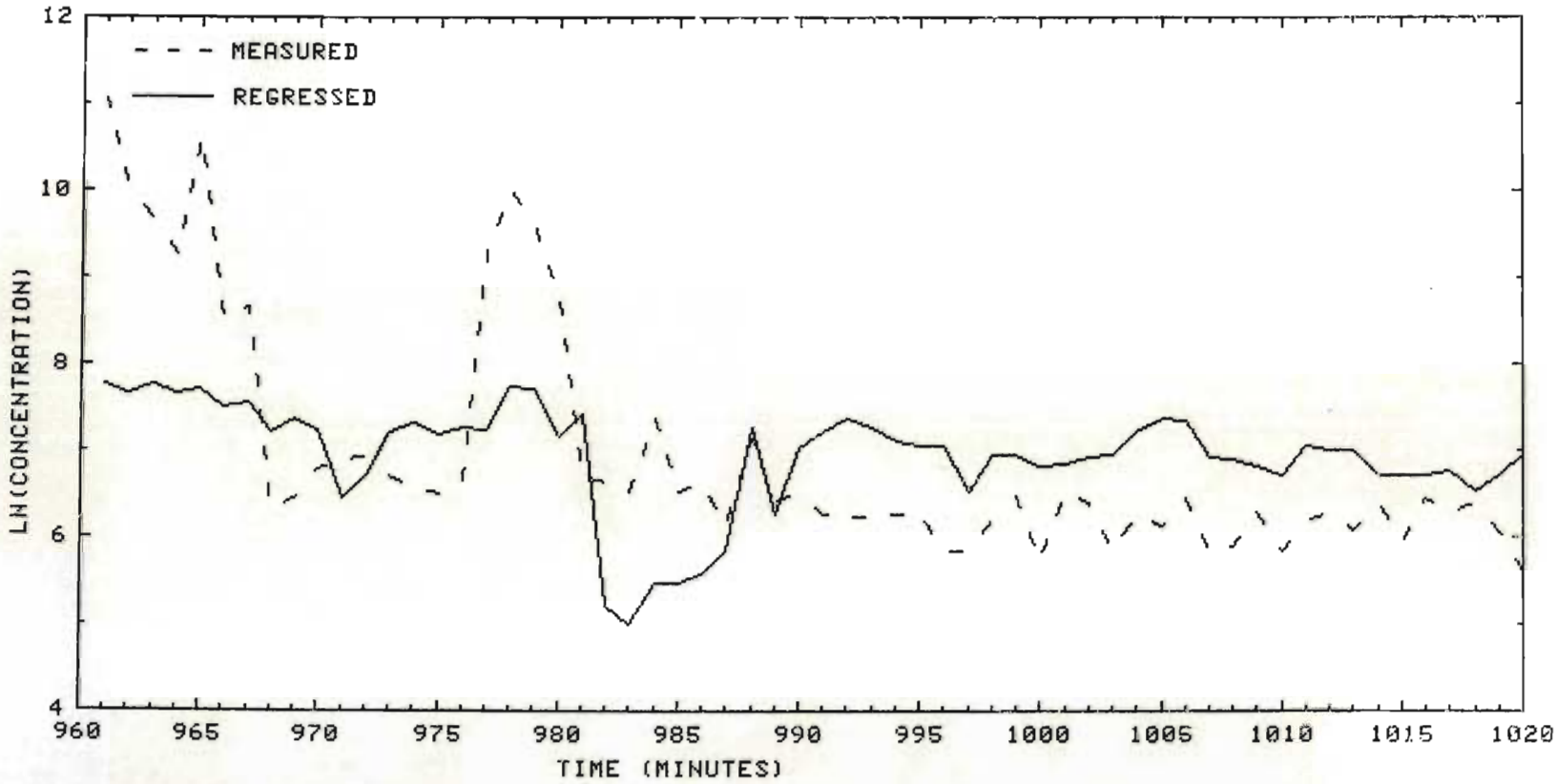

Figure D.7 : The best estimate of the concentration-time history from the fluctuating wind dispersion model compared with the measured history. Run 1 ; 960 to 1020 minutes

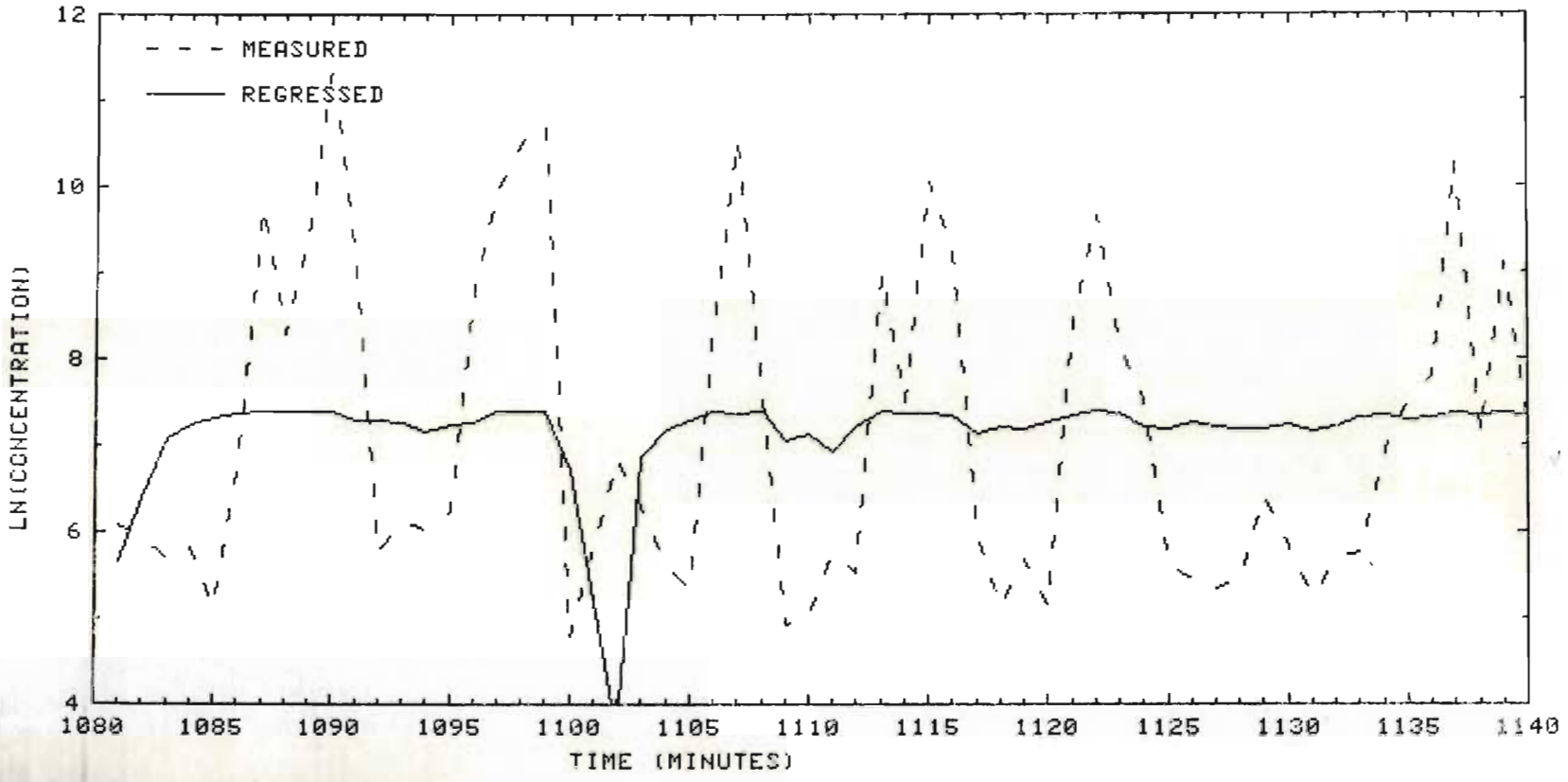

Figure D.8 : The best estimate of the concentration-time history from the fluctuating wind dispersion model compared with the measured history. Run 1 ; 1080 to 1140 minutes

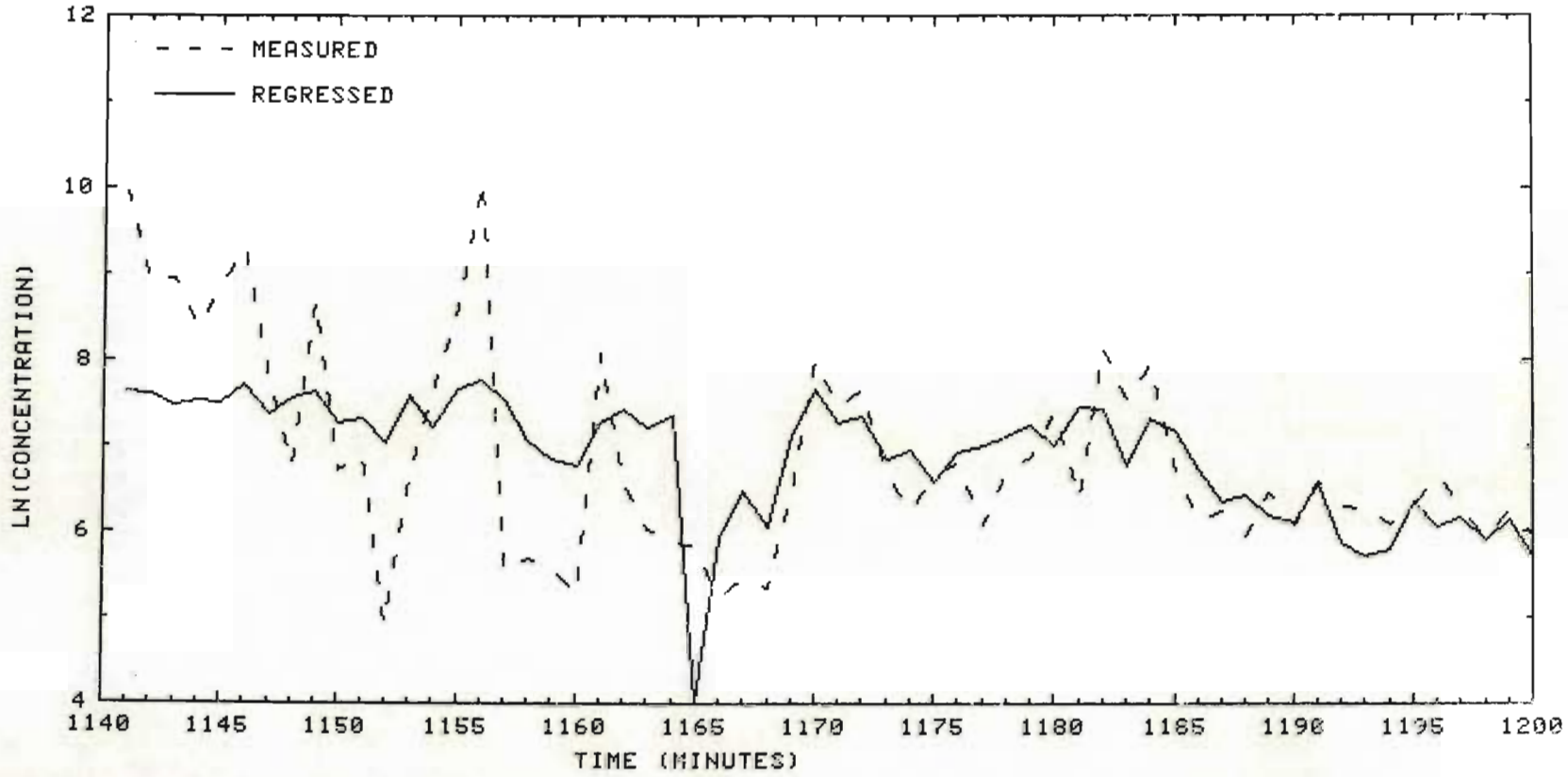

Figure D.9 : The best estimate of the concentration-time history from the fluctuating wind dispersion model compared with the measured history. Run 1 ; 1140 to 1200 minutes

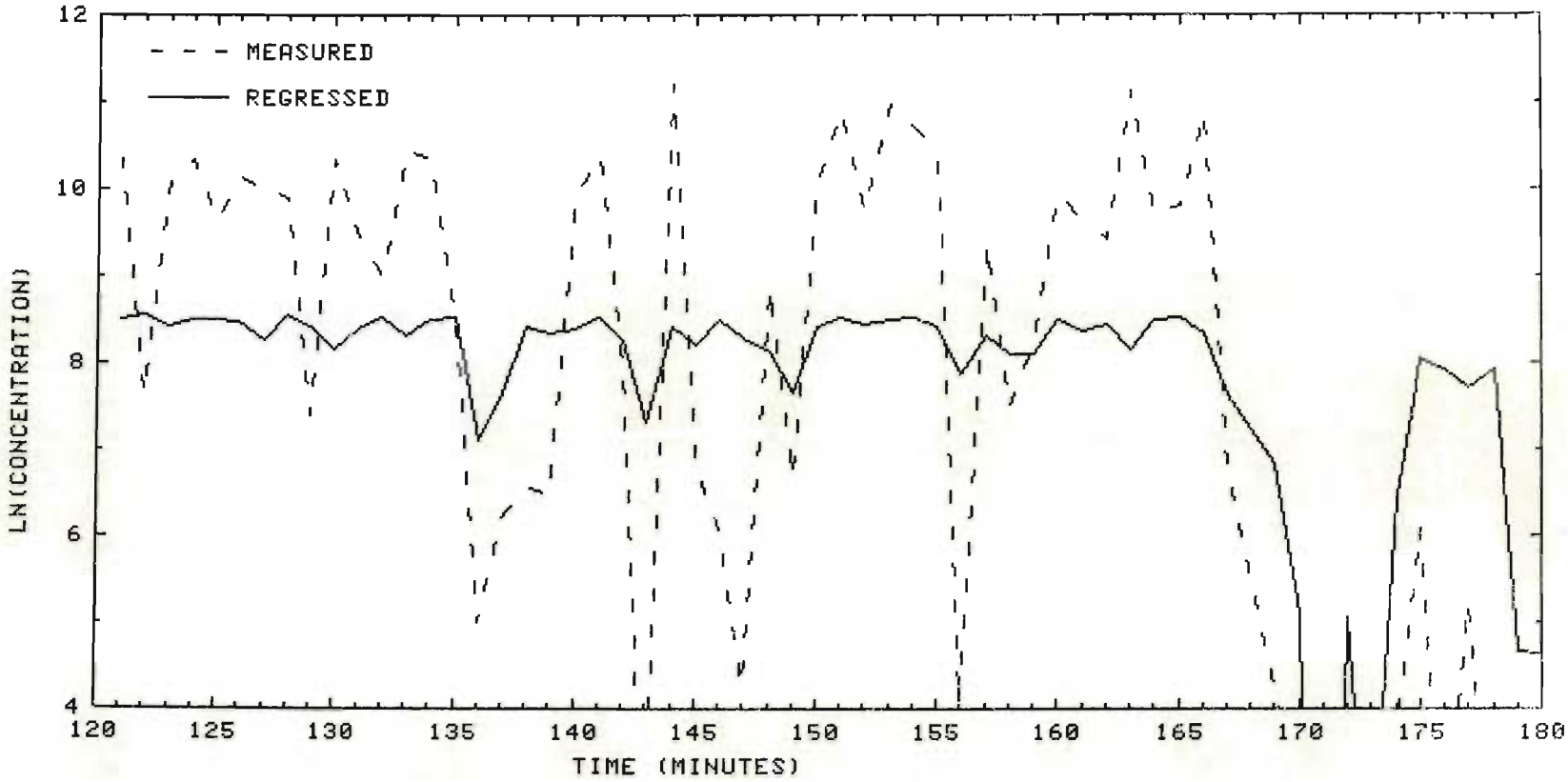

Figure D.10: The best estimate of the concentration-time history from the fluctuating wind dispersion model compared with the measured history. Run 2 ; 120 to 180 minutes

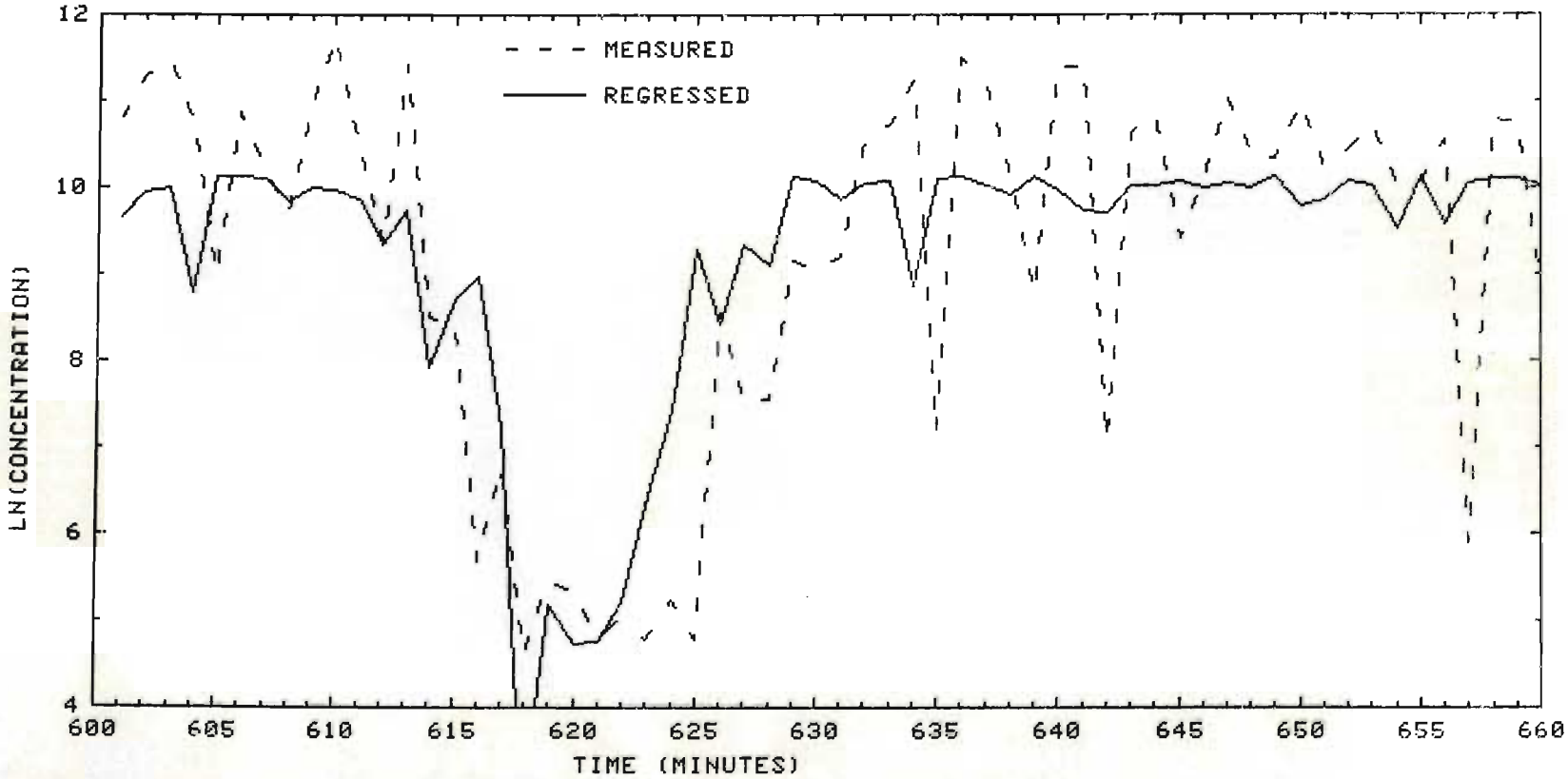

Figure D.11: The best estimate of the concentration-time history from the fluctuating wind dispersion model compared with the measured history. Run 3 ; 600 to 660 minutes

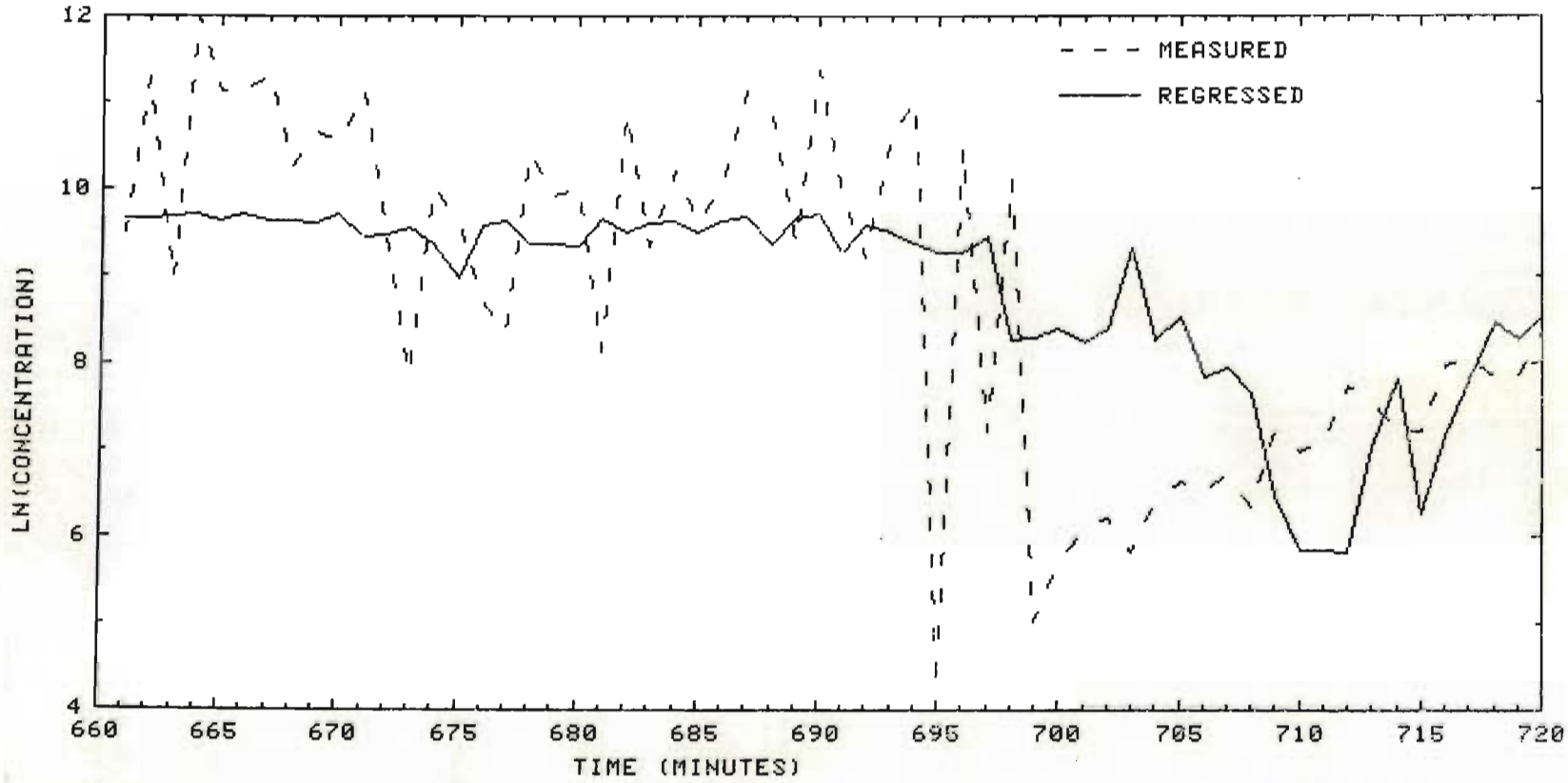

Figure D.12: The best estimate of the concentration-time history from the fluctuating wind dispersion model compared with the measured history. Run 3 ; 660 to 720 minutes

APPENDIX E: THEORETICAL RESPONSE OF THE FLUORESCENT PARTICLE COUNTER

Consider a geometrical arrangement of the various parts of the fluorescent particle counter as shown below :

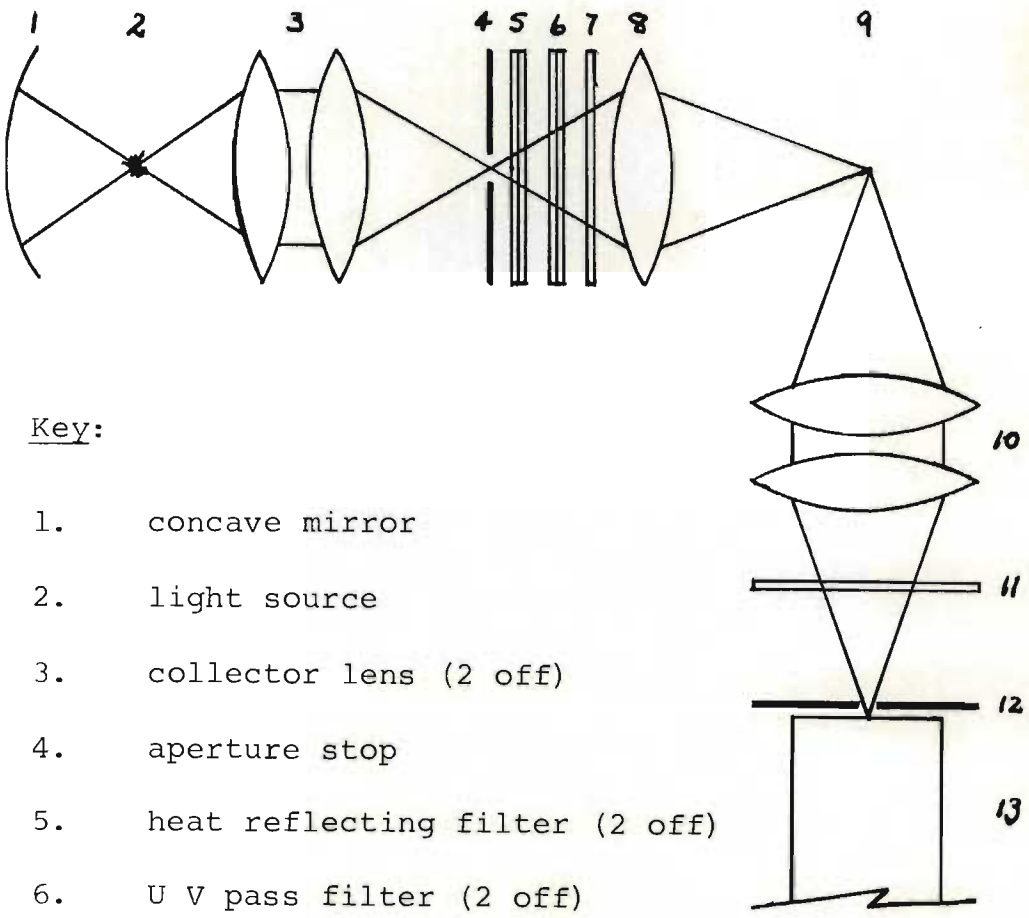

Key:

1. concave mirror
2. light source
3. collector lens (2 off)
4. aperture stop
5. heat reflecting filter (2 off)
6. U V pass filter (2 off)
7. red cut filter
8. projection lens
9. view volume containing a fluorescent particle
10. collector lens (2 Off)
11. U V cut filter
12. aperture stop

It can be shown that the anode current from the photomultiplier will be given by the following formula :

$$I_a = \frac{1}{2,5}(1 - \cos\alpha_{10}).T_{10}^2.G.\phi_f(\lambda_{max})\int_{\lambda_f} g(\lambda).T_{11}(\lambda).\varphi(\lambda).\lambda.d\lambda \qquad \text{(E.1)}$$

where $$\phi_f(\lambda_{max}) = \frac{\phi_i.\beta.\pi.D_p^2}{4A_q\int_{\lambda_f} g(\lambda)d\lambda.} \qquad \text{(E.2)}$$

and $$\left.\frac{\phi_i}{A_q}\right|_{\lambda=365nm} = h_2.A_2.2\pi(1-\cos\alpha_3).T_3^2.T_5^2.T_6^2.T_7.T_8.\Delta\lambda_i \qquad \text{(E.3)}$$

If the current I_a is assumed to pass through a $1M\Omega$ resistor and the resulting voltage signal further increased by a buffer amplifier gain of 18,2 the amplitude of the signal which can be obtained from a fluorescent particle of diameter D_p may be calculated. The result of this calculation is given in figure E.1.

The symbols for equations E.1 to E.3 are defined as follows : (all the constants have been given values and where appropriate the source has also been quoted)

A_2 Cross sectional area of the light source ($2,64 mm^2$; ref: technical literature from Osram)

A_q Cross sectional area of the view volume ($25\ mm^2$)

D_p Equivalent diameter of a fluorescent particle (m)

G Gain of the photomultiplier tube ($8,2 \times 10^6$; ref: 16)

$g(\lambda)$ Spectrum of fluorescence for fluorescent pigment FP2267 (ref: figure 3.7)

h_2 Intensity of radiation from the light source at a wavelength of 365 nm ($33 W/nm.\ mm^2$ steradian; ref: figure 3.2)

I_a Anode current from the photomultiplier (amps)

$Q(\lambda)$ Quantum efficiency of the photo-cathode of an EMI 9789B photomultiplier (ref: figure 3.7)

T_3, T_8, T_{10} Transmittance of the various lenses as numbered in sketch (0,95)

T_5, T_6, T_7 Transmittance of the filters in the excitation system, as numbered on the sketch, for a wavelength of 365nm (1,0; 0,7; 0,85; ref: figure 3.6)

$T_{11}(\lambda)$ Transmittance of the U V cut filter in the detection system (ref: figure 3.7)

α_3 Inlet pupil angle of the illumination system (30^o)

α_{10} Inlet pupil angle of the detection system (30^o)

β Proportion of the energy incident on a fluorescent particle which is converted to fluorescence (0,342; ref: 53)

λ Wavelength of light (nm)

λ_f Range of wavelengths over which a fluorescent particle fluoresces

$\Delta\lambda_i$ Width of the peak in the energy spectrum from the HBO 200 W/2 mercury lamp (12nm; ref: figure 3.2)

ϕ_i Total energy from the illumination system incident at the view volume (W)

$\phi_f(\lambda_{max})$ Energy fluoresced by a fluorescent particle at the wavelength of peak fluorescence (W)

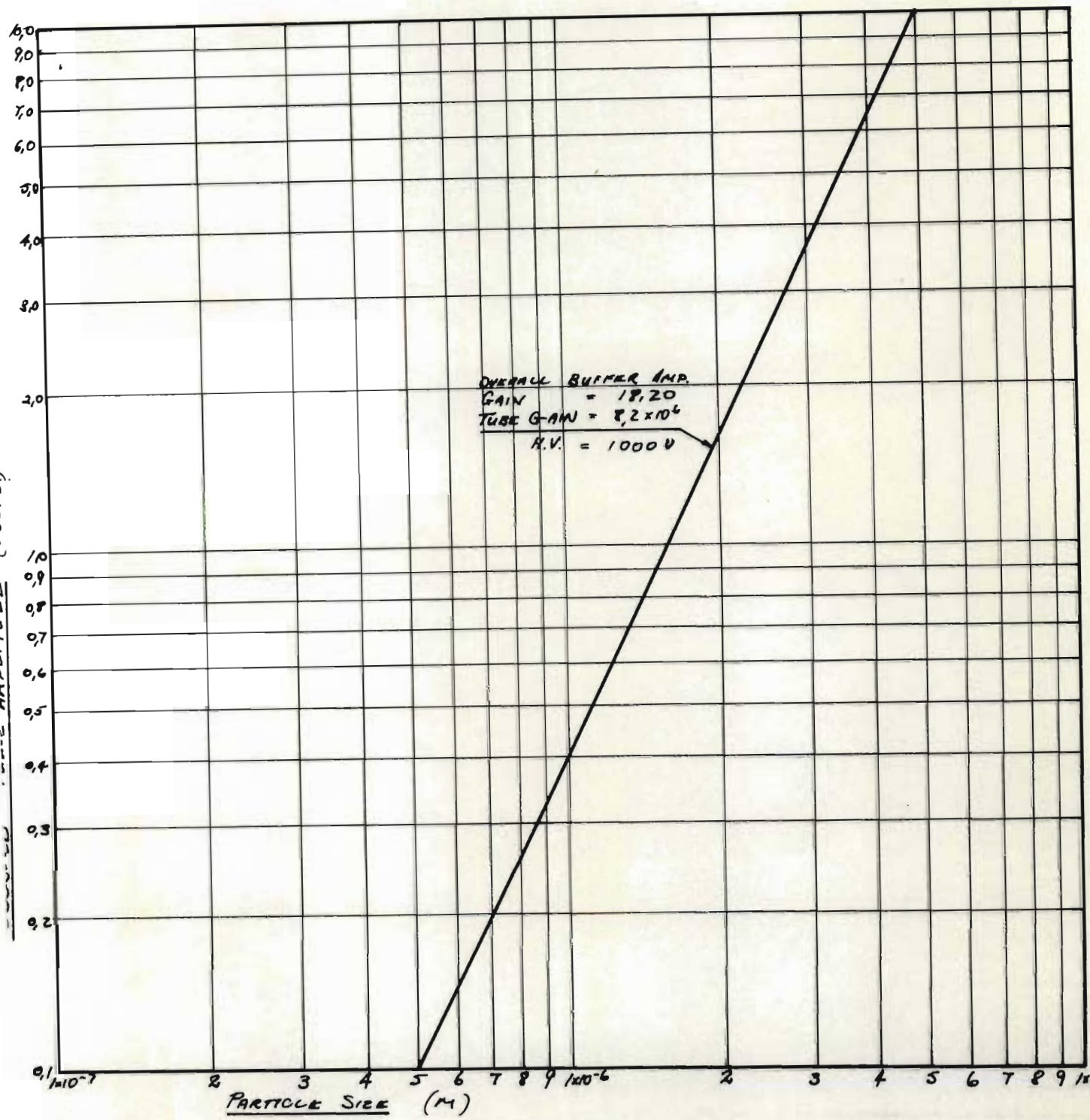

Figure E.1: Recorded pulse amplitude estimated from a theoretical consideration of the fluorescent particle counter, as a function of particle size